

PETROLEUM GEOLOGY OF THE TURNER  
SANDSTONE MEMBER OF THE CARLILE  
SHALES, WESTON COUNTY, WYOMING

by  
Courtney R. Bone

A thesis submitted to the Faculty and the Board of Trustees of the Colorado School of Mines in partial fulfillment of the requirements for the degree of Master of Science (Geology).

Golden, Colorado

Date \_\_\_\_\_

Signed: \_\_\_\_\_

Courtney R. Bone

Signed: \_\_\_\_\_

Dr. Stephen A. Sonnenberg  
Thesis Advisor

Golden, Colorado

Date \_\_\_\_\_

Signed: \_\_\_\_\_

Dr. Wendy Bohrson  
Professor and Department Head  
Department of Geology and Geological Engineering

## ABSTRACT

The Upper Cretaceous Turner Sandstone Member (Turner) of the Carlile Formation in the eastern Powder River Basin is a proven economic hydrocarbon producer with extensive potential for long term development and exploration. The Turner consists of shallow marine Turonian-aged deposits composed of interstratified sandstones, mudstones, and siltstones that were deposited on the western margin of the Western Interior Cretaceous Seaway and likely sourced from the Sevier Orogenic belt to the west. Hydrocarbon accumulation for the Turner is believed to be a result of long distance migration of the hydrocarbons from the Mowry Formation below with secondary sourcing from the Niobrara Formation above.

The Turner oil and gas play at Finn-Shurley Field in Weston County, Wyoming, is an unconventional stratigraphic trap characterized by low porosity and permeability on the eastern margin of the Powder River Basin. The field is a continuous accumulation of hydrocarbons that have migrated updip from mature source rock within the region, as the Mowry and the Niobrara Formations are not mature within Weston County. These hydrocarbons saturate the extremely heterolithic lower Turner sandstone reservoir, which is the primary target for operators in the field. Finn-Shurley Field, discovered in 1965 and producing since the 1980's, is a shallow, under-pressured, reservoir, where production seems to be limited by the facies, reservoir quality, such as porosity and permeability, and stage of diagenetic alteration. In recent years, Finn-Shurley has become a horizontal target because of its low porosity, low permeability, and tight oil nature.

Overall, the Turner is one of the most prolific plays in the basin. However, little work has been published on the Turner to understand the reservoir potential and its extent to predict future development and exploration. This thesis project researched the controls on reservoir quality and production in the Finn-Shurley Field in Weston County, Wyoming. The highly heterolithic nature of the Turner in the eastern PRB promotes studies to be conducted to

best understand the intervals that contain the best rock quality for hydrocarbon accumulations to occur throughout the region. This was accomplished by integrating four cores (271 ft) with supplemental core data, petrographic thin section analysis, X-ray Diffraction (XRD), X-ray Fluorescence (XRF), Field Emission Scanning Electron Microscopy (FE-SEM) imaging, historical production data, and petrophysical well logs. Due to the coarse nature of conventional reservoir characterization, this integrated dataset was critical in facies classification across the multiple scales required to accurately understand factors contributing to reservoir quality and their relation to production. The rock and source quality elements contributing to reservoir quality from core-based measurements were used to identify four reservoir facies out of eight total identified facies.

Within the study area, the Turner has been divided into eight facies based upon lithology, grain size, bioturbation intensity levels, diversity of ichnofauna, and sedimentary structures. Within these facies, porosity ranges between 10-16% and permeabilities generally range between 0.001-5 mD. There have been four potential reservoir facies identified which have porosity values greater than 12% and permeabilities greater than 0.1 mD, and suggest meso- to micro-pore throat sizes in these facies. These classifications aided in targeting the best reservoir intervals in the lower Turner interval for each core, which was scaled to petrophysical well logs for future targeting and completion of the Turner. The lower Turner one zone was determined to be the primary reservoir target in Finn-Shurley field based on the presence of reservoir facies, as well as high porosity, permeability, brittleness, and resistivity values.

The integrated use of this multi-scale approach gave a more comprehensive understanding of the diverse and interstratified facies observed within the Turner at Finn-Shurley field. The variations in reservoir quality are investigated at multiple scales, which lead to improved knowledge of factors controlling reservoir quality and hydrocarbon production in the Turner. This includes understanding the role of diagenesis in this unconventional reservoir, implications of depositional processes, and visualizing the reservoirs mineralogical and elemental makeup at multiple scales.

## TABLE OF CONTENTS

ABSTRACT . . . . .	iii
LIST OF FIGURES . . . . .	viii
LIST OF TABLES . . . . .	xviii
ACKNOWLEDGMENTS . . . . .	xix
CHAPTER 1 INTRODUCTION . . . . .	1
1.1 Overview . . . . .	1
1.2 Study Objectives and Purpose . . . . .	7
1.3 Study Area . . . . .	8
1.4 Dataset and Research Methods . . . . .	10
CHAPTER 2 BACKGROUND GEOLOGY . . . . .	14
2.1 Regional Geology . . . . .	14
2.2 Regional Structural Setting . . . . .	20
2.3 Regional Stratigraphy . . . . .	21
2.4 Petroleum Geology . . . . .	26
2.5 Previous Work . . . . .	30
CHAPTER 3 CORE ANALYSIS . . . . .	33
3.1 Overview . . . . .	33
3.2 Core Descriptions . . . . .	34
3.2.1 Colen 10-10 . . . . .	36
3.2.2 McTuillin Federal 1 . . . . .	36

3.2.3	Perpetual Finn 8 . . . . .	36
3.2.4	Dreiling Federal 7 . . . . .	36
3.3	Key Stratigraphic Surfaces . . . . .	37
3.3.1	Mid-Turonian Unconformity . . . . .	38
3.3.2	Flooding Surface . . . . .	39
3.3.3	Minor Flooding Surface . . . . .	41
3.3.4	Minor Erosional Surface . . . . .	42
3.4	Facies Description . . . . .	43
3.4.1	Facies 1: Bioturbated, Shaley, Very Fine-Grained Sandstone . . . . .	47
3.4.2	Facies 2: Laminated, Muddy, Very Fine- to Fine-Grained Sandstone . . . . .	49
3.4.3	Facies 3: Interbedded Burrowed, Laminated, Mudstone, Siltstone, and Sandstone . . . . .	50
3.4.4	Facies 4: Heterolithic, Bioturbated, Mudstone, Siltstone, and Sandstone . . . . .	52
3.4.5	Facies 5: Laminated Fine-Grained Sandstone . . . . .	53
3.4.6	Facies 6: Medium-Grained Sandstone . . . . .	55
3.4.7	Facies 7: Silty Argillaceous Mudstone . . . . .	56
3.4.8	Facies 8: Interbedded, Laminated, Sandstone, Siltstone, and Mudstone . . . . .	57
3.5	Ichnology and Bioturbation . . . . .	59
3.6	Sedimentary Structures . . . . .	64
3.7	Facies Distribution . . . . .	67
3.8	Subsurface Correlations . . . . .	70
3.9	Elemental Geochemistry . . . . .	73

3.9.1	Colen 10-10 Chemostratigraphy . . . . .	74
3.9.2	Colen 10-10 Chemofacies Classification . . . . .	80
CHAPTER 4	PETROGRAPHIC ANALYSIS . . . . .	86
4.1	Petrographic Analysis Overview . . . . .	86
4.2	Thin Section Analysis . . . . .	88
4.3	FE-SEM Analysis . . . . .	94
4.3.1	Diagenesis Summary . . . . .	107
CHAPTER 5	RESERVOIR CHARACTERIZATION . . . . .	110
5.1	Reservoir Characterization Overview . . . . .	110
5.2	Porosity and Permeability . . . . .	110
5.3	Source Rock . . . . .	113
5.4	Reservoir Targets . . . . .	117
5.5	Reservoir Mapping . . . . .	125
5.6	Production . . . . .	128
5.6.1	Historical Production . . . . .	128
5.6.2	Production Implications . . . . .	129
5.7	Discussion of Total Unconventional Petroleum System . . . . .	132
CHAPTER 6	CONCLUSIONS AND FUTURE RECOMMENDATIONS . . . . .	135
6.1	Conclusions . . . . .	135
6.2	Future Recommendations . . . . .	137
REFERENCES CITED	. . . . .	139

## LIST OF FIGURES

Figure 1.1	Map of the Powder River Basin Providence with the black box outlining the area of study in Weston County (Modified from Anna, 2009). . . . .	3
Figure 1.2	Stratigraphic column of the Upper Cretaceous stratigraphy in the PRB on the west and east margins of the basin. The Turner is outlined in blue. The known or potential source rocks are marked by a red square and known productive reservoir intervals are marked by green dots. Modified from Anna (2009). . . . .	4
Figure 1.3	Average oil and gas per well EUR by Formation in the PRB (Kegel, 2019). . . . .	5
Figure 1.4	Horizontal well completions since 2011 with average well EUR by producing formation in the PRB (Kegel, 2019). . . . .	5
Figure 1.5	Map of the PRB showing Frontier/Turner hydrocarbon production in relation to the area where the Niobrara Formation is greater than 8,000 ft and believed to be mature. The grey line outlines approximately where the Mowry is believed to be mature, and the purple line outlines the boundaries of the Frontier/Turner assessment unit. The black box shows the location of the study area, Finn-Shurley field. Modified from Anna (2009). . . . .	6
Figure 1.6	Map of the counties of Eastern Wyoming and the study location of Finn-Shurley Field within Weston County, Wyoming. . . . .	9
Figure 1.7	Map of core locations within Finn-Shurley. The yellow star is the Colen 10-10 core, the red star is the Perpetual Finn 8 core, the green star is the Dreiling Federal 7 core, and the blue star is the McTuillin Federal 1 core. The purple star is the Dixon-Smith 3 well which was used for a 1D basin model. . . . .	10
Figure 2.1	Structural definition of the PRB from Dolton and Fox (1995). . . . .	15
Figure 2.2	Generalized East to West cross section of the PRB (Modified from Anna, 2009). . . . .	16



Figure 2.3	Distribution of oil and gas fields and structural lineaments in the PRB. Lineaments BC=Bell Creek, SR=Springen Ranch, RZ=Rozet, SCC=South Coyote Creek, GB=Gose Butte, FC=Fiddler Creek, CT=Clareton Trend, PB=Parkman-Baker, BHC=Bighorn-Custer, BD=Buffalo-Douglas, BB=Black Butte, LC=Lightening Creek. Study area is outlined in the black box. (Modified from Martinsen, 2003). . . . .	17
Figure 2.4	Paleogeography map of the Western Interior Seaway during the late Turonian in the PRB (outlined in red). (Modified from Blakey, 2013). . . . .	18
Figure 2.5	Biostratigraphic chart for the Western Interior. Red box highlights the zones corresponding to the Turner age (Modified from Merewether et al., 2007). . . . .	19
Figure 2.6	Typical log pattern from Pierre Shale to the Belle Fourche Formation (Weimer and Flexer, 1985). . . . .	25
Figure 2.7	Illustration of the Cretaceous transgressive-regressive cycles defined by Haq (2014). Red box indicates the Turner depositional interval. . . . .	26
Figure 2.8	Petroleum system elements chart for the Turner Sandy Member of the Carlile Shale. (Modified from Anna, 2009). . . . .	27
Figure 2.9	Well penetration map showing completion date for Turner wells within the southern PRB (from Enverus, 2019). . . . .	28
Figure 2.10	Pressure gradient contours with first 18 months production of unconventional oil from Wall Creek-Turner reservoirs (From Toner, 2019). . . . .	29
Figure 3.1	Location and names of cores described for this study within Weston County, Wyoming. . . . .	34
Figure 3.2	Core description of the Colen 10-10 well. The facies legend is on the far right side with the core description showing depth, grain size, lithology, facies, and bioturbation index. Also included is a gamma ray log and interpreted key stratigraphic surfaces, which include a minor flooding surface (MnFS), a flooding surface ( <i>S. warreni</i> ), and an unconformity. . . . .	35

Figure 3.3	Core photos from the Colen 10-10 core displaying the Mid-Turonian unconformity (red dashed line) with the underlying Poole Creek member of the Carlile Shale at 5,307-5,308 ft. core depth. A minor flooding surface (blue solid line) with a medium- to fine-grained sandstone underlying a mudstone bed. at 5296-5297 ft. core depth. And a major flooding surface (red solid line) with a fine sandstone underlying an mudstone at 5263-6264 ft. core depth, capping the top of a Turner deposition cycle. . . . .	37
Figure 3.4	Core photo from the Colen 10-10 core displaying the Mid-Turonian unconformity (red dashed line) with the underlying Poole Creek member of the Carlile Shale at 5,307-5,308 ft. core depth. . . . .	39
Figure 3.5	Core photo from the Colen 10-10 core displaying the <i>Scaphites warreni</i> flooding surface that is present throughout the subsurface and at the top of an upward coarsening sequence at 5,263-5,264 ft. core depth. Argillaceous mudstones overlying fine-grained sands can be observed at each FS within the Turner interval. . . . .	41
Figure 3.6	Minor flooding surface within the Colen 10-10 core that shows a medium- to fine-grained sandstone underlying a mudstone and siltstone observed at the core depth of 5296-5297 ft core depth. . . . .	42
Figure 3.7	Minor erosional surface within the Colen 10-10 core that shows the observed sandstone facies eroding into the underlying bioturbated facies by scour surfaces at the core depth between 5246-5247 ft. . . . .	43
Figure 3.8	Summary of Facies 1, 2, and 3 for this study of the lower Turner in Finn-Shurley Field. Figure includes facies name, a representative core photo, a thin section photomicrograph, XRD mineralogy, porosity, permeability, number of available core data points, measured TOC, and a $R_{35}$ calculation. Blue epoxy in the thin section photomicrograph represents porosity. . . . .	45
Figure 3.9	Summary of Facies 4, 5, and 6 for this study of the lower Turner in Finn-Shurley Field. Figure includes facies name, a representative core photo, a thin section photomicrograph, XRD mineralogy, porosity, permeability, number of available core data points, measured TOC, and a $R_{35}$ calculation. Blue epoxy in the thin section photomicrograph represents porosity. . . . .	46

Figure 3.10	Summary of Facies 7 and 8 for this study of the lower Turner in Finn-Shurley Field. Figure includes facies name, a representative core photo, a thin section photomicrograph, XRD mineralogy, porosity, permeability, number of available core data points, measured TOC, and a $R_{35}$ calculation. Blue epoxy in the thin section photomicrograph represents porosity. . . . .	47
Figure 3.11	Facies 1: Bioturbated, shaley, very fine-grained sandstone. A) shows a representative core photo of the highly bioturbated and muddy facies. B) shows a representative photomicrograph of the facies in thin section at a depth at 5234 ft in the Colen 10-10 core. . . . .	48
Figure 3.12	Facies 2: Laminated, muddy, burrowed, very-fine sandstone. A) shows a representative core photo of the laminated muddy facies. B) shows a photomicrograph of the facies in thin section at a depth at 4884 ft in the McTuillin Federal 1 core. . . . .	50
Figure 3.13	Facies 3: Interbedded, burrowed, laminated, mudstone, siltstone, and sandstone. A) shows a representative core photo of the highly bioturbated and muddy facies. B) shows a representative photomicrograph of the facies in thin section at a depth at 4884 ft in the McTuillin Federal 1 core. . . . .	51
Figure 3.14	Facies 4: Heterolithic, bioturbated, mudstone, siltstone, and sandstone. A) shows a representative core photo of the heterolithic facies. B) shows a representative photomicrograph of the facies in thin section at a depth at 4876 ft in the McTuillin Federal 1 core. . . . .	53
Figure 3.15	Facies 5: Laminated fine-grained sandstone. A) shows a representative core photo of the laminated sandstone facies. B) shows a representative photomicrograph of the facies in thin section at a depth at 4851 ft in the McTuillin Federal 1 core. . . . .	54
Figure 3.16	Facies 6: Medium-grained sandstone. A) shows a representative core photo of the sandstone facies. B) shows a representative photomicrograph of the facies in thin section at a depth at 5297 ft in the Colen 10-10 core. . . . .	56
Figure 3.17	Facies 7: Argillaceous, silty mudstone. A) shows a representative photo of the mudstone facies. B) shows the facies in thin section at a depth at 4840 ft in the McTuillin Federal 1 core. . . . .	57

Figure 3.18	Facies 8: Interbedded, laminated, sandstone, siltstone, and mudstone. A) shows a representative core photo of the interbedded facies. B) shows a photomicrograph of the facies in thin section at a depth at 4838 ft in the McTuillin Federal 1 core. . . . .	58
Figure 3.19	Bioturbation index key with a 0-6 scale. Modified from Reineck (1963), Taylor and Goldring (1993) and Taylor et al. (2003) by MacEachern and Bann (2008). . . . .	61
Figure 3.20	Common marine ichnofacies. Modified from Seilacher (1954). . . . .	62
Figure 3.21	Core photos from the lower Turner two cycle. Most common trace fossils present include examples of <i>Skolithos</i> (Sk), <i>Planolites</i> (Pl), <i>Teichichnus</i> (Te), <i>Thalassinoides</i> (Th), <i>Asterosoma</i> (As), and <i>Ophiomorpha</i> (O). . . . .	63
Figure 3.22	Core photos from the lower Turner one cycle. Most common trace fossils present include examples of <i>Skolithos</i> (Sk), and <i>Planolites</i> (Pl). . . . .	64
Figure 3.23	Observed sedimentary structures. A) bi-directional ripples B) wavy-flaser laminations C) ripple cross sets D) planar laminations E) climbing ripples F) hummocky or swaley cross stratification G) mud rip-up clasts. . . . .	66
Figure 3.24	Pie distribution of facies in each core across Finn-Shurley. . . . .	68
Figure 3.25	Distribution of facies across Finn-Shurley. Left shows the distribution of facies in the lower Turner two. Right shows the distribution of facies in the lower Turner one. . . . .	68
Figure 3.26	Vertical distribution of facies across Finn-Shurley. The black dashed line represents the <i>S. Warreni</i> flooding surface. . . . .	70
Figure 3.27	Surface map showing cross section A-A' and B-B'. . . . .	71
Figure 3.28	Subsurface stratigraphic correlation N-S across Finn-Shurley from A-A'. Flattened on the top of the Turner. . . . .	72
Figure 3.29	Subsurface stratigraphic correlation E-W across Finn-Shurley from B-B'. Flattened on the top of the Turner. . . . .	72
Figure 3.30	Detrital elemental indicators from XRF for the Colen 10-10 core. Included is a core facies log, a lithology log, a gamma ray curve, and curves for Si (ppm), Al (ppm), Ti (ppm), K(ppm), and a Ti/Al ratio. . . . .	76

Figure 3.31	Carbonate elemental indicators from XRF for the Colen 10-10 core. Included is a core facies log, a lithology log, a gamma ray log, and curves for Ca (ppm), Sr (ppm), and Mn (ppm). . . . .	77
Figure 3.32	Provenance elemental ratios from XRF for the Colen 10-10 core. Included is a core facies log, a lithology log, a gamma ray log, and ratio curves for Nb/Th, K/Rb, Zr/Ti, K/Al, and P/Ti. . . . .	78
Figure 3.33	Comprehensive mineral model in weight percent generated from XRF for the Colen 10-10. Included is a core facies log, a lithology log, a petrophysical and pseudo gamma ray log, and mineralogy curves for calcite, clay, and quartz. Each individual mineralogy curve is then compared to XRD data points (black dots) for each mineral profile. A pseudo gamma ray log (green dashed line) is also calculated from K, U, and Th and superimposed on the petrophysical gamma ray log (black solid line). . . . .	79
Figure 3.34	PCA analysis image showing the interpreted general clusters and trends of elements in two dimensions. . . . .	82
Figure 3.35	Log plot of raw XRF data in ppm for each element through the vertical succession of the Colen 10-10 core. Also included is the euclidean distance from data average (FIT), vertical chemofacies log (XRF), and core description facies log (CORE). . . . .	84
Figure 3.36	Bar graph that shows the enrichment or depletion of each element for each defined chemofacies for the Colen 10-10. Enriched elements are in green, depleted elements are in red. Elements in black bars was the largest enrichment or depletion used to classify chemofacies. Chemofacies 2 and 4 are enriched in Si, with lower concentrations of Ca and Al, which correlate with better reservoir quality facies (green star). . . . .	85
Figure 4.1	Paragenetic sequence of the Wall Creek member of the Frontier Formation from Almon and Tillmon (1979). . . . .	88
Figure 4.2	Thin section photomicrograph in plane light (top) and cross polar light (bottom) from the Colen 10-10 at a core depth of 5275 ft. Photomicrograph displays epifluorescent yellow dye highlighting primary porosity and possible secondary porosity with observed chert grains. Porosity from core is 16% and permeability from core is 0.38 mD at this depth. . . . .	90

Figure 4.3	Thin section photomicrograph in plane light from the McTuillin Federal 1 at a core depth of 4851 ft. Photomicrograph displays chlorite coating of grains observed as partial green/brown dust rims around quartz grains with visible intergranular porosity. Porosity from core is 15.5% and permeability from core is 0.33 mD at this depth. . . . .	91
Figure 4.4	Thin section photomicrograph in plane light from the McTuillin Federal 1 at a core depth of 4876 ft. Photomicrograph displays quartz overgrowths as quartz cements interpreted to have grown in the initial pore space. . . . .	92
Figure 4.5	Thin section photomicrograph in plane light from the Colen 10-10 at a core depth of 5297 ft. The photomicrograph displays late calcite cements that have destroyed most of the initial porosity. Also displays partial feldspar dissolution, pressure solution, and quartz overgrowths. . . . .	93
Figure 4.6	FE-SEM BSE image from the Colen 10-10 core at 5300 ft. core depth. BSE image shows a early microcrystalline authigenic quartz grain coat (mQ) and a later secondary authigenic chlorite (Cl) grain coating on a framework grain. . . . .	97
Figure 4.7	FE-SEM BSE image from the Colen 10-10 core at 5300 ft. core depth. BSE image shows a large euhedral quartz overgrowth (Q) in the pore space. . . . .	98
Figure 4.8	FE-SEM BSE image from the Colen 10-10 core at 5297 ft. core depth. BSE image shows another large euhedral quartz (Q) overgrowth in the pore space. Also seen in the image is an interpreted detrital chert grain (Cht), a framework grain with authigenic chlorite grain coat (Cl), and an authigenic calcite grain (Ca). . . . .	99
Figure 4.9	FE-SEM CL image from the Colen 10-10 core at 5275 ft. core depth. A/D) shows SE image of thin section. B/E) shows combined red, blue, and green CL image. C/F) shows red CL image. Detrital quartz grain (dq) displays bright luminescence in contrast to the dull luminescence of the authigenic quartz overgrowth (og). . . . .	100
Figure 4.10	FE-SEM CL image from the Colen 10-10 core at 5297.2 ft. core depth. A/D) shows SE image of thin section. B/E) shows combined red, blue, and green CL image. C/F) shows red CL image. Detrital quartz grain (dq) displays bright luminescence in contrast to the dull luminescence of the authigenic quartz overgrowth (og). . . . .	101

Figure 4.11	FE-SEM BSE image from the Colen 10-10 core at 5297 ft. core depth. BSE image shows a close up of a detrital chert grain. Authigenic microcrystalline quartz (mQ) is interpreted to be using the detrital chert as a nucleation site. . . . .	104
Figure 4.12	FE-SEM BSE image from the Colen 10-10 core at 5273.6 ft. core depth. BSE image shows conchoidal fractures as a result of rock breakage. . .	105
Figure 4.13	FE-SEM BSE image from the Colen 10-10 core at 5297 ft. core depth. BSE image shows authigenic kaolinite (classic "book" morphology) growing in the pore space. . . . .	105
Figure 4.14	FE-SEM BSE image with EDS map from the Colen 10-10 core at 5297 ft. core depth. Authigenic microcrystalline quartz grain coat is shown in red, chlorite grain coat is seen in yellow, pore filling calcite cement is seen in blue, and pore filling authigenic kaolinite books are seen in green. . . . .	106
Figure 4.15	Paragenetic sequence of the Turner Sandy member created from thin section and FE-SEM analysis and interpretations. . . . .	109
Figure 5.1	Porosity versus permeability plot of the McTuillin Federal 1 core colored by facies. Where the red, purple, green, and yellow squares are representative of reservoir facies. Dashed lines show the separation of pore throat sizes interpreted from $R_{35}$ calculation from Hartmann and Beaumont (1999). . . . .	112
Figure 5.2	FE-SEM BSE image of an intergranular pore in a rock sample from Facies 5. This sample was from the Colen 10-10 core at a core depth of 5300 ft. . . . .	113
Figure 5.3	Maturity map of the Mowry Shale in the PRB. The black circle represents the study area and the purple star represents the well used for a 1D basin model. Modified from Modica and Lapierre (2012). . . .	115
Figure 5.4	Basin Model created for the Dixon Smith 3 well just outside of the study area with maturity windows. Black line highlights the burial history of the Mowry Formation. . . . .	116
Figure 5.5	Type log section for the Perpetual Finn 8 that shows the gamma ray, resistivity, and density porosity profile through the Turner. Pink stippled bar shows cored interval and pink dashed bar shows perforated interval. Resistivity is filled in red where $ILD \geq 5$ Ohm-m, and porosity is filled in blue where $DPHI \geq 12\%$ . Net productive pay intervals are indicated by zones where both these cutoffs are met. . . . .	120

Figure 5.6	Chosen reservoir targets (green shaded intervals) for the Colen 10-10 well based upon facies classification, gamma ray signature, a resistivity cutoff, an arbitrary brittleness index cutoff of 0.55, high porosity values, and high permeability values. Well location is shown on the map in the right corner, and current production information is on the right corner where the perforated interval is shown in pink. . . . .	121
Figure 5.7	Chosen reservoir targets (green shaded intervals) for the McTuillin-Federal 1 well based upon facies classification, gamma ray signature, a resistivity cutoff, an arbitrary brittleness index cutoff of 0.55, high porosity values, and high permeability values. Well location is shown on the map in the right corner, and current production information is on the right corner where the perforated interval is shown in pink. . . . .	122
Figure 5.8	Chosen reservoir targets (green shaded intervals) for the Dreiling-Federal 7 well based upon facies classification, gamma ray signature, a resistivity cutoff, high porosity values, and high permeability values. Well location is shown on the map in the right corner, and current production information is on the right corner where the perforated interval is shown in pink. . . . .	123
Figure 5.9	Chosen reservoir targets (green shaded intervals) for the Perpetual Finn 8 well based upon facies classification, gamma ray signature, a resistivity cutoff, high porosity values, and high permeability values. Well location is shown on the map in the right corner, and current production information is on the right corner where the perforated interval is shown in pink. . . . .	124
Figure 5.10	Stratigraphic cross section of key cored wells flattened on top of the Turner. Logs including gamma ray and resistivity logs with a cutoff of 5 ohm-m. Pink dotted bars show perforated interval and pink stippled bars show cored interval. . . . .	126
Figure 5.11	Maps generated for the entire Turner interval (Top Turner to Basal Unconformity). A) Isopach of the Turner in Finn-Shurley area. The thickest interval is located in the center of the study area. B) Net resistivity map of the Turner. Resistivity map is created by summing the thickness of the Turner where resistivity is greater than 5 ohm-m. Contoured map shows the thickest interval of resistive rock is located in the center of the study area. Stars represent the locations of the key cored wells for this study. . . . .	127



Figure 5.12	Maps generated for the lower Turner interval (Top Lower Turner to Basal Unconformity). A) Isopach of the lower Turner in Finn-Shurley area. The thickest interval is located in the center of the study area. B) Net resistivity map of the lower Turner. Resistivity map is created by summing the thickness of the lower Turner where resistivity is greater than 5 ohm-m. Contoured map shows the thickest interval of resistive rock is located in the center of the study area. Stars represent the locations of the key cored wells for this study. . . . .	128
Figure 5.13	Historical production chart of the Turner within the study area of Finn-Shurley field in south central Weston County. Shows cumulative oil (green line), gas (red line), and water (blue line) produced from the field with the total cumulative barrels of oil equivalent (BOE) (orange line). . . . .	130
Figure 5.14	Historical production map of the Turner within the study area of Finn-Shurley field in south central Weston County. Illustrates a bubble map of 3 year oil cum's from historical vertical wells (top). In addition, it illustrates a bubble map of 3 year cum's from historical horizontal wells (bottom). . . . .	131
Figure 5.15	Lower Turner (Top Lower Turner to Basal Unconformity) production map for Finn-Shurley field. A) IHS Production is displayed on top of the Lower Turner isopach. B) IHS Production is displayed on top of the net resistivity map for the lower Turner. . . . .	132

## LIST OF TABLES

Table 1.1	Core location information. . . . .	9
Table 1.2	Dataset acquired for conducted research. . . . .	11

## ACKNOWLEDGMENTS

I would first like to thank my advisor, Dr. Steve Sonnenberg, for his continued guidance and support throughout this whole research experience. I will be forever grateful for your willingness to accept me into MUDTOC and allowing me to continue my academic journey at CSM. Thank you for all the wonderful conversations about geology, career paths, and life.

I'm also in debt to my committee members, Dr. Marsha French and Jim Emme. Thank you to Marsha for spending hours with me on the SEM discussing everything from minerals and diagenesis, to dogs and travel. Thank you to Jim for all the encouragement and support throughout this process, your enthusiasm and guidance were so welcomed and appreciated. I would also like to thank MUDTOC for the financial support throughout this experience, and to Kathy Emme for her ability to keep things running smoothly and contagious positivity during every meeting.

Huge thank you to all my fellow graduate students and more importantly, friends. Thank you for all of the support, laughter, and memories I will cherish with me forever. I would also like to thank Emre Kondakci, Andrew Wood, Andrew Heger, Matt Bauer, and Cahill Kelleghan for teaching me and guiding me in various softwares, the XRF/SEM machines, coding aid, and creating workflows.

Finally, thank you to my parents, Karen and Dale, for their unconditional love and support through my several years at Mines. You guys have been my biggest fans throughout my entire life and I owe all my accomplishments and successes to you guys. To Mariah and Lauren, thanks for your love, encouragement, and laughs throughout my life. You guys are a blessing and I'm so grateful to be your sister. And to my aunt Cindy and uncle Jed for being my home away from home and safeguard these last six years. I could not have done this project without any of you.

# CHAPTER 1

## INTRODUCTION

### 1.1 Overview

In recent years, the Powder River Basin (PRB) has become a primary target for exploration and development for petroleum companies. The PRB acreage is attractive to companies because it has over 5,000 ft of potential stacked pay within the Cretaceous strata across the basin. Combined with advances in horizontal drilling and recovery methods for unconventional reservoirs, new resources can be assessed and targeted that previously could not be tapped in these historical basin plays. The PRB is host to multiple world class source rocks, ideal pressure conditions, strong reservoir seals, and high quality reservoir rocks. Due to these conditions, many extensive and economic unconventional hydrocarbon reservoirs in different play types have been discovered within the PRB and new research and technologies are only expanding the untapped potential within the basin.

The Powder River Basin is a prolific hydrocarbon basin within the Western Interior Seaway basins located in the United States, with several potential reservoirs located within Upper Cretaceous sediments. The Powder River basin is located in northeastern Wyoming and extends into southeastern Montana (Figure 1.1). Within the PRB, the Turner Sandy Member of the Carlile Shale (Turner) has been proven both as a prolific unconventional and conventional play within the basin. The Carlile Shale is composed of three members: the upper Sage Breaks Member, the middle Turner Sandy Member, and the lower Pool Creek Member. The sediments that make up these lithologies were deposited as distal shallow marine clastics prograding from the Sevier Orogenic belt, located in modern Utah and Idaho, from the west to the western margin of the Western Interior Seaway. The Carlile Shale unconformably underlies the Niobrara Formation and conformably overlies the Greenhorn Formation (Figure 1.2). The Turner is considered stratigraphically and chronologically

equivalent to the Wall Creek Member of the Frontier Formation in the west, where erosion over bathymetric highs erased the connection between the two units in the rock record (Anna, 2009). Historically, the Turner has produced conventionally from isolated fields in the eastern margin of the PRB from a favorable reservoir facies that retained porosity and permeability during diagenesis (Weimer and Flexer, 1985). However, with modern horizontal drilling and completion techniques, this interval has become a highly prolific unconventional target and dominates oil production and well estimated ultimate recovery (EUR) numbers across the PRB (Figures 1.3, 1.4). The Turner has seen one of the most extensive horizontal development to date with immense success, as the Turner currently has the highest production rate and largest well EUR numbers in the basin (Kegel, 2019).

The Turner that occurs in the eastern PRB is Late Turonian in age and ranges in thickness from 80 to 300 feet across the region. The Turner is characterized by multiple flooding surfaces that result in coarsening upward parasequences of interstratified mudstone, siltstone, and sandstones. The Turner has been interpreted to be a brackish to marine deposit in northeast trending valleys (Weimer and Flexer, 1985). Others have suggested that the Turner was deposited similar to the Wall Creek Sandstone of the Frontier Formation, by a prograding lowstand delta to an open shelf and reworked by storms, tides, and waves (Merewether et al., 1979). A specific field of interest is the 1,300 acre Finn-Shurley Field, located in Weston County, Wyoming (Figure 1.5). Finn-Shurley Field was discovered in 1965 and has cumulatively produced 23 million barrels of oil and 38 billion cubic feet of gas. Historically, Finn-Shurley Field has produced from vertical wells first completed in the 1980's. However, recently this field has become a horizontal target due to advances in horizontal drilling and enhanced oil recovery techniques. This field has also seen an increase in modern hydraulic fracturing of historical vertical wells that has also proved successful for extending production life. The Turner in this field has good porosity values, greater than 10 percent, and permeabilities from core plugs that exceed 2 mD from medium-grained, clean, well-sorted sands (Anna, 2009). There are two erosional surfaces, present within Finn-Shurley

Field that can be observed across the basin, one at the base of the Turner Sandy Member, and another at the base of the Niobrara Formation (Anna, 2009). The underlying Mowry Shale is believed to be the source rock for this field, with possible secondary sourcing from the Niobrara Formation via long distance migration, as the Turner is typically associated with the Niobrara Total Petroleum System (Anna, 2009). Pressure data suggests a pressure gradient of normal to sub-normal within this eastern region of the PRB (Toner, 2019).

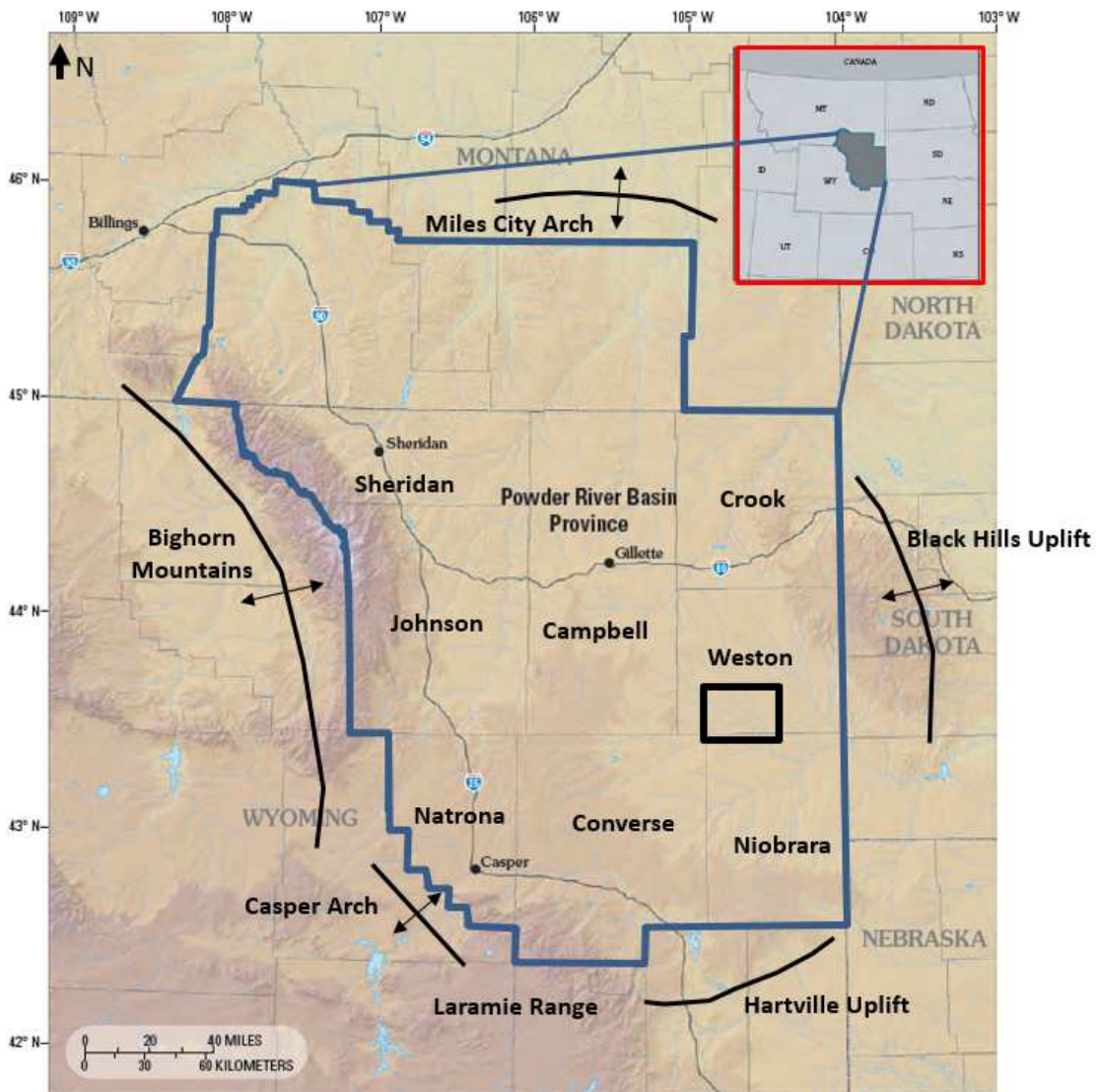


Figure 1.1: Map of the Powder River Basin Providence with the black box outlining the area of study in Weston County (Modified from Anna, 2009).

System	Series	Stage	West PRB	East PRB	
CRETACEOUS	Upper	Maastrichtian (part)	Fox Hills Formation	Fox Hills Formation	
		Campanian	Mesaverde Fm	Lewis Sh <span style="float:right">Teckla Ss Mbr</span> <span style="color:green">●</span>	Pierre Sh
				Teapot Ss Mbr <span style="color:green">●</span>	
				unnamed	
			Cody Sh	Parkman Ss Mbr <span style="color:green">●</span>	
				unnamed	
				Sussex Ss <span style="color:green">●</span>	
		Santonian	Cody Sh	Shannon Ss <span style="color:green">●</span>	Shannon Ss <span style="color:green">●</span>
				Steele Sh	Steele Sh
		Santonian	Cody Sh	Niobrara <span style="color:red">■</span> <span style="color:green">●</span>	Niobrara <span style="color:red">■</span> <span style="color:green">●</span>
		Coniacian			
		Turonian	Frontier Fm	Carlile Sh	Carlile Sh
	Wall Ck Mbr <span style="color:green">●</span>			Sage Breaks Mbr <span style="color:red">■</span>	
	Turner Sandy Mbr <span style="color:green">●</span>				
Cenomanian	Frontier Fm	Belle Fourche Mbr	Pool Ck Mbr		
		"Frontier" sandstones <span style="color:green">●</span>	Greenhorn Fm <span style="color:red">■</span>		
	Frontier Fm	Belle Fourche Sh <span style="color:red">■</span>			
Lower	Albian (part)	Mowry Shale <span style="color:red">■</span>	Mowry Shale <span style="color:red">■</span>		

Figure 1.2: Stratigraphic column of the Upper Cretaceous stratigraphy in the PRB on the west and east margins of the basin. The Turner is outlined in blue. The known or potential source rocks are marked by a red square and known productive reservoir intervals are marked by green dots. Modified from Anna (2009).

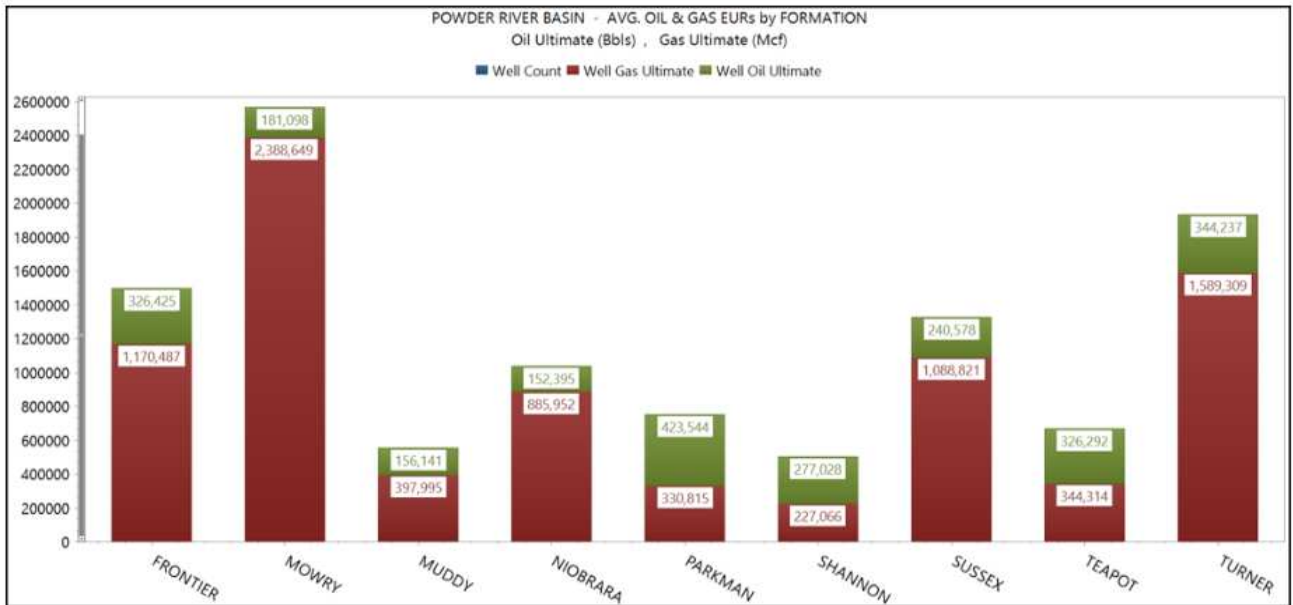


Figure 1.3: Average oil and gas per well EUR by Formation in the PRB (Kegel, 2019).

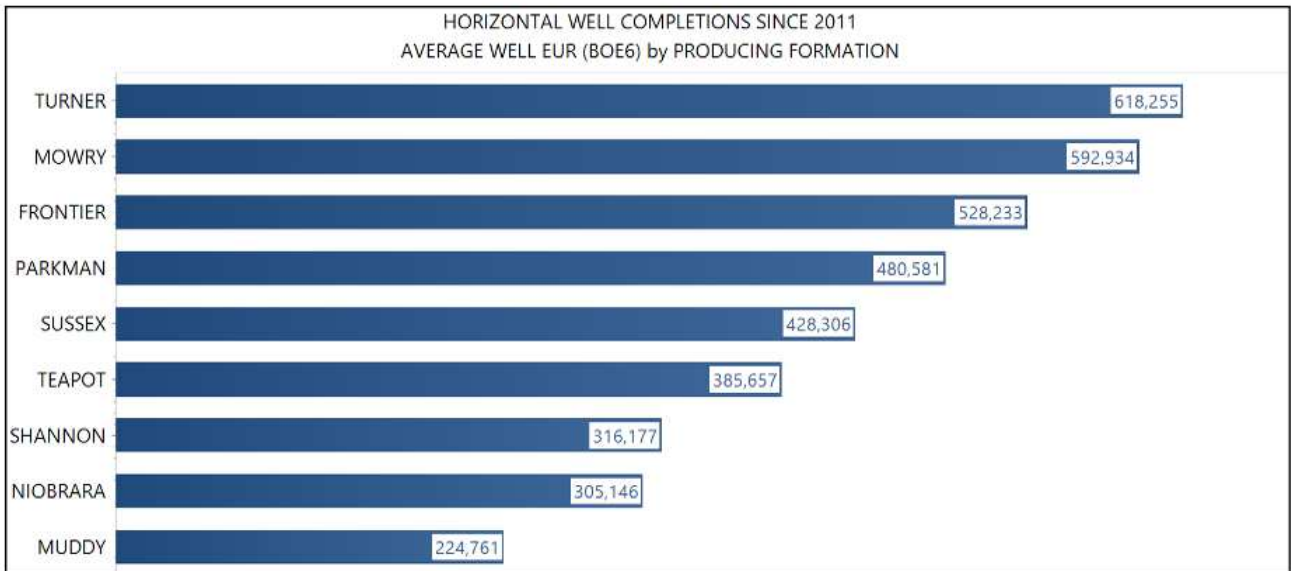


Figure 1.4: Horizontal well completions since 2011 with average well EUR by producing formation in the PRB (Kegel, 2019).



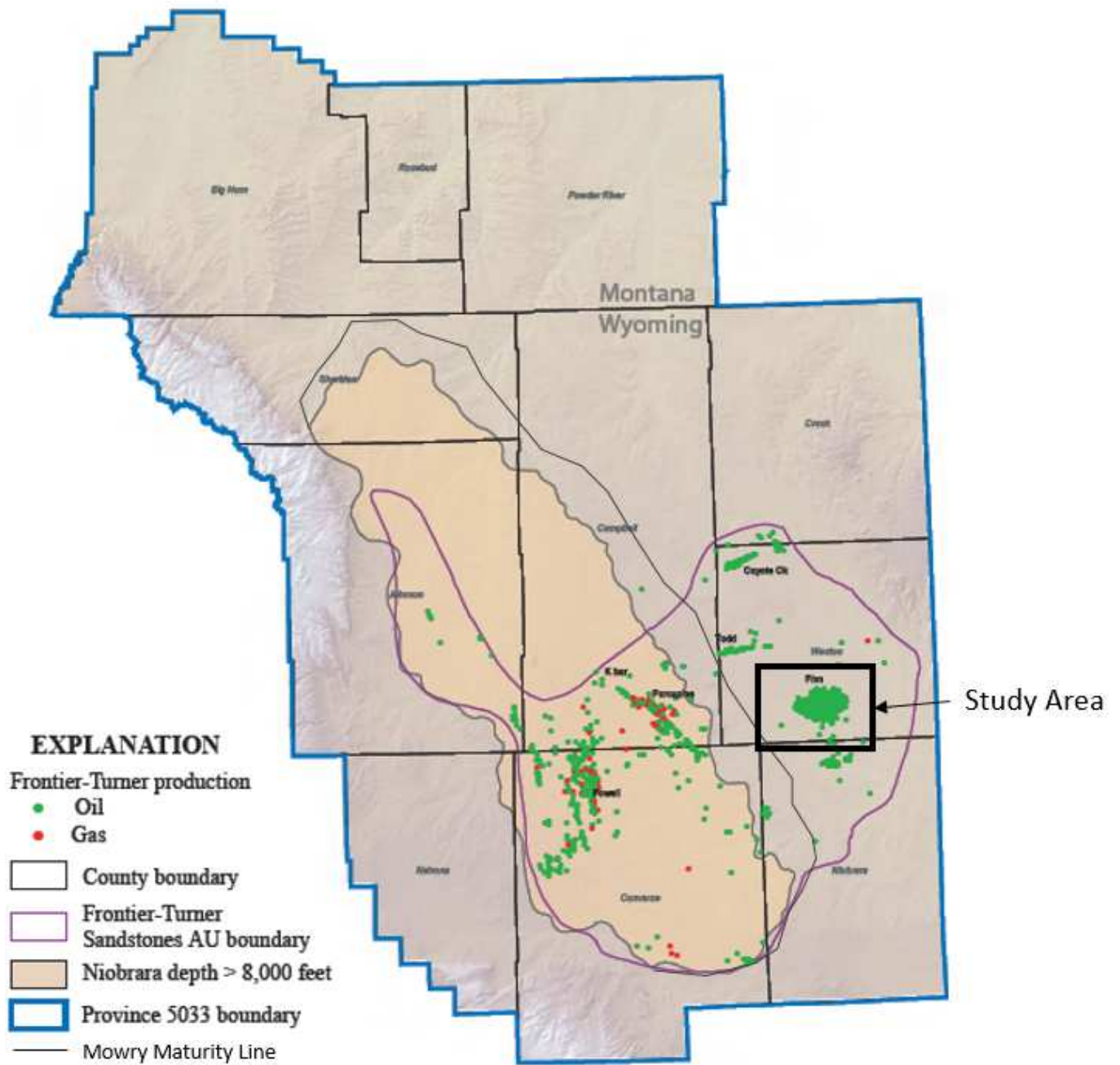


Figure 1.5: Map of the PRB showing Frontier/Turner hydrocarbon production in relation to the area where the Niobrara Formation is greater than 8,000 ft and believed to be mature. The grey line outlines approximately where the Mowry is believed to be mature, and the purple line outlines the boundaries of the Frontier/Turner assessment unit. The black box shows the location of the study area, Finn-Shurley field. Modified from Anna (2009).

## 1.2 Study Objectives and Purpose

The purpose of this study was the evaluation and characterization of the reservoir potential of the Turner Sandy member and to increase the understanding of controls on production within the Turner in the eastern PRB, specifically within Finn-Shurley Field of Weston County, Wyoming. The Turner has excellent reservoir quality within the central portion of the basin and has produced large economic quantities of hydrocarbons in Campbell and Converse counties. This research illustrates how productive this interval can be in the eastern region of the basin where hydrocarbons have migrated updip and outside of the maturity window of known source rocks where it is unconventionally stratigraphically trapped in low porosity and permeability rock with no apparent water leg. The Turner has historically produced from vertical wells in Finn-Shurley Field and has recently become a horizontal drilling target. Also investigated in this study are the recent incorporation of a successful hydraulic re-fracturing program for historical vertical wells and enhanced oil recovery methods in Finn-Shurley Field.

The main objectives of this project were achieved through an integrated study which includes: 1) reservoir characterization of the Turner interval using petrophysical well logs combined with core, thin section analysis, XRD, XRF, and FE-SEM; 2) facies and facies association descriptions to understand lateral and vertical variations throughout Finn-Shurley Field in the PRB using four cores; 3) source rock analysis, oil typing, and one dimensional basin modelling; 4) researching the productivity controls within this field by integrating all of the above data with known production information.

This is a multi-scale, integrated study from microscope scale to core and log scale in order to have a thorough understanding of the depositional and diagenetic controls on reservoir quality, which ultimately led to further identification of sweet spots within the region. This includes utilizing core descriptions, petrographic work, and routine core analysis data to characterize facies and facies associations. Well log data is necessary to understand petrophysical and geomechanical properties, as well as X-ray Fluorescence (XRF), X-ray

Diffraction (XRD), and Field Emission Scanning Electron Microscopy (FE-SEM) to interpret depositional environment and diagenetic history throughout the section. All the data was then integrated to understand the unconventional petroleum system and how the Turner in Finn-Shurley Field can be targeted and completed. The Turner lithology in Finn-Shurley is dominated by heterolithic mudstone, siltstones, and sandstones that are comprised of coarsening upward parasequences which contain oil stains of migrated hydrocarbon. This suggests multiple cycles in sea level fluctuation and varying sedimentation rates. The Turner is most productive in the central part of the basin where the lithology is more sandy, less heterolithic, and occurs within an overpressured cell of the PRB. By investigating these differences, there can be a better understanding of the variability of production in the Turner across the PRB.

### **1.3 Study Area**

The study area is located in Weston County, Wyoming, in the southern Powder River Basin (Figure 1.6). The townships and ranges included in this study area are T41-T43N and R64-R65W. Over 700 wells have been drilled in this area with active horizontal drilling occurring in or nearby this field. Up through December of 2019, the Turner at Finn-Shurley Field has cumulatively produced 23.5 million barrels of oil and 38 billion cubic feet of gas according to the Wyoming Oil and Gas Conservation Commission. This thesis will utilize four cores, all provided by the United States Geological Survey (USGS) Core Research Center (CRC) in Lakewood, Colorado (Table 1.1). The first core is the McTuillin Federal 1 located in Sec 31, T43N, R64W, Weston County, Wyoming and is denoted by the blue star on Figure 1.7. The second core is the Colen 10-10, which is located in Sec 10, T42N, R64W, Weston County, Wyoming and is denoted by the yellow star on Figure 1.7. The third core is the Perpetual Finn 8 located in Sec 5, T42N, R64W, Weston County, Wyoming and is denoted by the red star on Figure 1.7. The fourth and final core is the Dreiling Federal 7 located in Sec 15, T42N, R64W, Weston County, Wyoming and is denoted by the green star on Figure 1.7. All of these core locations in Finn-Shurley Field can be seen on Figure 1.7, with the

core information for each well located in Table 1.1.

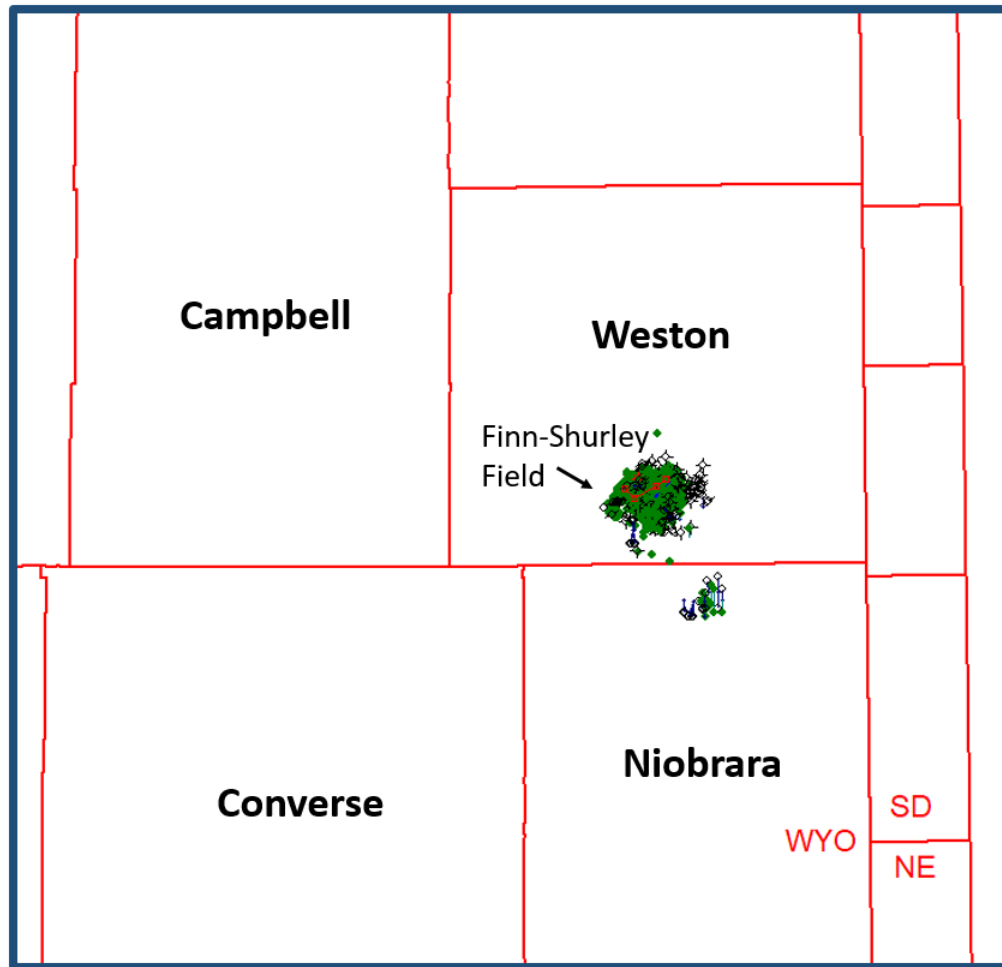


Figure 1.6: Map of the counties of Eastern Wyoming and the study location of Finn-Shurley Field within Weston County, Wyoming.

Table 1.1: Core location information.

Well	Colen 10-10	McTuillin Federal 1	Perpetual Finn 8	Dreiling Federal 7
Operator	M & K Oil Company	M & K Oil Company	Chemily Management	Chemily Management
API	49045220850000	490045217430000	49045221320000	49045219160000
Cored Formation	Lower Turner	Lower Turner	Turner	Lower Turner
Cored Interval	5234'-5320'	4824'-4889'	4900'-4960'	4839'-4899'
Core Length	86 ft	65 ft	60 ft	60 ft
Location	Sec 10, T42N, R65W	Sec 31, T43N, R64W	Sec 5, T42N, R64W	Sec 15, T42N, R64W

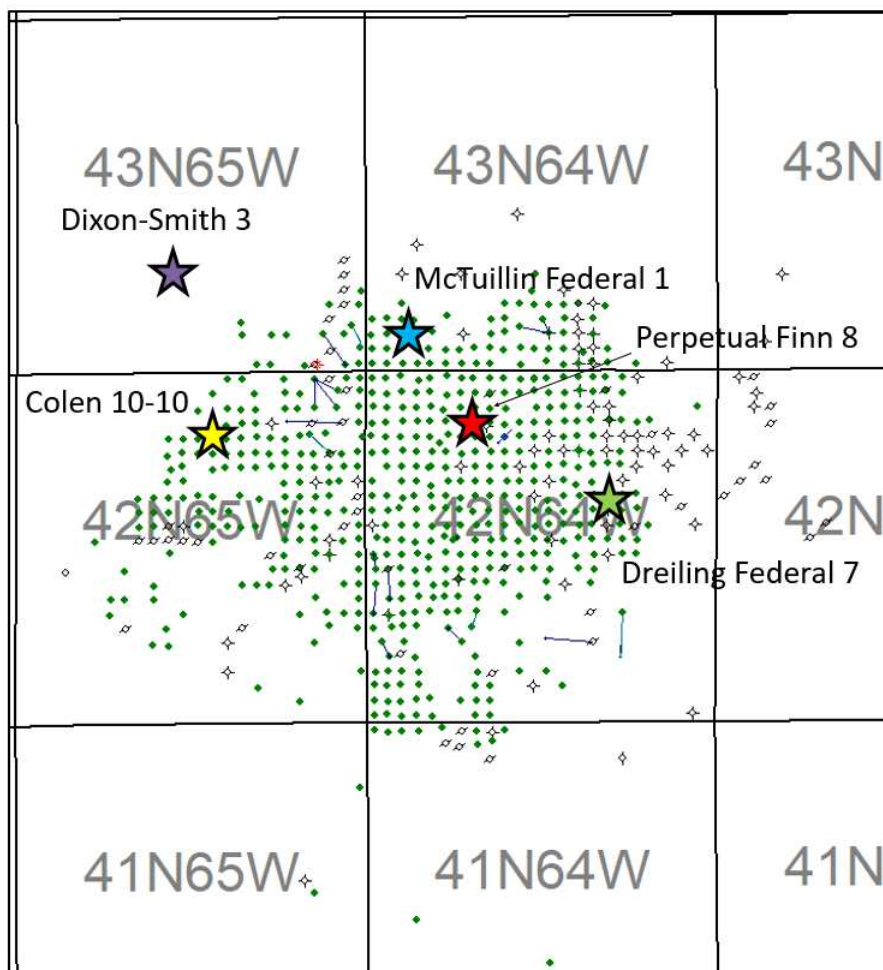


Figure 1.7: Map of core locations within Finn-Shurley. The yellow star is the Colen 10-10 core, the red star is the Perpetual Finn 8 core, the green star is the Dreiling Federal 7 core, and the blue star is the McTuillin Federal 1 core. The purple star is the Dixon-Smith 3 well which was used for a 1D basin model.

#### 1.4 Dataset and Research Methods

As mentioned previously, data from four Turner cores were integrated for this reservoir characterization study of the continuous oil accumulation in Finn-Shurley Field. This study utilized petrographic thin section analyses, X-Ray Fluorescence (XRF), X-ray Diffraction (XRD), source rock analysis (SRA) and petrophysical well logs. Field Emission Scanning Electron Microscopy (FE-SEM) was performed in greater detail on these cores as well. Table 1.2 displays the data that is available for each core. The integration of these data sets

provided optimal information to characterize the reservoir potential within the Turner in Finn-Shurley Field. From this dataset, well log correlations and reservoir maps using IHS Petra software were generated. This research also attempted to explain production variability trends across the field using available production information, stratigraphic variations, and one-dimensional basin modelling for future exploration and sweet spot identification.

For this study, all four cores were available with either respective datasets from the United States Geological Survey (USGS) Core Research Center (CRC). All cores were provided with thin sections, although more were made to analyze porosity trends in the interpreted reservoir intervals, as well as routine core analysis (RCA) and XRD data. In addition, twenty five samples were taken for Field Emission Scanning Electron Microscopy (FE-SEM) and 200 samples taken through a X-Ray Fluorescence (XRF) handheld gun.

Table 1.2: Dataset acquired for conducted research.

Well	Colen 10-10	McTuillin Federal 1	Perpetual Finn 8	Dreiling Federal 7
Operator	M & K Oil Company	M & K Oil Company	Chemily Management	Chemily Management
API	49045220850000	490045217430000	49045221320000	49045219160000
Cored Interval	5234'-5320'	4824'-4889'	4900'-4960'	4839'-4899'
Formation	Turner	Turner	Turner	Turner
Thin Sections & Photos	Yes(46)	Yes(5)	Yes(40)	Yes(6)
Core Analysis	Yes	Yes	Yes	Yes
FE-SEM	Yes	Yes	No	No
Rock-Eval Data	Yes	No	No	No
XRD	Yes	Yes	No	No
Log Suite	Yes	Yes	Yes	Yes

### *Core Description*

Four cores were observed for sedimentary structures, key stratigraphic surfaces, textures, and lithology to best characterize facies and facies associations within the Turner. From these observations, depositional environment interpretation were made, as a result of understanding depositional processes and ichnofauna. Due to the heterogeneous nature of the Turner in this region, an iterative multi-scale approach was taken to incorporate microscopic scale observations to best characterize and sub-divide the Turner into eight facies.

### *Thin Sections*

Between the four cores, 97 thin sections were available to use from the USGS CRC, with six extra thin sections made for supplemental use. These aided in making interpretations of mineralogy, provenance, diagenetic history, depositional processes, and to characterize the facies at a finer scale. The heterolithic nature of the Turner makes thin section texture analysis necessary to identify small scale variations within the core.

#### *X-Ray Fluorescence and X-Ray Diffraction*

To further understand the diagenetic effects, provenance, and mineral makeup on reservoir quality, XRD data was available for two cores, the Colen 10-10 and the McTuillin Federal 7, aiding in the geomechanical and petrophysical understanding of the reservoir rock. The XRF data was collected on 80 feet of the Colen 10-10 core. XRF was collected to help better understand the elemental and mineralogical changes within the facies and help better define the depositional history and rock composition within the study area.

#### *FE-SEM*

Photomicrographs from the FE-SEM, located at the Colorado School of Mines, were taken for the McTuillin Federal 1 core and the Colen 10-10 core. Twenty-five total samples were utilized from different facies throughout the two cores. They were gathered from the cores at the CRC and then taken to the thin section lab at CSM for sample preparation and gold coating to ensure image quality. This aided in analyzing textures, mineralogy, and porosity trends throughout the rock. The variability within the diagenetic affects on reservoir quality was also analyzed in a finer detail using the FE-SEM backscattered electrons, secondary electron imaging, and electron dispersive spectroscopy mineral mapping options. Cathodoluminescence was also utilized for this study on three thin sections to best visualize diagenetic effects and secondary quartz growth.

#### *Source Rock Analysis*

Source rock analysis was provided for the Colen 10-10 core to help determine if there are any total organic carbon content (TOC) relationships with the target intervals. Three Rock-Eval pyrolysis peaks were observed (S1, S2, and S3), which can help to determine

maturity, timing, and potential of hydrocarbon generation in the immediate area. Further investigation of oil type and migration of potential source rocks was done in this study with the aid of one-dimensional basin modelling.

#### *Basin Modelling*

A basin model was created using the Dixon Smith 3 well, a nearby well outside of Finn-Shurley Field (Figure 1.7), but within close enough proximity that there is confidence for its use as a proxy for the maturation profile of Finn-Shurley Field. BasinMod, from Platte River Associates, was used to create a one-dimensional basin model. This model attempts to display the thermal maturities for the stratigraphy displayed within the well by matching modelled curves to known source rock and temperature data measured within the well. This model shows what stratigraphic units are likely to be within the maturity windows, based on their burial history in the study area.

#### *Petrophysics*

A suite of well logs, which include both raster and digital logs, were available for the Finn-Shurley area. These were used to establish petrophysical trends and help with sweet spot identification, regional mapping of the reservoir, and correlation of intervals, to develop a stratigraphic framework. Ideally, the lateral variability of reservoir intervals can be mapped using these log suites across a larger region. The primary log suite available was gamma ray, spontaneous potential, and resistivity.

#### *Subsurface Correlations and Mapping*

After analyzing the petrophysical responses of the strata within Finn-Shurley, subsurface correlations were made across the study area to illustrate the lateral and vertical extent of the Turner and its internal flooding surfaces. Maps were generated in Petra using well log correlations in approximately 750 wells across Finn-Shurley in Weston county. Isopach and structure maps were vital in understanding the depositional environment and thickness changes. Pay maps were created to visually represent zones of thick hydrocarbon accumulation in the Turner interval.



## CHAPTER 2

### BACKGROUND GEOLOGY

#### 2.1 Regional Geology

During the Late Jurassic and Early Cretaceous, the Western Interior Cretaceous Basin was developed as a complex retro-arc foreland basin in the western region of the United States, due to the subduction of the oceanic Farallon Plate under the continental North American Plate following the breakup of Pangea. The onset of the Sevier Orogeny event was created from this subduction, allowing for this geologic province to experience rapid subsidence. Beginning in the Cretaceous, episodes of shallow flooding filled the Western Interior Cretaceous Basin resulting in an epicontinental seaway during the Barrenian-Aptian time period (Kauffman, 1985). The Sevier Orogeny was a mountain building event in modern Utah and Idaho that created pathways for terrigenous sediments to infill the rapidly subsiding Western Interior Cretaceous Basin. The regional stratigraphy of the Western Interior Cretaceous Basin has an extensive tectonic history, which has resulted in its diverse make up of sandstones, siltstones, shales, and carbonates. Dynamic and complex plate tectonics and sedimentation during this time period provided the Western Interior Basin with prolific hydrocarbon reservoirs and world class source rocks within the Rocky Mountain foreland structural basins.

The Powder River Basin, located in northeastern Wyoming and southeastern Montana, is an asymmetrical synclinal basin that developed during the Laramide Orogeny (Late Cretaceous to Eocene), and is similar to other Rocky Mountain foreland structural basins. The basin is defined by multiple structural features (Figure 2.1) including the Black Hills in the east, the Hartville uplift and Laramie Range to the south, the Casper arch, Bighorn mountains, and Hardin platform on the west and the Miles City arch, Bull mountains, and Porcupine dome to the north (Dolton and Fox, 1995). The PRB is asymmetrical with a deep

basin axis to the west (Figure 2.2). The eastern flank of the basin has a gradual dip of 100 ft/mi to the west and increases to 500 ft/mi along the west, near the basin axis, which is demonstrated in Figure 2.2 (Anna, 2009).

Throughout the basin history, multiple conjugate northeast and northwest trending structures in the basement rocks have surfaced as faults or other shear zones associated with the Laramide Orogeny (Figure 2.3) and could have impacted local and regional sedimentation patterns (Anna, 1986). It was also observed by Weimer and Flexer (1985) that the Turner Sandy Member thicknesses, as well as other Cretaceous interval thicknesses, seem to be strongly influenced by these northeast-southwest and northwest-southeast trending fault block lineaments. Figure 2.3 demonstrates the relationship of these basement lineaments with producing Cretaceous aged oil fields within the PRB.

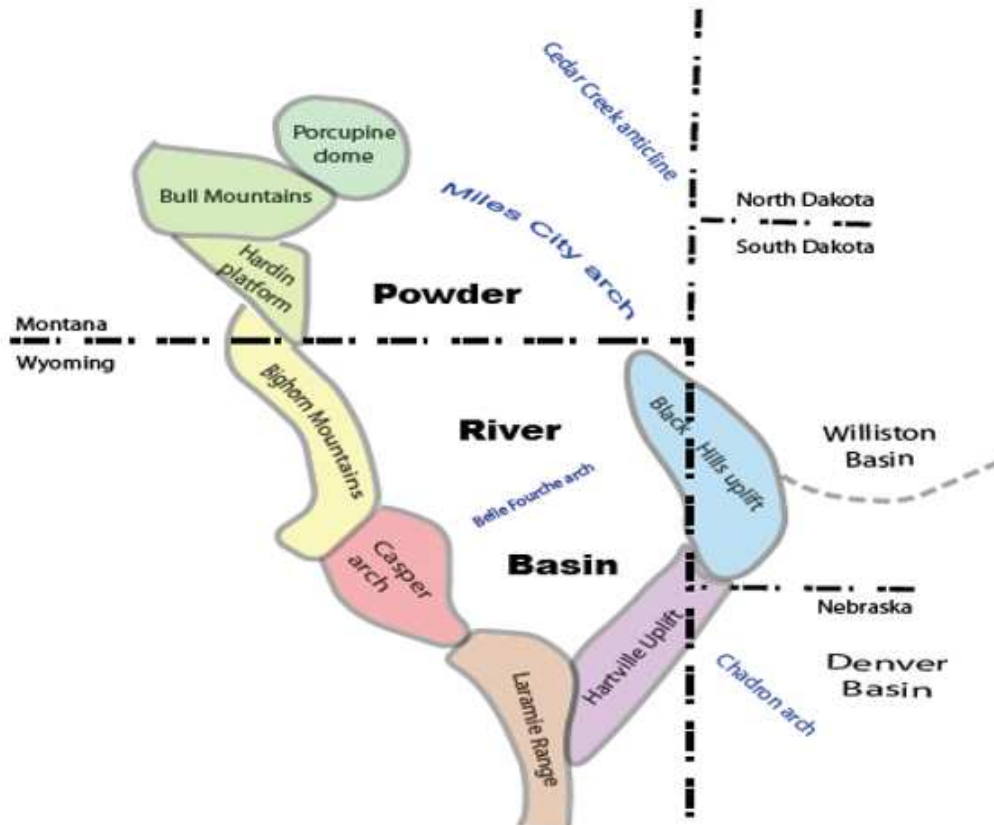


Figure 2.1: Structural definition of the PRB from Dolton and Fox (1995).

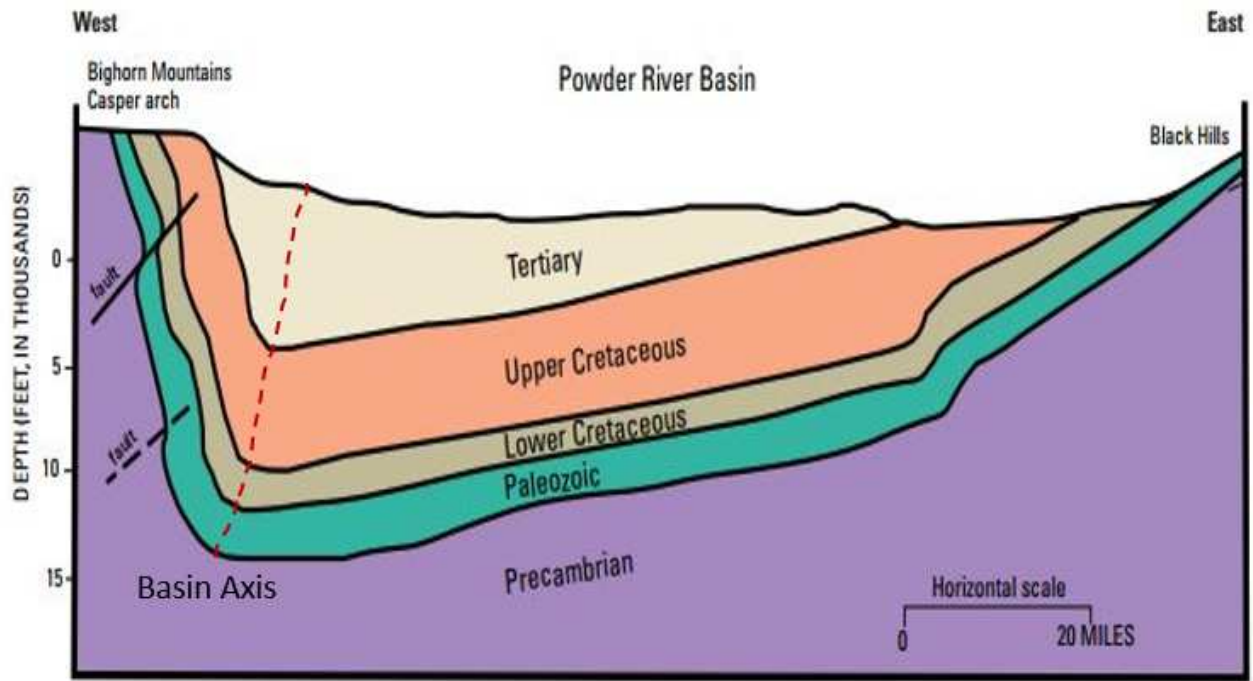


Figure 2.2: Generalized East to West cross section of the PRB (Modified from Anna, 2009).

The Western Interior Seaway extended from the Arctic Sea to the Gulf of Mexico and had a relatively shallow water depth. Figure 2.4 shows a paleogeographic map of the Western Interior Seaway during the late Turonian time period and the time of deposition of the Turner (Blakey, 2013). The Sevier Highlands, a north-south trending mountain range, can be seen throughout modern Idaho and Nevada from which sediments were being transported during this transgressive lowstand. Crustal loading and subsequent subsidence allowed for sediments to travel from the Sevier Orogenic belt down to the paleo-shelf where they could prograde into the Powder River Basin and be deposited.

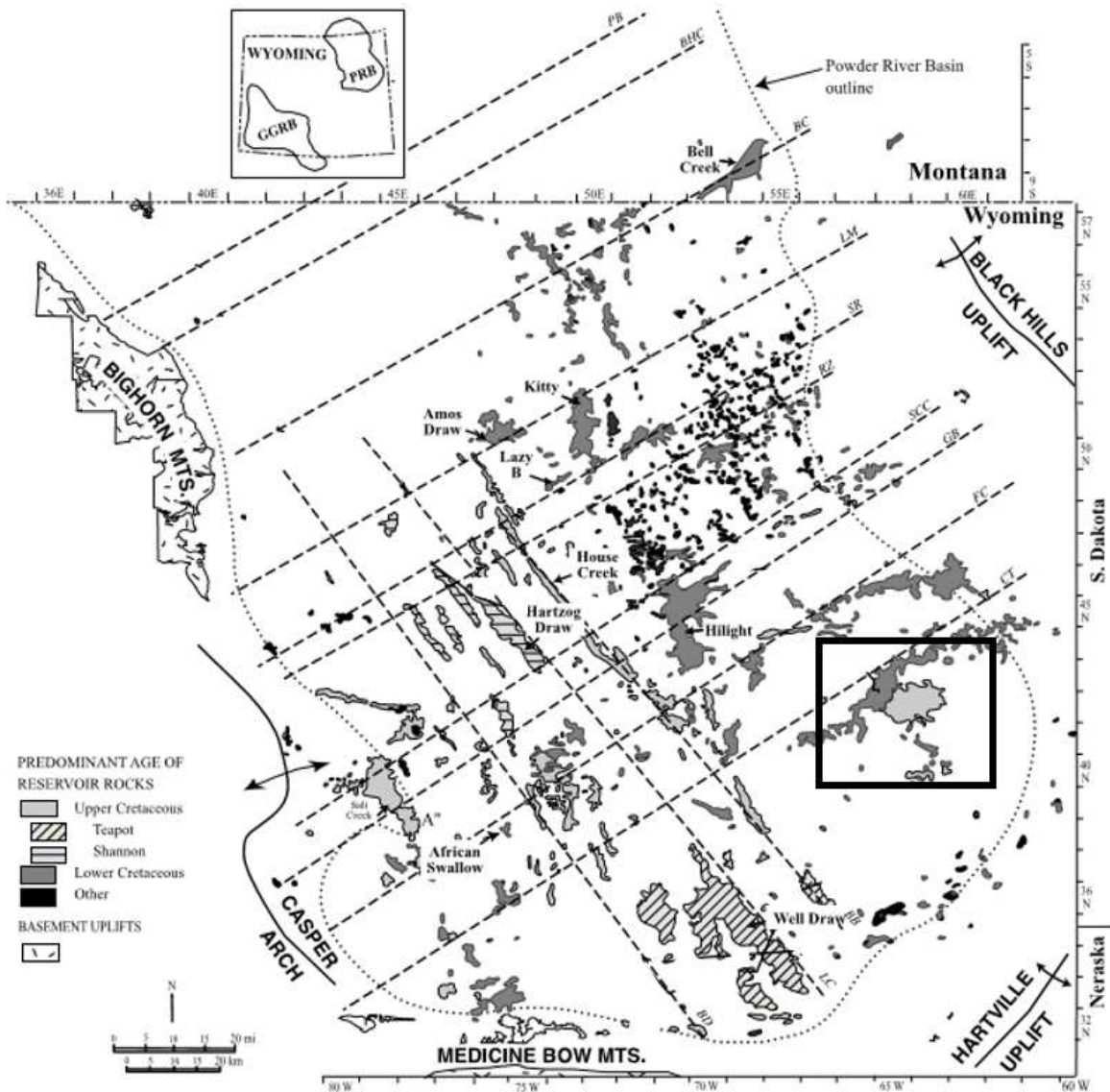


Figure 2.3: Distribution of oil and gas fields and structural lineaments in the PRB. Lineaments BC=Bell Creek, SR=Springen Ranch, RZ=Rozet, SCC=South Coyote Creek, GB=Gose Butte, FC=Fiddler Creek, CT=Clareton Trend, PB=Parkman-Baker, BHC=Bighorn-Custer, BD=Buffalo-Douglas, BB=Black Butte, LC=Lightning Creek. Study area is outlined in the black box. (Modified from Martinsen, 2003).

The Upper Turonian aged Turner Sandy Member of the Carlile Shale is composed of interstratified mudstones, siltstones, and sandstones, which were deposited near the end of the middle Turonian after a worldwide drop in sea level (Hancock and Kauffman, 1979). Merewether et al. (2007) further refined the stratigraphy and determined the biostratigraphic

zones from *Scaphites warreni* to *Prionocyclus germari* to constrain the Turner and equivalent Wall Creek Member of the Frontier Formation (Figure 2.5). The *Scaphites warreni* is the first depositional cycle within the lower Turner and can be identified within the subsurface as a major flooding surface. The *Prionocyclus germari* caps the upper Turner cycle and can also be identified and correlated within the subsurface as the top of the Turner member. There is a third depositional cycle that occurs within the Turner, the *Scaphites whitfieldi*, which can also be traced within the subsurface. This specific cycle is used to divide the Turner into a lower and an upper unit. With the refined stratigraphy, the Turner can be separated into three zones that represent larger depositional cycles capped by flooding surfaces and represent changes in the Western Interior ammonite zone.



Figure 2.4: Paleogeography map of the Western Interior Seaway during the late Turonian in the PRB (outlined in red). (Modified from Blakey, 2013).

SERIES	Stages		Western Interior ammonite range zones and radiometric ages (Ma)	Zone nos.	Western Interior inoceramid range zones	Intercalated radiometric ages (Ma)	2 <sup>nd</sup> order sea-level fluctuations
	San tobian (part)	Informal subranges					
UPPER CRETACEOUS (part)	Coniacian	Lower	<i>Clioscaphites saxitonianus</i>		<i>Cladoceramus undulatopticatus</i>		Niobrara
		Upper	<i>Scaphites depressus</i> 87.14 ± 0.39	1	<i>Magadiceramus crenelatus</i> <i>Magadiceramus subquadratus</i>		
			Middle	<i>Scaphites ventricosus</i>	2 3	<i>Volviceramus involutus</i> <i>Volviceramus koeneni</i>	
		Lower	<i>Scaphites preventricosus</i> 88.55 ± 0.59	4	<i>Cremlnoceramus crassus crassus</i>	88.70	
				5	<i>Cremlnoceramus crassus inconstans</i>	88.85	
		6	<i>Cremlnoceramus deformis dobrogensis</i>	89.00			
	Turonian	Upper	<i>Scaphites mariasensis</i>	7	<i>Cremlnoceramus waltersdorfensis</i>	89.15	
			<i>Prionocyclus germari</i>	8	<i>Mytiloides scupini</i>	89.30	
			<i>Scaphites nigricollensis</i>	9	<i>Mytiloides incertus</i>	89.45	
			<i>Scaphites whitfieldi</i>	10 11	<i>Inoceramus dakotensis</i> <i>Inoceramus perplexus</i>	89.60 89.75	
		Middle	<i>Scaphites ferronensis</i>	12		89.90	
			<i>Scaphites warreni</i>	13	<i>Inoceramus dimidius</i>	90.05	
			<i>Prionocyclus macombi</i> 90.21 ± 0.54	14	<i>Inoceramus aff. dimidius</i>		
			<i>Prionocyclus hyatti</i> 92.46 ± 0.58	15	<i>Inoceramus howelli</i>		
			<i>Collignonicerias praecox</i>	16	<i>Inoceramus n. sp.</i>	92.72	
			<i>Collignonicerias woolgari</i>	17	<i>Mytiloides hercynicus</i> <i>Mytiloides subhercynicus</i>	92.97	
			<i>Mammites nodosoides</i>	18	<i>Mytiloides mytiloides</i>	93.23	
	Lower	<i>Vascoceras birchbyi</i> 93.48 ± 0.58	19	<i>Mytiloides kossmati</i>			
		<i>Pseudaspidoceras flexuosum</i> 93.19 ± 0.42	20				
		<i>Watinoceras devonense</i>	21	<i>Mytiloides puebloensis</i>	93.32		
	Cenomanian (part)	Upper	<i>Nigericeras scotti</i>	22	<i>Mytiloides hattini</i>	93.44	
			<i>Neocardioceras juddii</i> 93.32 ± 0.38 93.82 ± 0.30	23	<i>Inoceramus pictus</i>	93.57	
			<i>Burroceras clydense</i>	24		93.62	
			<i>Euomphaloceras septemseriatum</i> 93.68 ± 0.50	25			
			<i>Vascoceras diartianum</i> 93.99 ± 0.72	26			
			<i>Dunveganoceras conditum</i>	27		94.17	
			<i>Dunveganoceras albertense</i>	28	<i>Inoceramus ginterensis</i>	94.35	
			<i>Dunveganoceras problematicum</i>	29		94.53	
			<i>Dunveganoceras pondi</i> 94.71 ± 0.49	30	<i>Inoceramus prefragilis</i>		
			<i>Plesiocanthoceras wyomingense</i>	31		94.83	

Figure 2.5: Biostratigraphic chart for the Western Interior. Red box highlights the zones corresponding to the Turner age (Modified from Merewether et al., 2007).

## 2.2 Regional Structural Setting

The Sevier Orogeny took place during the late Jurassic to Eocene, approximately 120 to 50 million years ago, which created a north to south trending fold and thrust belt along the western margin of North America. Syn-orogenic deposition and crustal loading resulted in increased subsidence within the Western Interior Cretaceous Basin east of the Sevier highlands. The Western Interior Cretaceous Basin was one of the largest foreland basins in the world, extending all the way from the Arctic to the modern Gulf of Mexico (Weimer and Flexer, 1985). Turonian-aged reservoirs are comprised of sediments that were derived from this western fold and thrust belt called the Sevier Highlands. Global tectonics and eustasy during this time dramatically controlled changes in sea level and sedimentation patterns in the Western Interior Seaway. Thickness of the Turner seems to be strongly influenced by these northeast to southwest trending fault block movements (Weimer and Flexer, 1985). However, on a broad scale, the Turonian aged sediments show a thinning to the southeast, which may be related to the Belle Fourche Arch (Slack, 1981). Transgressive and regressive episodes caused progradation and retrogradation of near shore sediments, resulting in deposition of the reservoirs, seals, and source rocks that occur within the PRB. A sea level curve showing these transgressive and regressive events is shown in Figure 2.7. The Powder River Basin developed as a Laramide structural feature and an asymmetrical foreland basin within the Western Interior between 75 and 35 million years ago (Anna, 2009). Rapid subsidence resulted in high rates of sedimentation along the shoreline, shelf, and slope environments. Deeper parts of the basin experienced much slower sedimentation rates allowing for large amounts of organic matter to accumulate.

As mentioned previously, during the Laramide Orogeny, northeast-southwest trending basement features were reactivated and controlled local deposition and erosion. These lineaments were identified from gravity surveys, satellite images, and stratigraphic thickness anomalies. Figure 2.3 shows the alignment of hydrocarbon fields with these structural lineaments that occur throughout the basin. This image shows a correlation between the Upper

Cretaceous oil fields and the locations of these features. The majority of the production from Cretaceous aged sandstones is from structural closures along the western margin of the PRB or from normally pressured stratigraphic traps on the eastern flank of the PRB. The central, highly overpressured, part of the basin has been historically lightly explored (Parks and Gale, 1996) but is now the focus of more intense horizontal drilling (Figure 2.9).

### **2.3 Regional Stratigraphy**

Cretaceous strata within the PRB have an extensive and complex tectonic history that resulted in highly variable thicknesses, lithologies, and depositional patterns. The stratigraphic sequence from the base of the Mowry Formation to the top of the Niobrara Formation is composed of marine shales, siltstones, sandstones, chalks, and limestones (Weimer and Flexer, 1995). Variations in tectonic activity, sea level fluctuations, and sediment supply create a complex stratigraphic record that was either preserved or eroded away. Within the PRB, the Mowry Shale was deposited following the deposition of the Muddy Sandstone and was succeeded by the deposition of the Belle Fourche Formation and then the Greenhorn Limestone. Following this, the Carlile Formation (which includes the Pool Creek member, Turner Sandy member, and the Sage Break member), was deposited on top of the Belle Fourche Formation. Above the Carlile Shale, the Niobrara was deposited in open-marine conditions.

A typical log pattern for the Upper Cretaceous sediments, as well as major erosional surfaces can be seen in Figure 2.6. Most of the disconformities in the Upper Cretaceous strata are distinguished by hiatuses in the fossil record (Merewether and Cobban, 1985). Although there are many, the ones concerning this study will be the Turonian and Coniacian disconformities from Merewether et al. (2007). Within the eastern PRB, the Coniacian disconformity occurs at the base of the Niobrara Formation, while the Turonian disconformity occurs at the base of the Turner Sandy member, or the chronostratigraphic equivalent, the Wall Creek member of the Frontier Formation.



*a. Mowry Formation*

The Mowry Shale is a prominent Lower Cretaceous hydrocarbon source rock within the PRB. It was deposited as a siliceous organic-rich mudrock during maximum marine transgression from the end of the Lower Cretaceous Albian to Cenomanian (Merewether, 1996). It ranges in thickness from 100 ft to 400 ft in the central part of the basin (Momper and Williams, 1984). The organic matter is dominantly Type II kerogen with minor amounts of Type III present, suggesting a strong marine influence. The average total organic carbon content (TOC) weight percent across the basin for the Mowry Shale is approximately 3 weight percent (Modica and Lapierre, 2012). In addition, there are multiple bentonite beds within this stratigraphic unit that can be correlated throughout the PRB in petrophysical well logs (Slaughter and Early, 1965).

*b. Belle Fourche Formation*

Conformably overlying the Mowry Shale, is the Belle Fourche Formation. This is composed of very fine- to fine-grained sandstones interbedded with bentonite beds. This formation can occur greater than 50 ft thick in some regions and can be easily identified on well logs by the widespread Clay Spur Bentonite present at the basal contact with the Mowry Shale. The top of the Belle Fourche Formation is marked by another thick bentonite bed. This upper bentonite bed is equivalent to the X-Bentonite of the Denver Basin. Reservoir quality in this unit occurs in sandstones known as the Frontier sandstones which have variable porosity, ranging from 5 to 15 percent, and permeabilities, which range from less than 1 to 100 mD. The Belle Fourche is early to middle Cenomanian in age and is typically confined to the southwestern part of the basin.

*c. Greenhorn Limestone*

Conformably overlying the Belle Fourche Formation is the Greenhorn Limestone. The Greenhorn consists of interbedded calcareous and organic-rich shale, limestones, and bentonite beds deposited in an open-marine environment. The Greenhorn Limestone is middle Cenomanian to early Turonian in age and generally thickens to the west, closer to the sed-

iment source. This thickness pattern is also seen within the Greenhorn Formation within the Denver Basin, as mapped by Sonnenberg and Weimer (1981). The Greenhorn is clearly distinguished on well logs in the subsurface, as well as in outcrop that are located in Weston County, Wyoming.

*d. Carlile Shale: Pool Creek Member*

Conformably overlying the Greenhorn Limestone is the Pool Creek member of the Carlile Shale, the lowest member of the Carlile Shale Formation. The Pool Creek Member is a middle Turonian, dark gray, silty, marine shale (Weimer and Flexer, 1985). This unit wedges out westward and can reach up to 140 ft thick in the east and southeast. At the top of the Pool Creek, an erosional surface is present and is characterized by a chert and quartz pebble lag containing shark's teeth (Rubey, 1930; Cobban, 1952; Weimer and Flexer, 1985; Merewether, 1996). This erosional surface removes the shale moving westward until it eventually cuts into the Greenhorn Limestone. Weimer and Flexer (1985) interpret the Pool Creek as being deposited during the early stages of the Greenhorn Sea Regression, prior to the prolonged lowstand of Turner deposition (Figure 2.7).

*e. Carlile Shale: Turner Sandy Member*

Unconformably deposited on top of the Pool Creek member is the stratigraphic interval of interest for this study, the Turner. It has been delineated into upper and lower sandstone intervals (Rice and Gaskill, 1988) with multiple flooding surfaces containing multiple cycles of coarsening upward parasequences. The Turner is considered to be a chronostratigraphic equivalent to the Wall Creek Member of the Frontier Formation in central and western Wyoming. It is also equivalent to the Codell Sandstone within the Denver Basin, and the Ferron Sandstone in Utah. The lithology of the Turner is characterized by interstratified mudstone, siltstone, and sandstones that were deposited near the end of the middle to late Turonian during a worldwide drop in sea level (Figure 2.7). Thickness averages between 80 to 300 ft and this unit thins to the west. Most of the hydrocarbon production occurs in areas of thicker strata.

*f. Carlile Shale: Sage Breaks Member*

The upper member of the Carlile Shale is the Sage Breaks member, which was deposited on top of the Turner Sandstone. It is upper Turonian to Coniacian in age from fauna data. It is composed of laminated marine shale and is conformable with the underlying Turner Sandy Member. In outcrop, many calcareous concretions layers are present. The Sage Break ranges from 100 to 300 ft thick with a large erosional surface at the top directly below the contact with the Niobrara Formation. Major areas of thinning within this unit are associated with this widespread erosional surfaces.

*g. Niobrara Formation*

The final stratigraphic unit that is pertinent to this study, is the Niobrara Formation. The formation was deposited in early Campanian time as pelagic carbonates and limestones in the Western Interior Seaway during a prolonged highstand where water depths ranged from 200 to 500 ft deep. Regionally, the Niobrara is composed of allochems such as chalk pellets, inoceramids, oyster shell fragments, and forams. The primary matrix is composed of mud, clay, and silt (Anna, 2009). The Niobrara Formation contains Type II kerogen and averages more than three weight percent TOC, suggesting marine input. The permeability within the Niobrara is generally lower than 0.01 mD and porosity averages 10 percent. The carbonates of the Niobrara are considered the primary hydrocarbon source for Upper Cretaceous reservoirs within the PRB. Hydrocarbons were generated and began migration upon reaching burial depths in excess of 7,000 ft (Anna, 2009). At this depth, models suggest significant generation should have started with 8,000 ft of overburden (Figure 3).

*h. Other Cretaceous Units*

Although not relevant for this study, some of the other Upper Cretaceous units that occur in the eastern PRB include the Shannon Sandstone, which is a local reservoir, the Pierre Shale, and Steele Shale units (Figure 1.2). These units are all Campanian in age and are primarily targeted on the western and central regions of the Powder River Basin.

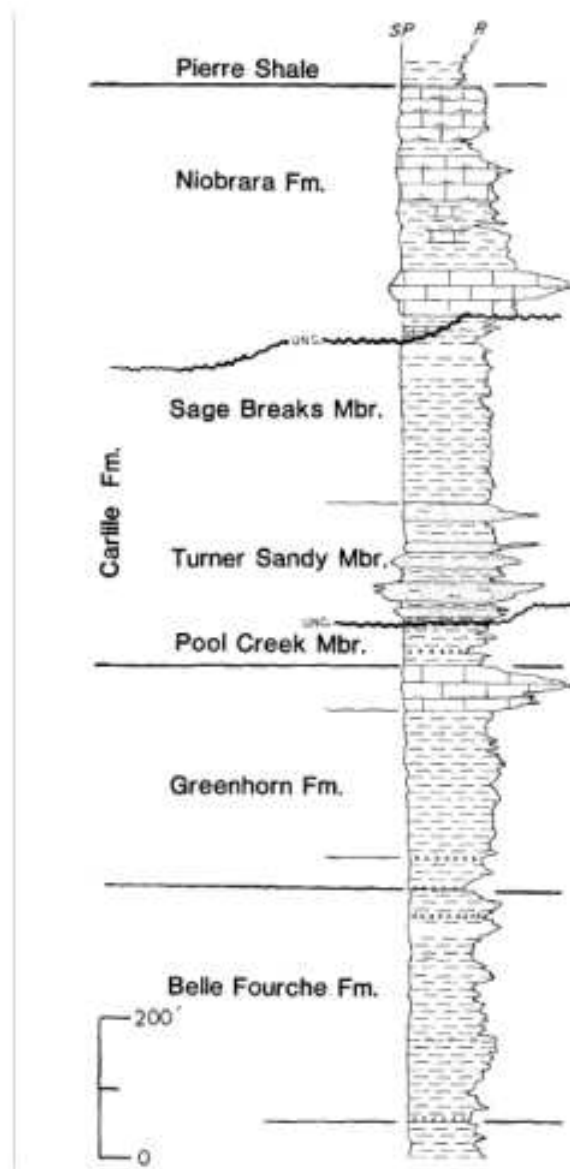


Figure 2.6: Typical log pattern from Pierre Shale to the Belle Fourche Formation (Weimer and Flexer, 1985).

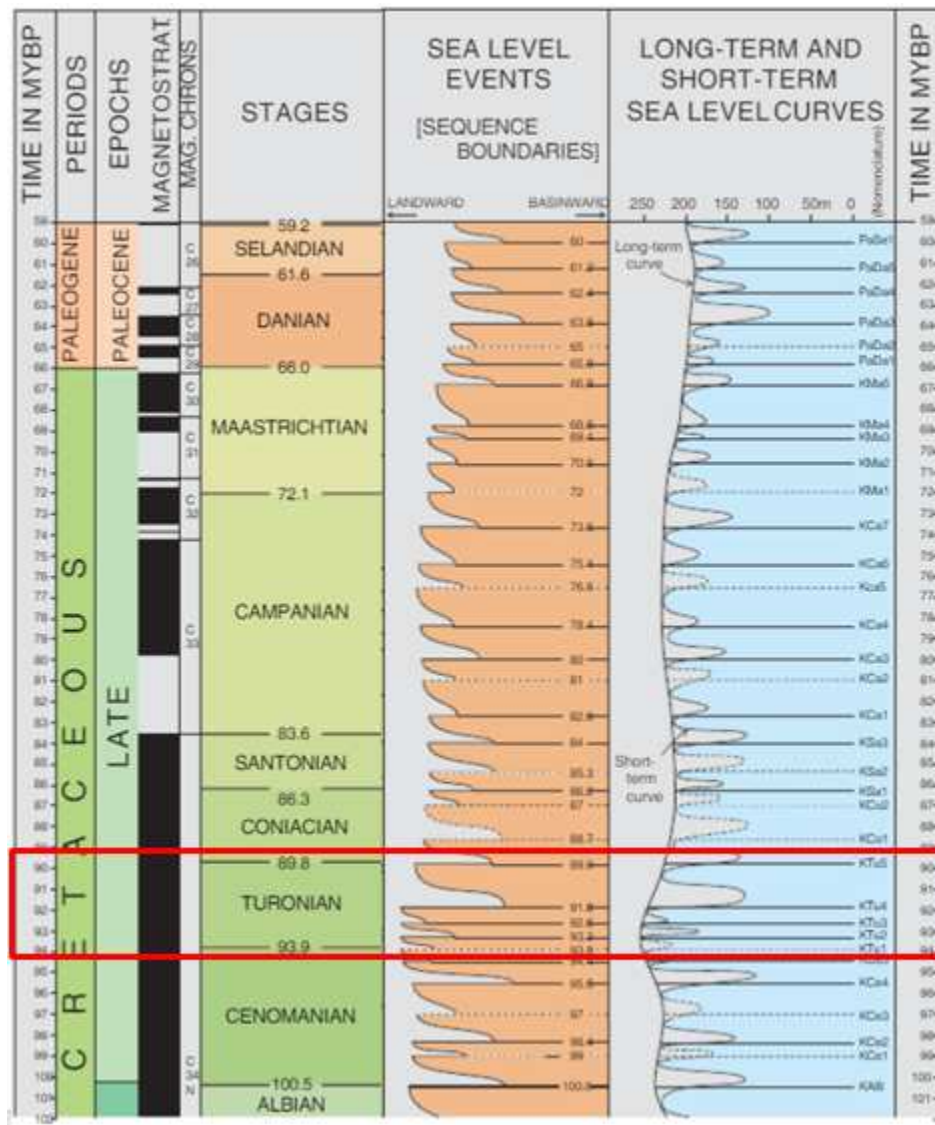


Figure 2.7: Illustration of the Cretaceous transgressive-regressive cycles defined by Haq (2014). Red box indicates the Turner depositional interval.

## 2.4 Petroleum Geology

The Turner is part of a well developed petroleum system that has produced significant amounts of hydrocarbons within the Rocky Mountain basins in the United States. It has been defined by the United States Geological Survey (USGS) as a conventional assessment unit (Frontier-Turner) within the Niobrara Total Petroleum system with huge undiscovered resources (Anna, 2009). Both the overlying Niobrara Formation and the underlying Mowry

Shale serve as world class source rocks for this reservoir interval. However, within Finn-Shurley Field, the Niobrara is not buried deep enough to be thermally mature (Anna, 2009); Therefore, hydrocarbons would have had to migrate from the region where the Niobrara Formation is mature and buried greater than 8,000 feet. Momper and Williams (1984) show that the Mowry Formation, although mature, is in the early oil window within the eastern PRB. Migration could have taken place through faults and fracture systems from where the Mowry has reached peak maturity in the central part of the basin. Momper and Williams (1984) also suggested that migration from the Sage Breaks Member, the Belle Fourche Shale, and the Greenhorn Limestone, are also possible to have sourced the Turner. The Turner reservoir produces light crude oil with API gravities that average 43 API, as well as associated gas. Thus suggesting a highly mature source for the Turner.

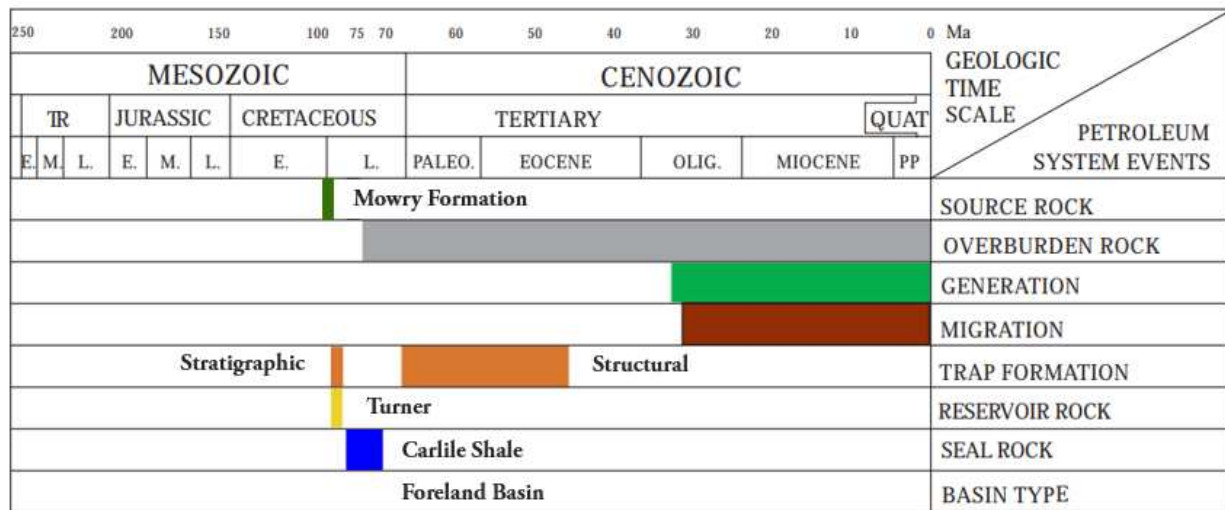


Figure 2.8: Petroleum system elements chart for the Turner Sandy Member of the Carlile Shale. (Modified from Anna, 2009).

The Turner is a low permeability reservoir with porosity values ranging between 8 to 12 percent in the highest quality reservoir intervals. These values are not uniform across the entire PRB due to facies, diagenesis, and paleo-environment changes (Heger, 2016). Both structural and stratigraphic trapping mechanisms are present within the PRB. However, stratigraphic trapping mechanisms dominate the Turner reservoirs, due to the low perme-

ability values and its heterogeneous lithologies. The Turner is considered a unconventional stratigraphic trap, due to its geologic criteria of a low permeability, tight reservoir, and engineering criteria of its ability to be drilled horizontally and completed with a large volume multi-stage completion.

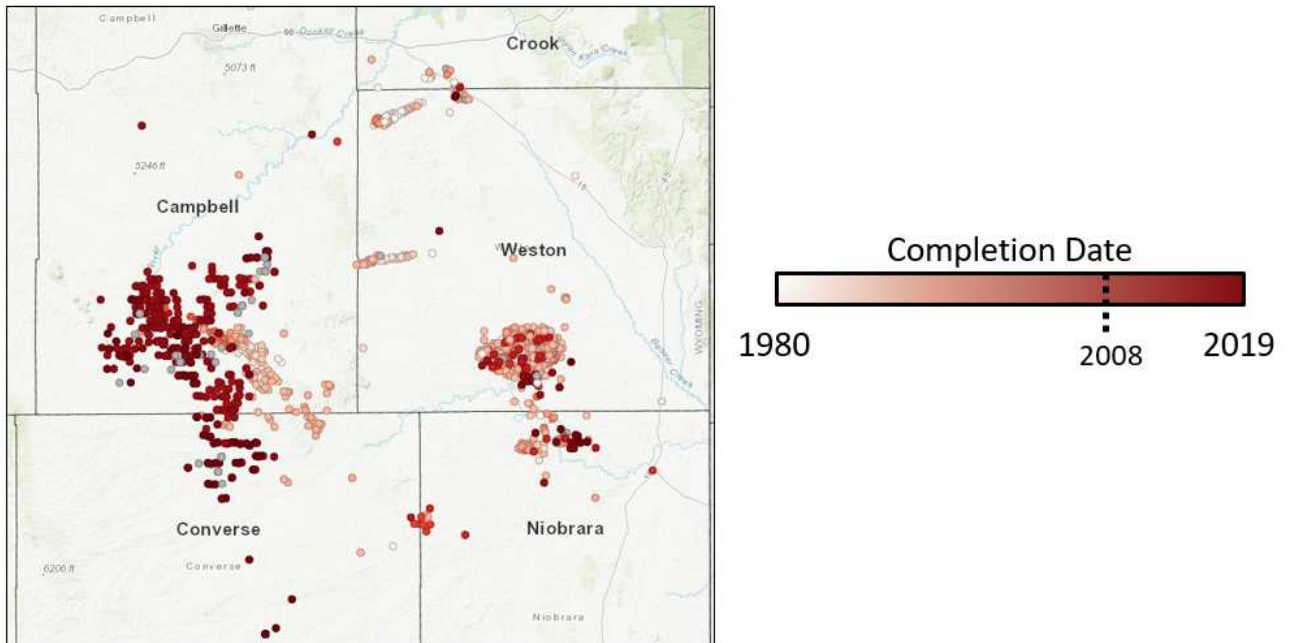


Figure 2.9: Well penetration map showing completion date for Turner wells within the southern PRB (from Enverus, 2019).

Operators producing from the prolific Wall Creek and Turner members use an average of 21 fracture stages to complete their horizontal wells. Well attributes, such as lateral length and orientation, do not appear to influence the production of the wells within the Turner (Toner, 2019). Figure 2.9 shows a well penetration map with completion dates throughout the southern PRB since 1980. Although most of the Turner completion activity is located in Campbell and Converse counties, Weston County has also become a horizontal target as denoted by the darker red circles (Figure 2.9). Operators are able to produce large amounts of oil and gas volumes from both normally pressured and abnormally pressured reservoir conditions. This is important as the Turner pressures vary throughout the basin. The dis-

continuity of overpressuring throughout the Turner implies that compartmentalization may exist within this unit (Figure 2.10). When compared to the equivalent Wall Creek Member of the Frontier Formation, the Turner is shallower and at a lower reservoir temperature than its counterpart. However, each formation is a target for horizontal drilling for various reasons such as reservoir depth, pressure, rock quality, and hydrocarbon saturation.

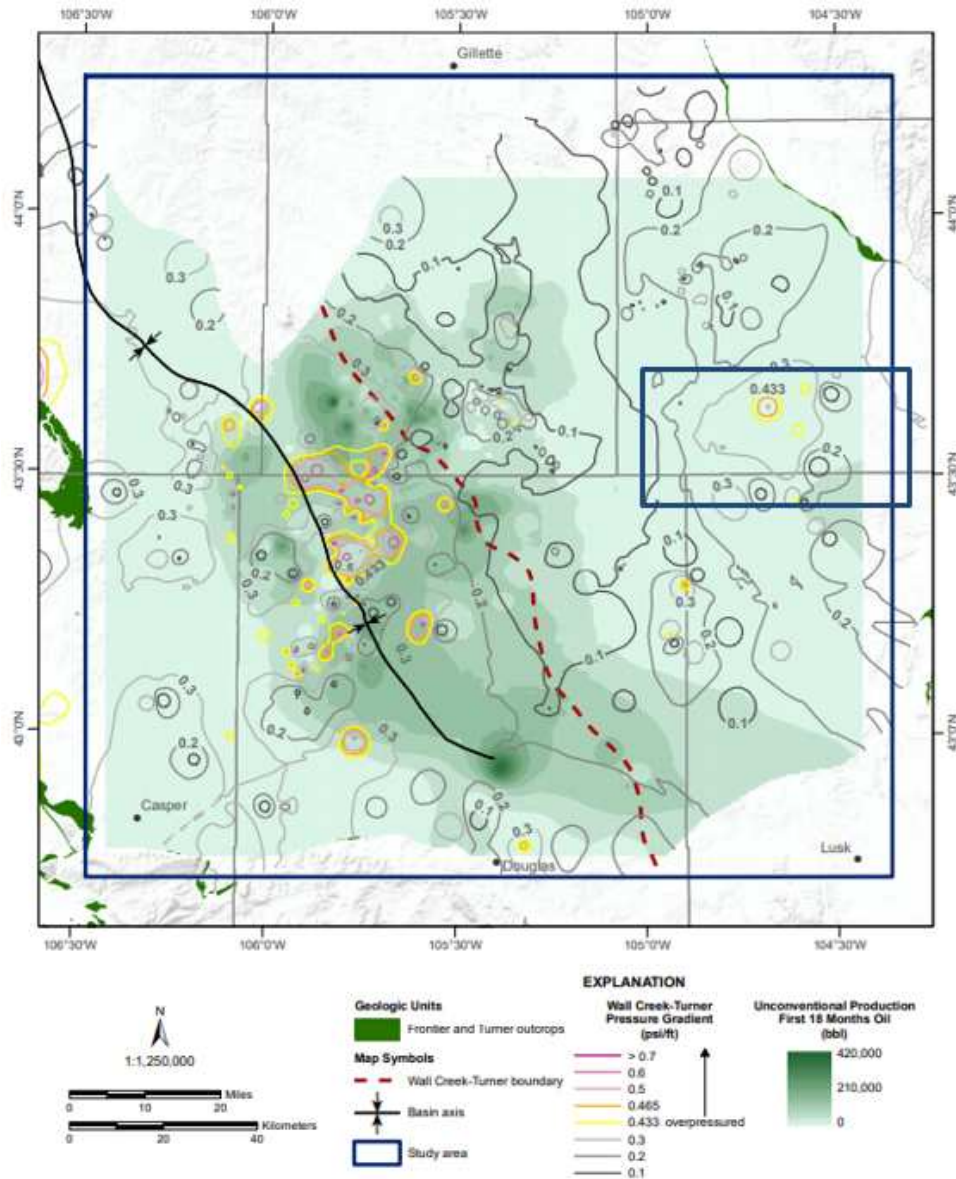


Figure 2.10: Pressure gradient contours with first 18 months production of unconventional oil from Wall Creek-Turner reservoirs (From Toner, 2019).



## 2.5 Previous Work

Although the Turner is one of the most targeted reservoirs within the PRB, very little work has been published in the last decade about its reservoir characteristics and exploration potential. The majority of the work done on the Turner, although minimal, is on the depositional environment for mapping purposes and facies distribution. However, the depositional interpretation for the Turner is vastly debated and argued. This section will attempt to explain some of the more common interpretations, as well as the uncertainty for even the most recognized and accepted interpretations.

The first publication that studied the Upper Cretaceous strata in the PRB was Rubey (1930) who named the Turner Sandy Member of the Carlile Shale from outcrop located in Weston County, Wyoming. Rubey (1930) noticed a possible unconformity at the base of the unit with abundant shark teeth near the erosional surface. The Turner was described as a sandy shale, siltstone, thin bedded sandstone, and conglomeratic unit that outcropped along Turner Creek.

There are some authors who group the Turner into the same depositional environment as the Wall Creek member of the Frontier Formation (Merewether et al., 1979; Winn, 1991; Gustason, 2015). The most common interpretation for the Wall Creek's depositional environment is a prograding, top-truncated lowstand deltaic system influenced by waves, tides, and storms. Merewether et al. (1979) proposed a north-northeast sediment transport direction during the Turonian. However, cross-bedding within the Turner suggest a paleocurrent from the southeast, which was interpreted as storm reworking of the original deposit which transported sediments away from the delta-strandplain system.

In contrast, there are several authors who do not group the Wall Creek and the Turner together and have made new or different interpretations. Haun (1958) observed outcrops on both the western and eastern margins of the PRB. He suggested that the Turner occupied a similar stratigraphic and biostratigraphic position as the Wall Creek member of the Frontier Formation in the west and contained three different members.

Merewether (1980, 1996) suggests that the Turner was deposited in a more distal setting than the Wall Creek, with shelf sand bars fed by high energy deltas. Merewether (1996) noticed progradational parasequences and then suggested that the sandy lithology of the Turner was deposited in a shallow-marine environment on a shelf, particularly where the member is sandy, as a distal delta lobe, and possibly close to lowland vegetation.

Weimer and Flexer (1985) used petrophysical well logs to correlate reservoir intervals and map them throughout the PRB. They observed three different lithologies within the Turner: 1) a lower lens of gray, fine to medium grained, pebbly conglomeratic sandstone occurring in an overall fine-grained sandstone body. 2) A middle gray, fine-grained sandstone alternating with thin layers of siltstone or shale with light bioturbation. 3) an upper gray, fine-grained and highly bioturbated, glauconitic sandstone. Weimer and Flexer (1985) interpreted the lower Turner as brackish to marine deposits filling erosional valleys, which cut in to the Greenhorn and Pool Creek.

Rice and Gaskill (1988) subdivided the Turner into upper and lower sand intervals where Rice and Keighin (1989) then further split them into two stratigraphic parasequences that could act as a stratigraphic trap. The upper interval contains *Scaphites whitfieldi* and lower contains *Scaphites warreni*, separated by a marine mudrock. They suggest that as sea levels rose during the late Turonian, a wave dominated shelf with storm influence setting deposited the lower Turner, while the upper Turner sediments were deposited below fair weather wave base.

Melick (2013) described the Turner as being deposited below fair weather wave base on a shallow shelf. Melick (2013) specifies that sediment input was from hyperpycnal flows, or sediment gravity flows. Heger (2016) generally agrees with this interpretation, but suggests that the lower Turner was deposited near storm wave base.

The Mowry Shale and the Niobrara Formation are considered two possible source rocks for the Turner reservoir (Momper and Williams, 1984; Dolton and Fox, 1995; Anna, 2009). Momper and Williams (1984) suggest that oil began to expel from Cretaceous source rocks

starting in the early Tertiary, where expulsion was controlled by structural features. Anna (2009) suggested that within the eastern margin of the basin, near the location of Finn-Shurley Field, hydrocarbons sourced from the mature Mowry migrated up along faults into the reservoir and that the Niobrara is not within the maturity window. Momper and Williams (1984) show that within the eastern margin of the PRB, the Mowry is in the early oil window. Rahman et al. (2016) confirmed migrated hydrocarbon contributions to the Turner from both the Mowry Shale and the Niobrara Formation.

There have been numerous Turner wells drilled within the PRB, and nearly 800 within the study area. Of these vertical wells, very few have drill stem tests or production tests available, even though oil staining can be seen in outcrop. With the advances in horizontal drilling, past production testing and methods do not accurately evaluate the potential for Turner production. Nearly a decade ago the USGS assessment of the Frontier-Turner Sandstone assessment unit gave an average estimate of total undiscovered resources of 10.18 million barrels of oil, 40.47 billion cubic feet of gas, and 2.91 million barrels of natural gas liquids (Anna, 2009).

The increasing attention on the Turner reservoir will aid in continued research to better understand the petroleum potential throughout the PRB. The Turner has been subject to several stratigraphic and structural framework studies. However, not much has been done in terms of reservoir characterization and geochemical analysis. This study will attempt to bridge those gaps and help better define an interpretation for the depositional environment of the Turner within Weston County, Wyoming. Facies and facies associations, reservoir characterization, well log analysis, and basin modelling will be used extensively within this study along with the information from previous studies to better understand the Turner in the Powder River Basin.

## CHAPTER 3

### CORE ANALYSIS

#### 3.1 Overview

This chapter focuses on the classification and discrimination of facies observed within the lower Turner interval through the utilization and integration of core description, petrographic thin sections, and FE-SEM analysis. A total of four cores were made available from the United States Geological Survey (USGS) Core Research Center (CRC) for the study area. Cores in Finn-Shurley field were all viewed and described in detail at the CRC. Cored intervals were all within the Turner Sandstone member of the Carlile Formation, and will be referred to as the Turner. More specifically, the four cored intervals are within the lower Turner, which is defined in this study as below a correlatable flooding surface that separates the upper and lower Turner zones, and totals 271 feet of core across three townships (Figure 3.1). In general, conventional characterization efforts are sufficient to capture larger scale changes in lithology within the Turner. However, these characterization methods are generally too coarse to observe small scale changes in mineralogy, rock properties, and reservoir quality that govern potentially economic wells. In order to account for and observe these small changes, supplemental and iterative work with thin section petrography, FE-SEM analysis, X-ray Fluorescence (XRF), and X-ray Diffraction (XRD) were necessary for facies classification of the Turner. The primary objective of this project was to characterize the reservoir potential within the highly heterolithic strata of the lower Turner, the primary producing interval in Finn-Shurley Field. Four core descriptions were compiled to identify eight facies, which are described below, based upon lithology, grain size, mineralogy, sedimentary structures, ichnofauna, and bioturbation levels. Of these eight facies, four reservoir facies were identified by integrating routine core analysis, XRF, and XRD to make assumptions about the rock quality and the mechanical stratigraphy. Distribution of these facies

across Finn-Shurley was also investigated and compared across the four key cored wells to then be discussed in relation to stacking patterns and interpreted depositional processes and environments.

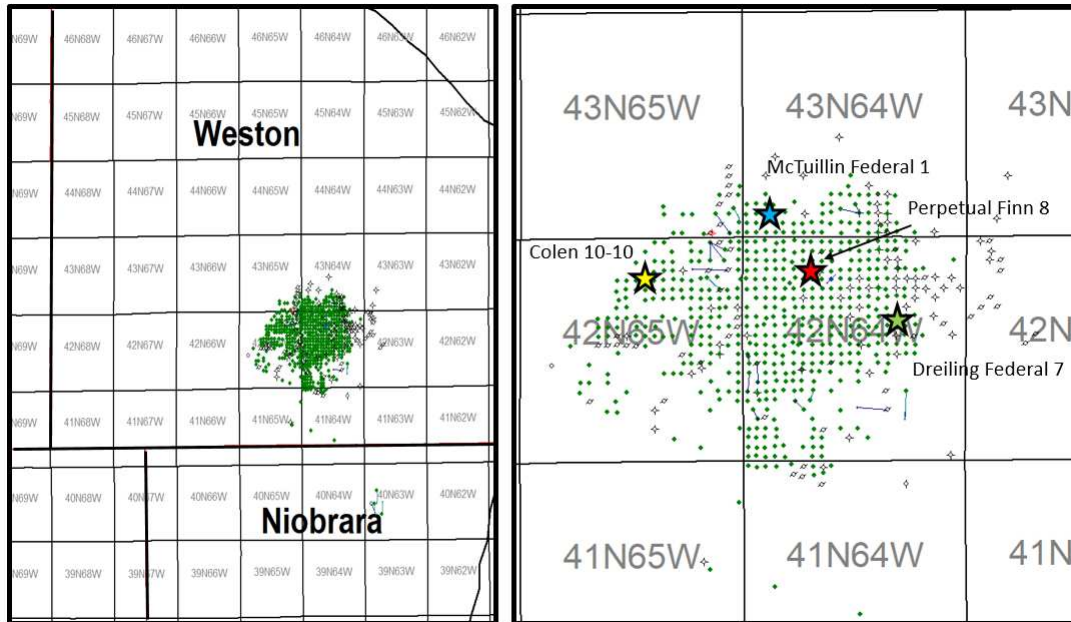


Figure 3.1: Location and names of cores described for this study within Weston County, Wyoming.

### 3.2 Core Descriptions

The Colen 10-10, McTuillin-Federal 1, Perpetual Finn 8, and Dreiling-Federal 7 cores were the four cores described in detail for this study. This detailed description includes lithology, bioturbation intensity levels, abundance and diversity of ichnofauna, sedimentary structures, percentage of mud, and grain size. All four wells were cored through the lower Turner, where only the Perpetual Finn 8 is interpreted to have been cored through the surface that separates the lower and upper Turner. This means the Perpetual Finn includes approximately 9 feet of the upper Turner interval and 51 feet of the lower Turner interval, where the Colen 10-10, McTuillin-Federal 1, and the Dreiling-Federal 7 are only cored in the lower Turner interval and do not appear to intersect the *Scaphites whitfieldi* flooding surface.

The *Scaphites whitfieldi* is defined as the separation between the upper and lower Turner intervals (Heger, 2016). Each core was described in detail by hand drawings at the USGS CRC, then digitized in Strater (Figure 3.2). The descriptions illustrate variations in grain size, sedimentary structures, levels of bioturbation, and facies classification throughout the cored stratigraphy.

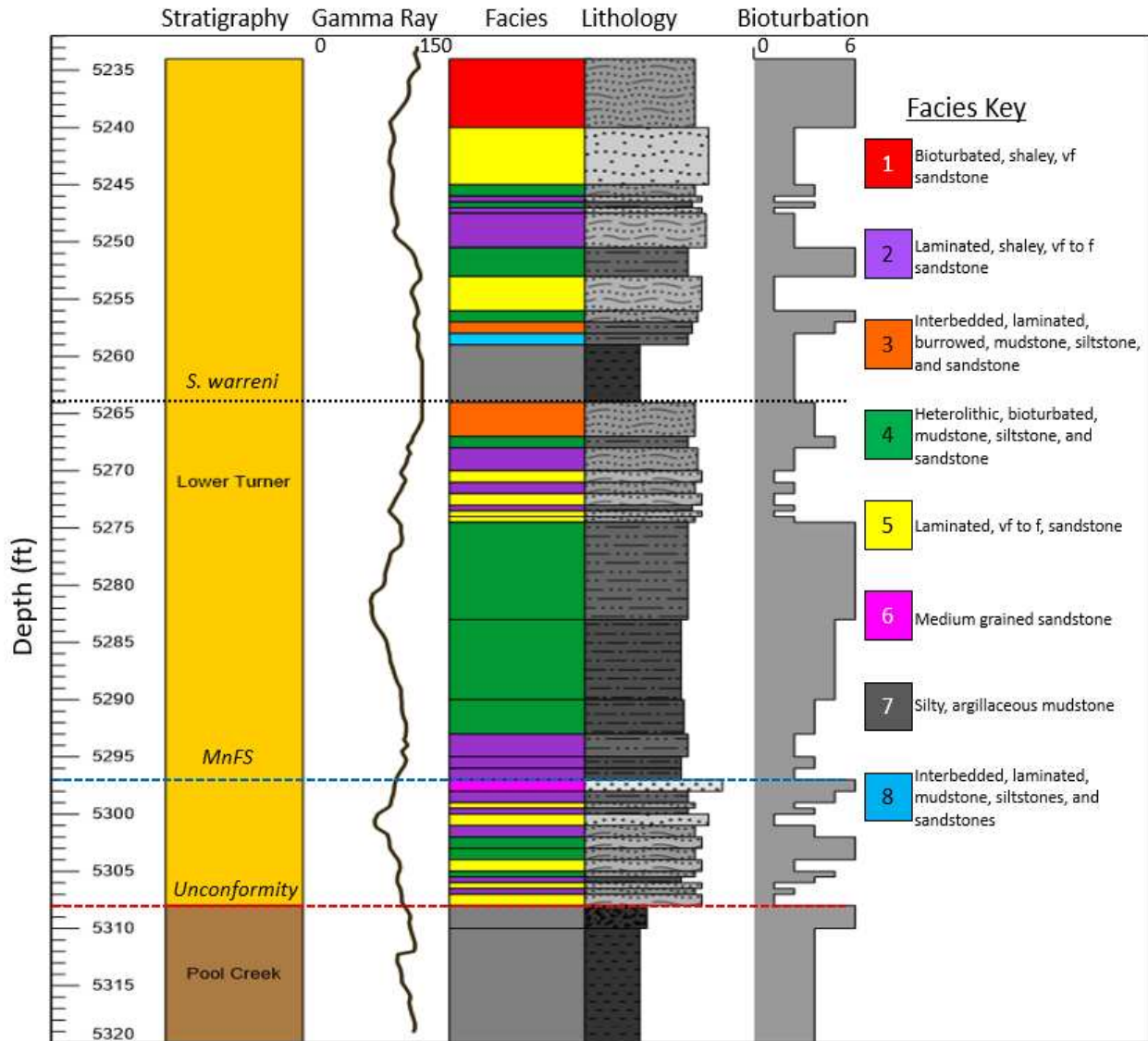


Figure 3.2: Core description of the Colen 10-10 well. The facies legend is on the far right side with the core description showing depth, grain size, lithology, facies, and bioturbation index. Also included is a gamma ray log and interpreted key stratigraphic surfaces, which include a minor flooding surface (MnFS), a flooding surface (*S. warreni*), and an unconformity.

### **3.2.1 Colen 10-10**

The Colen 10-10 core is a vertical well operated by M & K Oil Company and is located in Sec 31, T42N, R64W within Weston County, Wyoming. According to the Wyoming Oil and Gas Conservation Commission (WOGCC), the Colen 10-10 was completed on November 30th, 1983. This well has produced 42 thousand barrels of oil (MBO) and 90 thousand cubic feet of gas (MMCF) to date. This core is 86 feet long through the Turner, and the longest of all the Turner cores in this study.

### **3.2.2 McTuillin Federal 1**

The McTuillin Federal 1 core is a vertical well operated by M & K Oil Company and is located in Sec 31, T43N, R64W within Weston County, Wyoming. According to the WOGCC the McTuillin Federal 1 was completed on January 12th, 1982. This well has produced 49 MBO and 106 MMCF of gas to date. This core is 65 feet long through the Turner and is the second longest Turner core in this study.

### **3.2.3 Perpetual Finn 8**

The Perpetual Finn 8 core is a vertical well operated by Chemily Management Company and is located in Sec 5, T42N, R64W within Weston County, Wyoming. According to the WOGCC the Perpetual Finn 8 was completed on February 2nd, 1983. This well has produced 56 MBO and 96 MMCF of gas to date. This core is 60 feet long through the Turner.

### **3.2.4 Dreiling Federal 7**

The Dreiling Federal 7 core is a vertical well operated by Chemily Management Company and is located in Sec 15, T42N, 64W within Weston County, Wyoming. According to the WOGCC the Dreiling Federal 7 was completed on March 2nd, 1983. This well has produced 38 MBO and 71 MMCF of gas to date. This core is 60 feet long through the Turner.

### 3.3 Key Stratigraphic Surfaces

Based on observation of the four Finn-Shurley cores and previous surface outcrop work throughout Wyoming conducted by Rubey (1930), Haun (1958), Merewether (1979, 1980), and Heger (2016), four key stratigraphic surfaces were observed throughout the four cores within the study area. A key stratigraphic surface is defined for this study as a lithologic boundary with observed juxtaposition across the interpreted stratigraphic boundary. Figure 3.3 shows an example of 3 of the key surfaces and their interpreted location on the Colen 10-10 core. These interpreted surfaces include an unconformity, a major flooding surface, and a minor flooding surface. Minor erosional surfaces are not visible at this scale, but observed in closer proximity in several locations throughout the core.



Figure 3.3: Core photos from the Colen 10-10 core displaying the Mid-Turonian unconformity (red dashed line) with the underlying Poole Creek member of the Carlile Shale at 5,307-5,308 ft. core depth. A minor flooding surface (blue solid line) with a medium- to fine-grained sandstone underlying a mudstone bed. at 5296-5297 ft. core depth. And a major flooding surface (red solid line) with a fine sandstone underlying an mudstone at 5263-6264 ft. core depth, capping the top of a Turner deposition cycle.



### 3.3.1 Mid-Turonian Unconformity

The three members that make up the entirety of the Carlile shale, include the Pool Creek Member, the Turner Sandy Member, and the Sage Breaks Member. These individual members are separated by distinct lithologic boundaries, both conformable and disconformable, of Turonian age. The base of the Turner is a prominent lithologic boundary. The base of the Turner is identified by a very fine-grained sandstone overlying the argillaceous Pool Creek mudstone (Figure 3.4). This boundary is visible in petrophysical well logs and core, when data across the boundary is available. This boundary is interpreted as an unconformity representing 2-3 missing ammonite zones or approximately 2.42 million years of missing time from the geologic record, or a period of no deposition (Merewether et al., 2011).

This unconformity is correlatable across the entire PRB at the base of the Turner in the eastern PRB and at the base of the Wall Creek Member of the Frontier Formation, the time equivalent formation in the western PRB (Merewether, 1979). Sea level curves from Haq (2014) denote that this beginning of the Turner time period was marked by a lowstand after a regional drop in sea level of the Greenhorn Sea following Pool Creek deposition. This forced regression is interpreted to be what allowed for the fine-grained sandstones and siltstones of the Turner to prograde out and deposit across the eastern PRB. Although there is no evidence for sub-aerial exposure during this regression of sea level within these cores, some authors have suggested sub-aerial exposure could have occurred (Weimer and Flexer, 1985).



Figure 3.4: Core photo from the Colen 10-10 core displaying the Mid-Turonian unconformity (red dashed line) with the underlying Poole Creek member of the Carlile Shale at 5,307-5,308 ft. core depth.

### 3.3.2 Flooding Surface

Major flooding surfaces (FS) are present within the four cores located in Finn-Shurley Field. These surfaces are observed as sharp, non-gradational contacts between an underlying fine-grained sandstone and an overlying argillaceous mudstone (Figure 3.5). These lithological changes are a result of an increase in water depth within a local region. From core and log observation, the Turner is composed of multiple coarsening upward sequences, capped with a flooding surface. These surfaces are visible on petrophysical well logs and some are even correlatable in the Turner across Finn-Shurley. Across the four cores, the deepest, or first occurring, major flooding event marks the top of a Turner deposition cycle, which will be referred to as the Turner one zone. The Turner one zone is interpreted to be present within each core in Finn-Shurley Field and can be correlated in well logs as a sharp increase

in gamma ray response within the subsurface across the study area. Although it is necessary to point out, in two of the cores, Colen 10-10 and Perpetual Finn 8, there is a minor flooding surface seen both in well logs and core, that occurs prior to the major flooding event that marks the top of the Turner one zone. However, this is interpreted as a minor and local flooding event within those two cores. The top of Turner one has also been interpreted to be the top of the Western Interior ammonite zone *Scaphites warreni*. Based upon outcrop to subsurface work and observations of ammonites on the surface by Heger (2016), the top of this surface is correlatable into the subsurface using well logs and core across the study area, however, there are no visible ammonites within the core to confirm the subsurface correlation.

The second major flooding surface present is only present in the core of the Perpetual Finn 8, but is visible and correlatable in petrophysical well logs across the field as a sharp increase in gamma ray response. This marks the top of a second cycle of deposition within the Turner, or the Turner two zone. This specific surface is interpreted as the top of a second ammonite zone present within the Turner from outcrop work, the *Scaphites whitfieldi*. The top of this depositional cycle is also typically used as the separation between the lower Turner and the upper Turner intervals.

The lower Turner is separated from the upper Turner largely due to variations in facies assemblage and distribution, diversity of ichnofauna and intensity of bioturbation, as well as reservoir characteristics such as porosity, permeability, and reservoir thickness. This is an important distinction, as the lower Turner is the primary reservoir target in the eastern region of the PRB, where the upper Turner is the primary reservoir target in the central portion of the basin. Comparison of these variations is considered outside the scope of this study due to limited core data of this upper unit in Finn-Shurley Field.



Figure 3.5: Core photo from the Colen 10-10 core displaying the *Scaphites warreni* flooding surface that is present throughout the subsurface and at the top of an upward coarsening sequence at 5,263-5,264 ft. core depth. Argillaceous mudstones overlying fine-grained sands can be observed at each FS within the Turner interval.

### 3.3.3 Minor Flooding Surface

Multiple minor flooding surfaces (MnFS) are interpreted to be present in the cores in the study area. A correlatable MnFS is present in two of the cores, Perpetual Finn 8 and Colen 10-10, where a medium-grained sandstone is present below approximately 6 inches of interbedded mudstone and siltstone (Figure 3.6). The MnFS typically occur within a larger depositional cycle, such as the Turner one or two zones. They can also be seen in petrophysical well logs as a slight increase in gamma ray when compared to the major flooding surfaces. This is due to the fact that these MnFS have a smaller thickness of preserved mudstones, typically 3-6 inches thick. These surfaces could represent small periods, potentially 3rd or 4th order cycles, of flooding during the overall transgression of sea level.



Figure 3.6: Minor flooding surface within the Colen 10-10 core that shows a medium- to fine-grained sandstone underlying a mudstone and siltstone observed at the core depth of 5296-5297 ft core depth.

### 3.3.4 Minor Erosional Surface

Minor erosional surfaces (MnES) were also pervasive throughout the cores within the study area. Figure 3.7 shows two examples in the Colen 10-10 core where the observed fine-grained sandstone are found overlying a bioturbated shaley, very fine-grained sandstone with another minor erosional surface at the base of this facies. These surfaces are representative of pre-existing sediment being eroded away from indications of scour surfaces and non-deposition in the core. These surfaces are post depositional events and cannot give accurate assessment of sedimentation rate. However, they can explain periods of non deposition and increased bioturbation levels.



Figure 3.7: Minor erosional surface within the Colen 10-10 core that shows the observed sandstone facies eroding into the underlying bioturbated facies by scour surfaces at the core depth between 5246-5247 ft.

### 3.4 Facies Description

The Turner is a highly heterolithic interval composed of varying thickness of interstratified mudstone, siltstone, and sandstone beds. The Turner facies can vary anywhere from an argillaceous silty mudstone, to a well preserved fine-grained sandstone with sharp sedimentary structures and heavily defined mud drapes. Ultimately, proper and detailed multi-scale facies description can help with understanding the controls on the best porosity and permeability intervals within the lower Turner. By understanding the primary drivers on the best reservoir quality rock, this study can optimize targeting of these sandstones intervals for horizontal drilling and be in zones with ideal mechanical properties for completion. Eight facies were identified and described in detail within the Turner through the integration of core,

thin sections, and XRD mineralogy data, when available. The Turner is primarily composed of very fine-grained sandstones, which can be discerned and classified with a hand lens. The mud and silt size grains needed to be supplemented with thin section photomicrographs for successful classification. Once classified, each facies was determined to be a reservoir facies or a non-reservoir facies, based upon core analysis and bulk mineralogy. Also noted were common sedimentary structures, bioturbation types and diversity, and grain size with mud abundance, all which vary heavily from facies to facies. These additional observations help reveal distinct features if facies have similar grain size and mineralogy. From petrographic analysis, secondary cements and diagenetic fabrics were incorporated to better comprehend diagenetic effects on reservoir and non-reservoir facies.

Figures 3.8-3.10 summarize the defining characteristics and variations in the eight identified facies and their rock properties. This includes core photos, thin section photomicrographs, mineralogical makeup, and rock quality. Rock quality properties include average porosity, permeability, total organic carbon content (TOC), and an estimated pore throat size ( $R_{35}$ ) (Equation 3.1). The  $R_{35}$  calculation gives information of fluid flow and storage quality of the rock by estimating pore throat radii with 35 percent non-wetting phase saturation during capillary pressure tests. Using the Hartman et al. (1999) classification, porosity and permeability values can be used to estimate the pore throat size of a rock without the need for mercury injection capillary pressure tests. This aids in understanding the pore network and pore geometries in addition to the flow capacity and storage capacity of the reservoir rocks.

$$R_{35} = 10^{(0.732+0.588\log K_a-0.864\log\phi)} \quad (3.1)$$


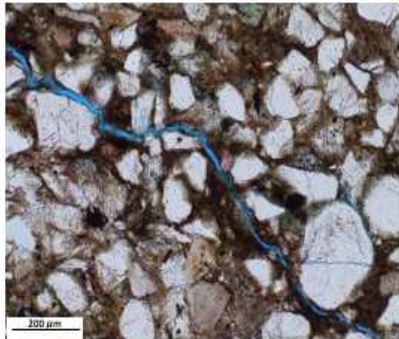
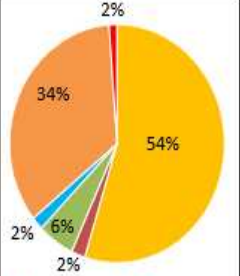

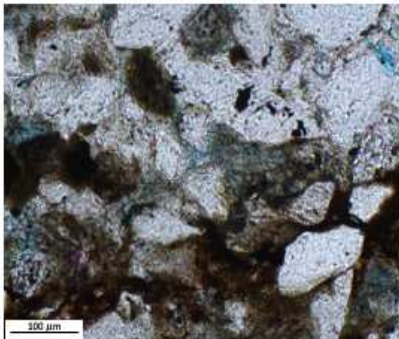
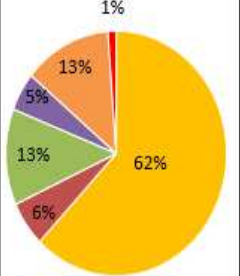

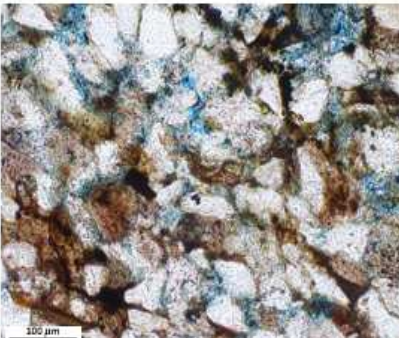
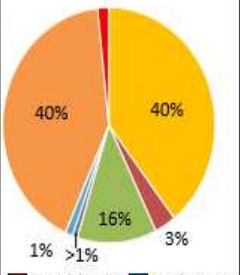
	Facies Name	Core Photo	Thin Section	XRD	Rock Properties
<b>Facies 1</b>	Bioturbated, Shaley, Very Fine-Grained Sandstone	 2 in.	 200 µm Colen 10-10 (5234')	 2% 34% 54% 2% 6% 2% K-Feldspar Carbonate Clay Quartz Other Plagioclase Chlorite	$\Phi = 14\%$ Range (10-16%) $K = 0.12$ mD Range (0.06-0.26 mD) $N = 3$ $TOC = 0.45$ wt% $R_{35} = 0.43$ µm
<b>Facies 2</b>	Laminated, Muddy, Very Fine- to Fine-Grained Sandstone	 2 in.	 100 µm McTuillin Federal 1 (4884')	 1% 13% 62% 5% 13% 6% K-Feldspar Carbonate Clay Quartz Other Plagioclase Chlorite	$\Phi = 13\%$ Range (9-16%) $K = 2$ mD Range (0.08-8 mD) $N = 8$ $TOC = 1.2$ wt% $R_{35} = 0.51$ µm
<b>Facies 3</b>	Interbedded, Burrowed, Laminated, Mudstone, Siltstone, and Sandstone	 2 in.	 100 µm Colen 10-10 (5289')	 1% 40% 40% 16% 3% 1% >1% K-Feldspar Carbonate Clay Quartz Other Plagioclase Chlorite	$\Phi = 12\%$ Range (11-13%) $K = 0.04$ mD Range (0.001-0.07 mD) $N = 3$ $TOC = 0.89$ wt% $R_{35} = 0.41$ µm

Figure 3.8: Summary of Facies 1, 2, and 3 for this study of the lower Turner in Finn-Shurley Field. Figure includes facies name, a representative core photo, a thin section photomicrograph, XRD mineralogy, porosity, permeability, number of available core data points, measured TOC, and a  $R_{35}$  calculation. Blue epoxy in the thin section photomicrograph represents porosity.




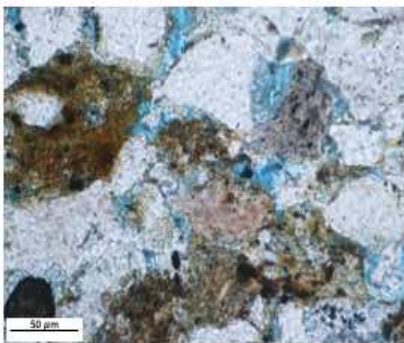
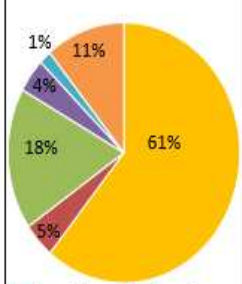
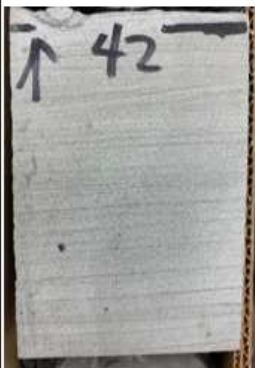
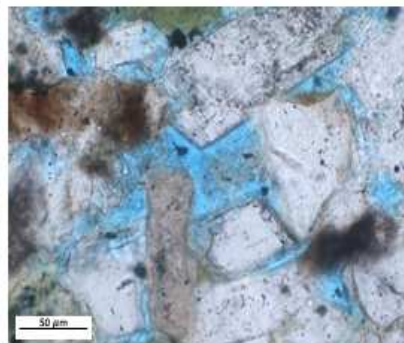
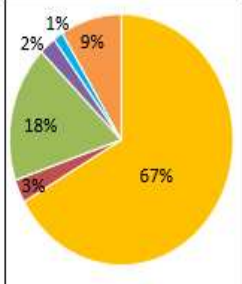

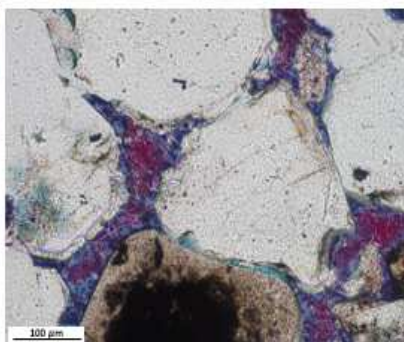
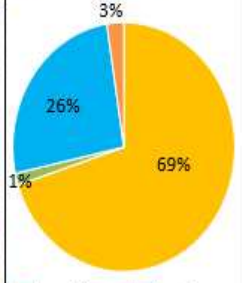
	Facies Name	Core Photo	Thin Section	XRD	Rock Properties
Facies 4	Heterolithic, Bioturbated, Mudstone, Siltstone, and Sandstone	 2 in.	 McTuillin Federal 1 (4876')	 K-Feldspar Carbonate Clay Quartz Other Plagioclase Chlorite	$\Phi = 14\%$ Range (10-16%) $K = 0.16 \text{ mD}$ Range (0.001-6 mD) $N = 16$ $\text{TOC} = 0.57 \text{ wt}\%$ $R_{35} = 0.52 \mu\text{m}$
Facies 5	Laminated Very Fine- to Fine-Grained Sandstone	 2 in.	 McTuillin Federal 1 (4851')	 K-Feldspar Carbonate Clay Quartz Other Plagioclase Chlorite	$\Phi = 14\%$ Range (13-16%) $K = 0.31 \text{ mD}$ Range (0.06-0.5 mD) $N = 6$ $\text{TOC} = 0.45 \text{ wt}\%$ $R_{35} = 0.55 \mu\text{m}$
Facies 6	Medium-Grained Sandstone	 2 in.	 Colen 10-10 (5297')	 K-Feldspar Carbonate Clay Quartz Other Plagioclase Chlorite	$\Phi = 13\%$ Range (n/a) $K = 0.003 \text{ mD}$ Range (n/a) $N = 1$ $\text{TOC} = 0.07 \text{ wt}\%$ $R_{35} = 0.38 \mu\text{m}$

Figure 3.9: Summary of Facies 4, 5, and 6 for this study of the lower Turner in Finn-Shurley Field. Figure includes facies name, a representative core photo, a thin section photomicrograph, XRD mineralogy, porosity, permeability, number of available core data points, measured TOC, and a  $R_{35}$  calculation. Blue epoxy in the thin section photomicrograph represents porosity.

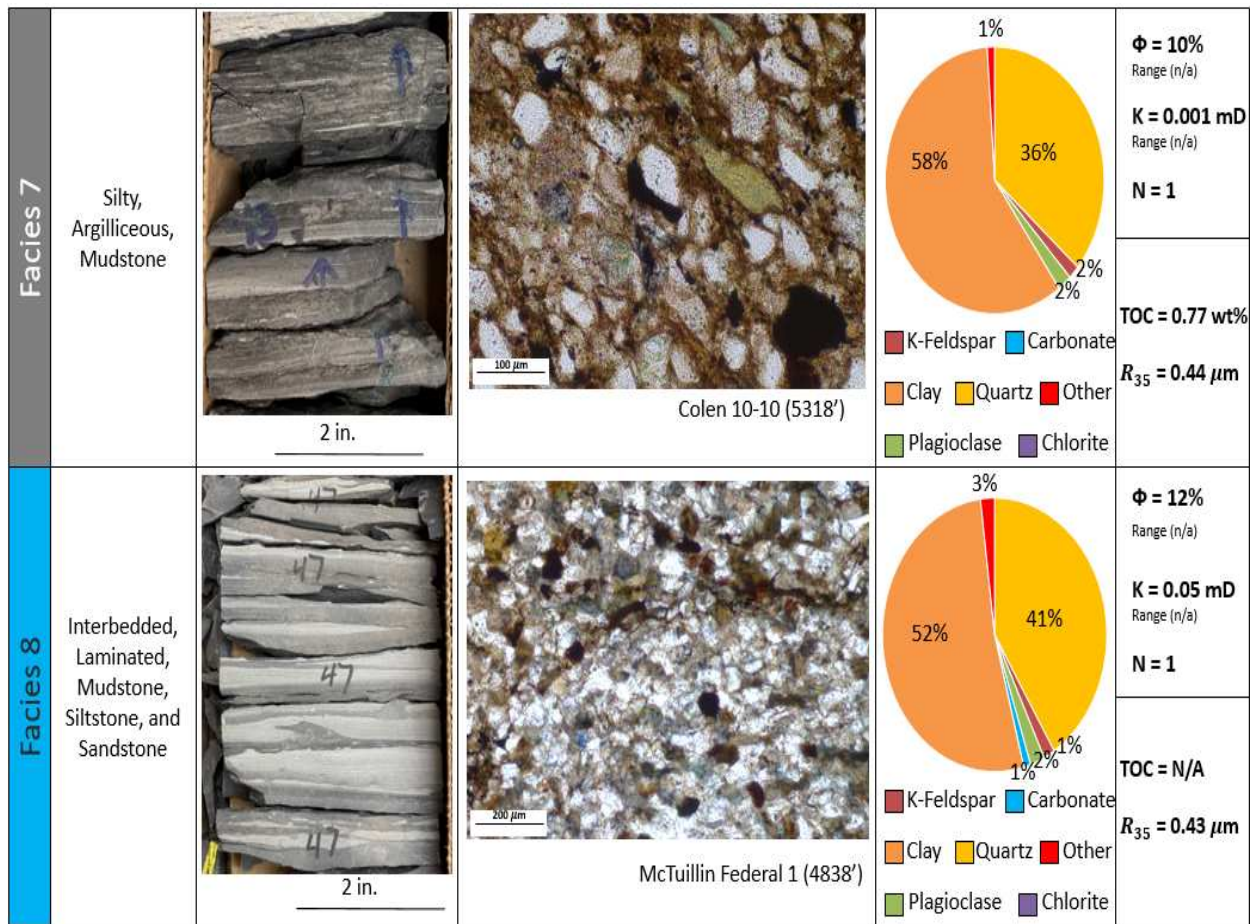


Figure 3.10: Summary of Facies 7 and 8 for this study of the lower Turner in Finn-Shurley Field. Figure includes facies name, a representative core photo, a thin section photomicrograph, XRD mineralogy, porosity, permeability, number of available core data points, measured TOC, and a  $R_{35}$  calculation. Blue epoxy in the thin section photomicrograph represents porosity.

### 3.4.1 Facies 1: Bioturbated, Shaley, Very Fine-Grained Sandstone

Facies 1 is composed of light grey to grey, shaley, fine- to very-fine grained sandstone with a high intensity of bioturbation (Figure 3.11). This facies dominantly occurs in the upper Turner and the shallowest cycle of the lower Turner, or the Turner two zone, in each of the cores throughout Finn-Shurley Field. Trace fossils, when preserved, are *Asterosoma*, *Thalassinoides*, and *Teichichnus* with a bioturbation index (BI) of 5-6. This facies has a high diversity of trace fossils preserved, and due to the large intensity of bioturbation, no

sedimentary structures were observed in this facies. Porosity from core suggest this facies has an average porosity of 14% percent, with a range from 10-16%, and permeability of 0.12 mD with a range from 0.06-0.26 mD. From these core data points, an average  $R_{35}$ , which is used as a proxy for pore throat size, of  $0.43 \mu\text{m}$  was calculated, suggesting that this facies is dominated by micropore throat sizes. From these average values, this facies was interpreted to be a potential reservoir facies. TOC values from source rock analysis done on the Colen 10-10 core determined a value of 0.45 weight percent TOC from one core point for this facies.

X-ray Diffraction (XRD) show that this facies is dominated by quartz, greater than 50%, with a clay percentage of 34%. Clay types from XRD suggest mostly illite/muscovite and mixed layer clays. Other constituent minerals include plagioclase and potassium feldspar, which range between 2% and 6%, respectively.

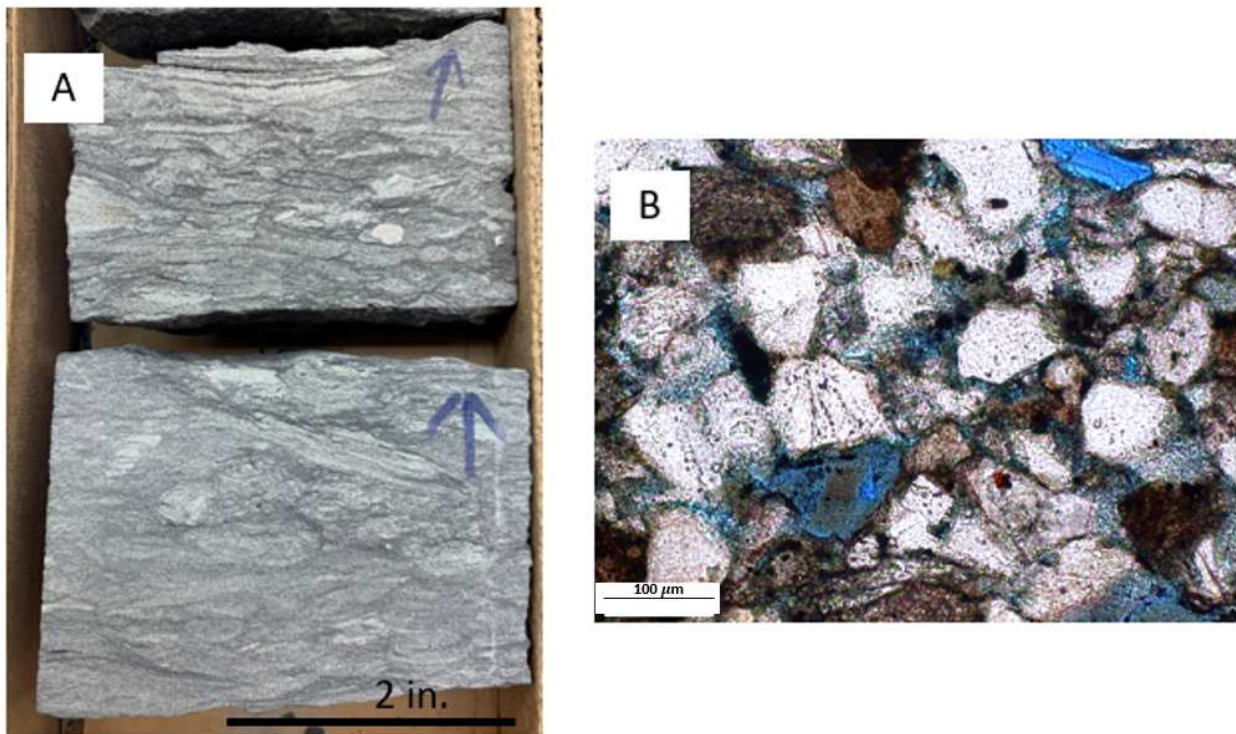


Figure 3.11: Facies 1: Bioturbated, shaley, very fine-grained sandstone. A) shows a representative core photo of the highly bioturbated and muddy facies. B) shows a representative photomicrograph of the facies in thin section at a depth at 5234 ft in the Colen 10-10 core.

### 3.4.2 Facies 2: Laminated, Muddy, Very Fine- to Fine-Grained Sandstone

Facies 2 is a light grey, laminated, muddy, very fine- to fine-grained sandstone. This facies preserves well developed sedimentary structures and laminations (Figure 3.12). Laminations include wavy and flaser lamina, as well as planar to low angle laminations, hummocky and swaley cross stratification, and ripples. It is also distinguished by mud drapes and paired mud drapes between sand beds. These interstratified sand beds can range in thickness from centimeter scale, to several inches thick separated by mud drapes, paired mud drapes, or even 1-2 inch thick mud beds. This facies has slight to no bioturbation, or a BI of 1-2. When bioturbation is observed, it is primarily *Planolites* that occur within the mud drapes. Overall, this facies has a low diversity of trace fossils. From core analysis, it has an average porosity of 13%, with a range from 9-16%, and an average permeability of 2 mD, with a range from 0.08-8 mD. From these values, an average  $R_{35}$  value of 0.51  $\mu\text{m}$  was calculated, suggesting mesopore throat size. From these values, this facies was interpreted to be a potential primary reservoir facies due to the high porosity and permeability values and a high  $R_{35}$  for produceability. TOC values from source rock analysis show that this facies has an average of 1.2 wt % TOC value, with a range of 0.37-1.2 wt %, which could suggest that the mud drapes are slightly organic rich.

From XRD, this facies is composed of 62% quartz with 6% and 13% potassium feldspar and plagioclase respectively. This facies is composed of 18% clay, with 5% of the clay being chlorite. From Almon and Tillman (1979) work in the chronostratigraphic equivalent Wall Creek member of the Frontier Formation, chlorite can be an indicator of early diagenesis within these intervals. Suggesting that this large percentage of chlorite within XRD means there is a potential that the sandstone grains were coated by chlorite clays early during compaction, which preserved porosity and permeability during diagenesis. This is investigated in further detail for this study in Chapter 4, which deals with the petrographic analysis of the Turner Sandy member in Finn-Shurley.

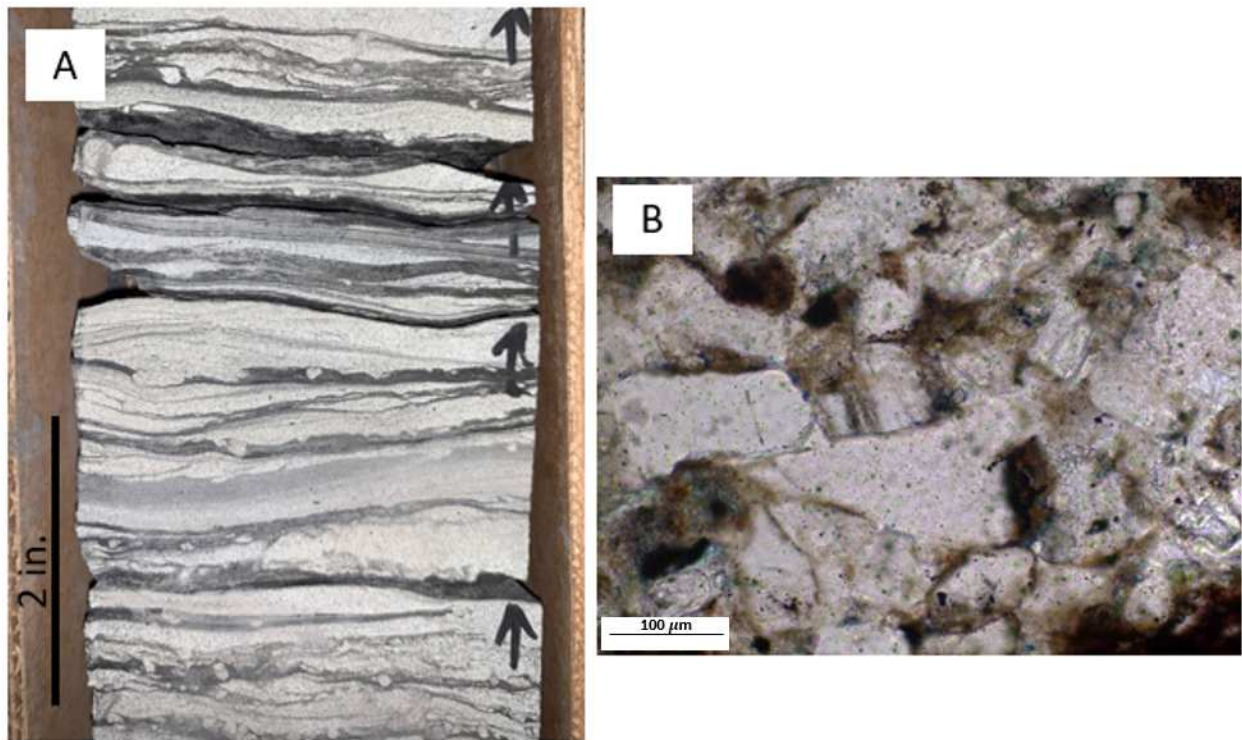


Figure 3.12: Facies 2: Laminated, muddy, burrowed, very-fine sandstone. A) shows a representative core photo of the laminated muddy facies. B) shows a photomicrograph of the facies in thin section at a depth at 4884 ft in the McTuillin Federal 1 core.

### 3.4.3 Facies 3: Interbedded Burrowed, Laminated, Mudstone, Siltstone, and Sandstone

Facies 3 is a dark to light grey, interbedded, burrowed, laminated, mudstone, siltstone, and sandstone (Figure 3.13). It has a bioturbation index of 3-4 and is easily identified by cyclic beds of mudstones, siltstones, and sandstones that range from a few centimeters to a few inches in thickness. The sandstone beds are typically laminated, either with wavy, flaser lamina or low angle to planar lamina, whereas the siltstone and mudstone beds have little to no laminations. Burrows are also present throughout this facies, with majority of the preserved burrows being identified as *Planolites* and *Skolithos*, with their burrows being filled with fine- to very fine- grained sand and typically are preserved within the mudstone and siltstone beds. From core analysis, the average porosity of this facies is 12%, with a

range from 11-13%, and an average permeability of 0.04 mD, with a range from 0.001-0.07 mD. An  $R_{35}$  calculation suggests an average pore throat size of 0.41  $\mu\text{m}$ . From source rock analysis, the value for TOC is 0.89 wt % for this facies from one core data point, suggesting some of the mud beds could have a slightly elevated amount of organics in them.

From XRD, this facies is made up of 40% quartz and 40% clay with the remaining makeup being 3% potassium feldspar, 16% plagioclase, and the other 1% including a small fraction of constituent minerals such as calcite and pyrite. However, due to the cyclic nature of this facies, the mineralogy can vary in these facies based upon the specific bed that is being measured.

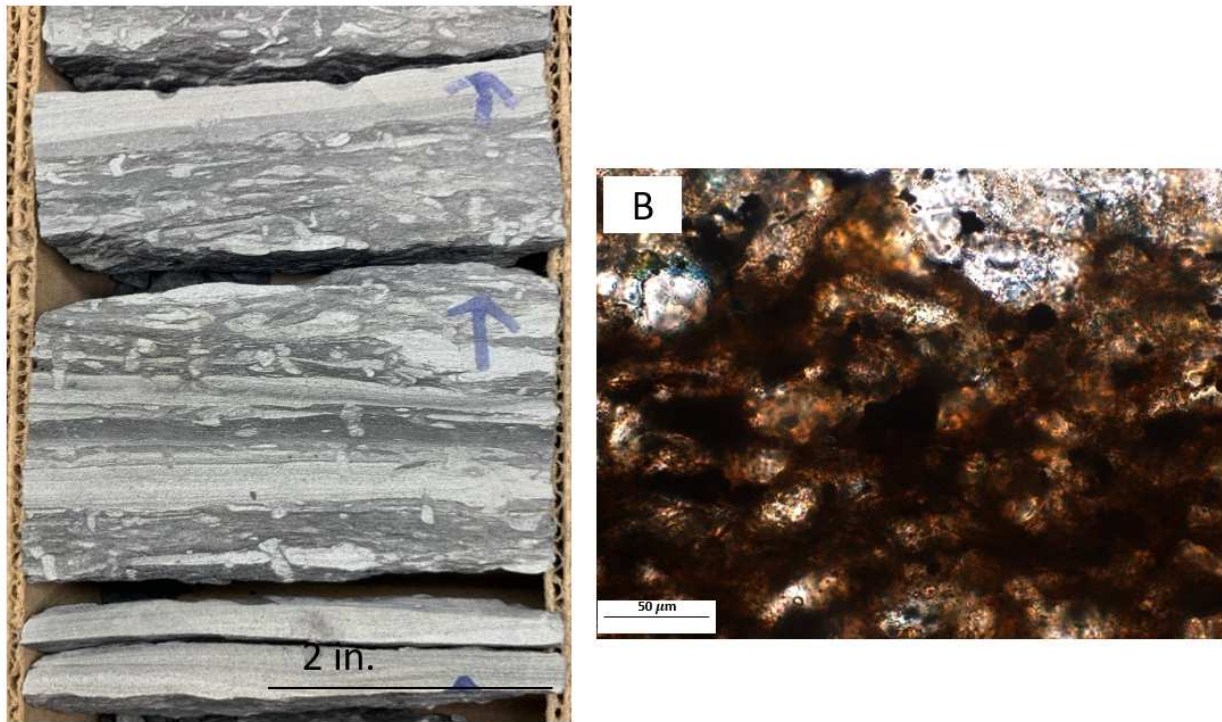


Figure 3.13: Facies 3: Interbedded, burrowed, laminated, mudstone, siltstone, and sandstone. A) shows a representative core photo of the highly bioturbated and muddy facies. B) shows a representative photomicrograph of the facies in thin section at a depth at 4884 ft in the McTuillin Federal 1 core.

#### 3.4.4 Facies 4: Heterolithic, Bioturbated, Mudstone, Siltstone, and Sandstone

Facies 4 is a light grey to dark grey, heterolithic, bioturbated, mudstone, siltstone and sandstone (Figure 3.14). This is the most abundant facies throughout the study area and dominates the Turner one cycle of the lower Turner. This facies generally has a higher degree of bioturbation intensity, and was assigned a bioturbation index of 4-5. In general, the dominant ichnofauna that are observed within this facies are *Skolithos*, *Thalassinoides*, and *Planolites*. This facies has a slightly elevated level of diversity in ichnofauna. Because of this level of bioturbation, if any sedimentary structures are observed they are discontinuous wavy lamina as a result of the degree of bioturbation. From core analysis, the average porosity is 14%, with a range from 10-16%, and the average permeability is 0.16 mD, with a range from 0.001-6 mD. An  $R_{35}$  calculation suggests an average pore throat size of 0.52  $\mu\text{m}$ , or mesopores. The source rock analysis done on the Colen 10-10 core shows an average TOC value of 0.57 wt % for this facies, with a range from 0.39-0.72 wt %. Due to the rock quality with high porosity and permeability, this facies is interpreted to be a potential reservoir facies. However, the quality of this facies does appear to vary across the study area, which is likely related to variations in mineralogy, diagenetic cements, or bioturbation intensity.

From XRD, this facies is primary composed of quartz, up to 61%. It also is composed of 5% potassium feldspar and an elevated amount of plagioclase, around 18%. The other makeup is composed of 4% chlorite, 1% calcite, and 11% clay.

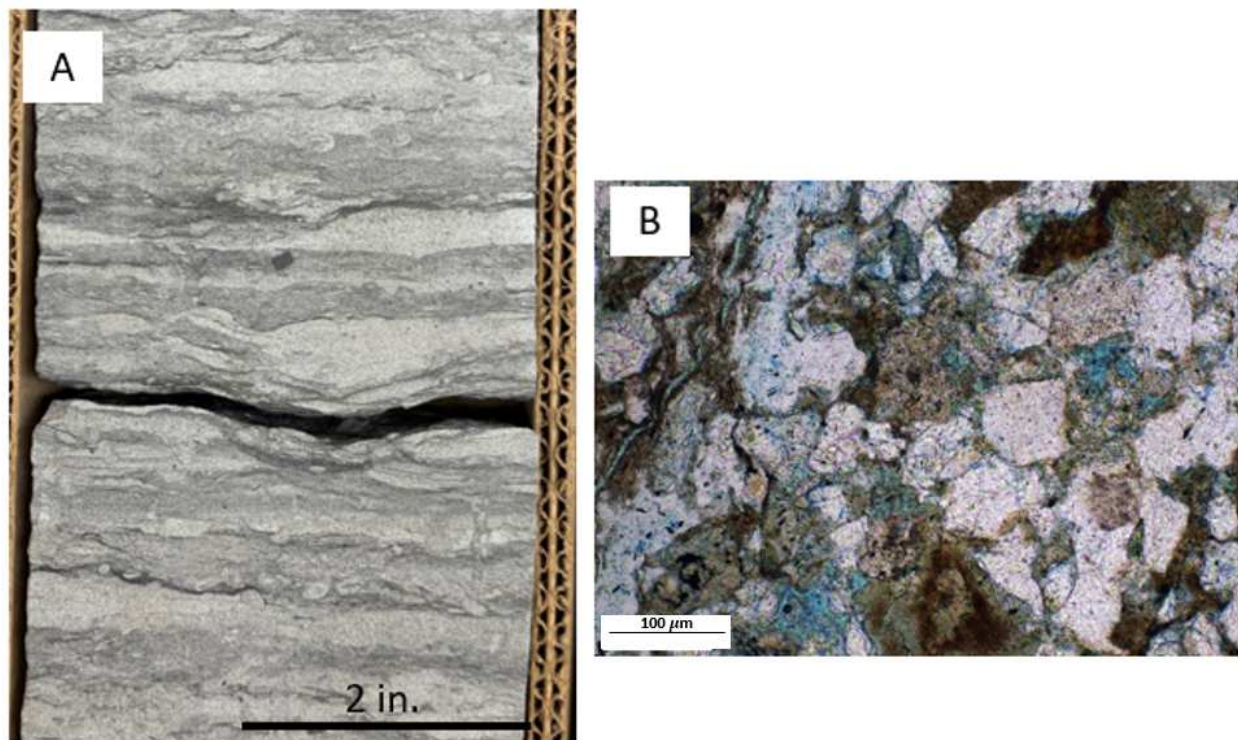


Figure 3.14: Facies 4: Heterolithic, bioturbated, mudstone, siltstone, and sandstone. A) shows a representative core photo of the heterolithic facies. B) shows a representative photomicrograph of the facies in thin section at a depth at 4876 ft in the McTuillin Federal 1 core.

### 3.4.5 Facies 5: Laminated Fine-Grained Sandstone

Facies 5 is a light grey, laminated, very fine- to fine-grained sandstone (Figure 3.15). There is little to no bioturbation present within this facies, so it was assigned a BI of 1. Because of this, laminations and other sedimentary structures dominate this facies and are well preserved within the core. These structures include planar to low angle laminations, ripples, and hummocky and swaley cross stratification with pervasive mud drapes. From core analysis this facies has an average porosity of 14%, with a range from 13-16%, and permeability of 0.31 mD, with a range from 0.06-0.5 mD. An average  $R_{35}$  value of  $0.55 \mu\text{m}$  was calculated for this facies as well, suggesting it primarily has a mesopore throat size. The source rock analysis done on the Colen 10-10 core shows an average TOC value of 0.45 wt %



for this facies, with a range from 0.41-0.49 wt %. From detailed description and analysis, this facies was interpreted to be a potential reservoir facies due to its high porosity, permeability, and  $R_{35}$  value.

From XRD, this facies is composed of 67% quartz, 3% potassium feldspar, 18% plagioclase. A few minor minerals that makeup this facies are chlorite, calcite, and various clay types, their volume percentage is 2%, 1%, and 9% respectively.

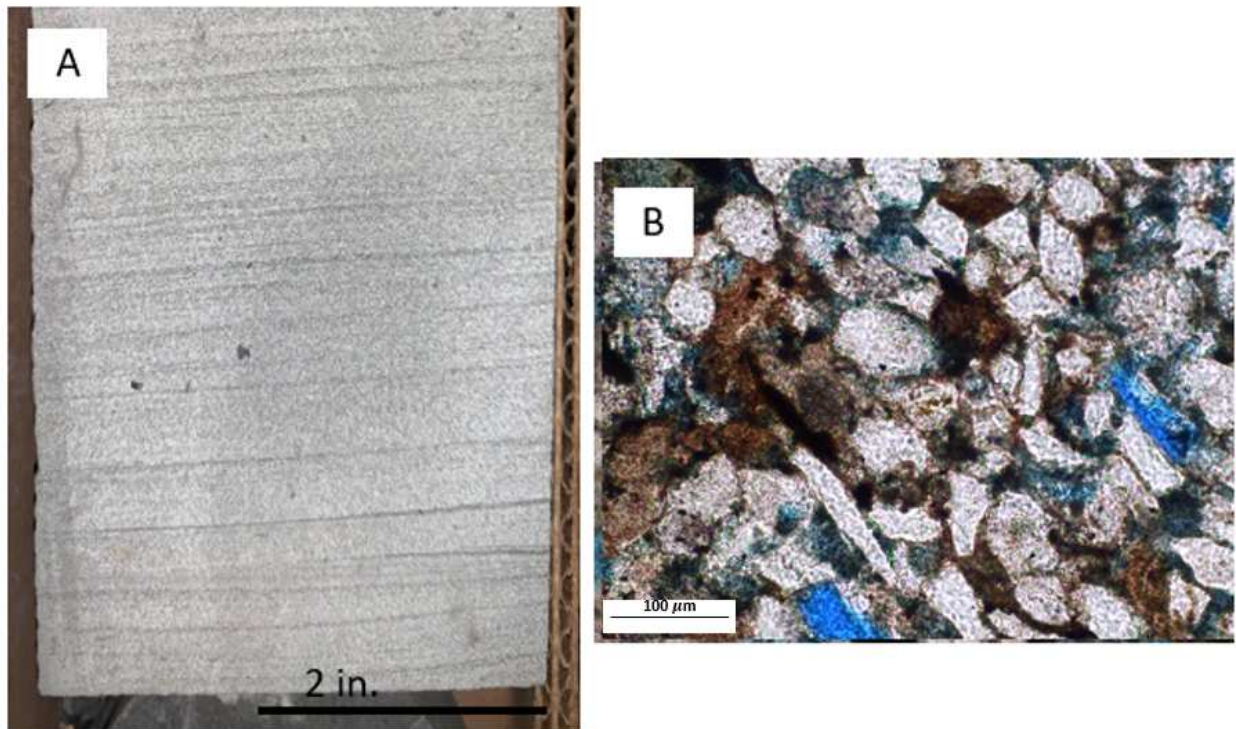


Figure 3.15: Facies 5: Laminated fine-grained sandstone. A) shows a representative core photo of the laminated sandstone facies. B) shows a representative photomicrograph of the facies in thin section at a depth at 4851 ft in the McTuillin Federal 1 core.

### 3.4.6 Facies 6: Medium-Grained Sandstone

Facies 6 is a light grey, medium-grained sandstone (Figure 3.16). There is no visible bioturbation within this facies and it appears structureless. The lack of visible bioturbation suggests that cryptic bioturbation could be responsible for the structureless texture (Howard and Frey, 1975). It occurs in two of the four cores within the larger Turner one depositional cycle and its upper contact is interpreted as a minor flooding surface, making this surface the basal coarsening sequence noted in the well logs. However, this facies was only observed in two of the four cores for the study area.

From XRD, this facies is dominated by quartz, nearly 70% from bulk mineralogy. It is also composed of 25% calcite from XRD. The rest of the mineral makeup is 1% plagioclase, 3% clay and 1% of other mineral constituents (K-feldspar, pyrite, etc.). In thin section, this facies was stained with alizarin red, which will appear red in the presence of calcite. It appears such that the large quartz grains have been cemented by calcite, where the alizarin red stained calcite is observed intergranular in the pore space (Figure 3.16b). This calcite cement is interpreted to be a late stage in diagenesis and to have significantly decreased the initial porosity and permeability of this facies. This interpretation is investigated in more detail in Chapter 4 which covers petrographic analysis and diagenesis. From core analysis, this facies has a porosity value of 13% and a permeability value of 0.003 mD from one core measurement. Based upon the source rock analysis conducted on the Colen 10-10 core, this facies has an average TOC of 0.77 wt %, with ranges from 0.5-0.99 wt %. From porosity and permeability measurements, an average  $R_{35}$  value of 0.38  $\mu\text{m}$  was calculated.

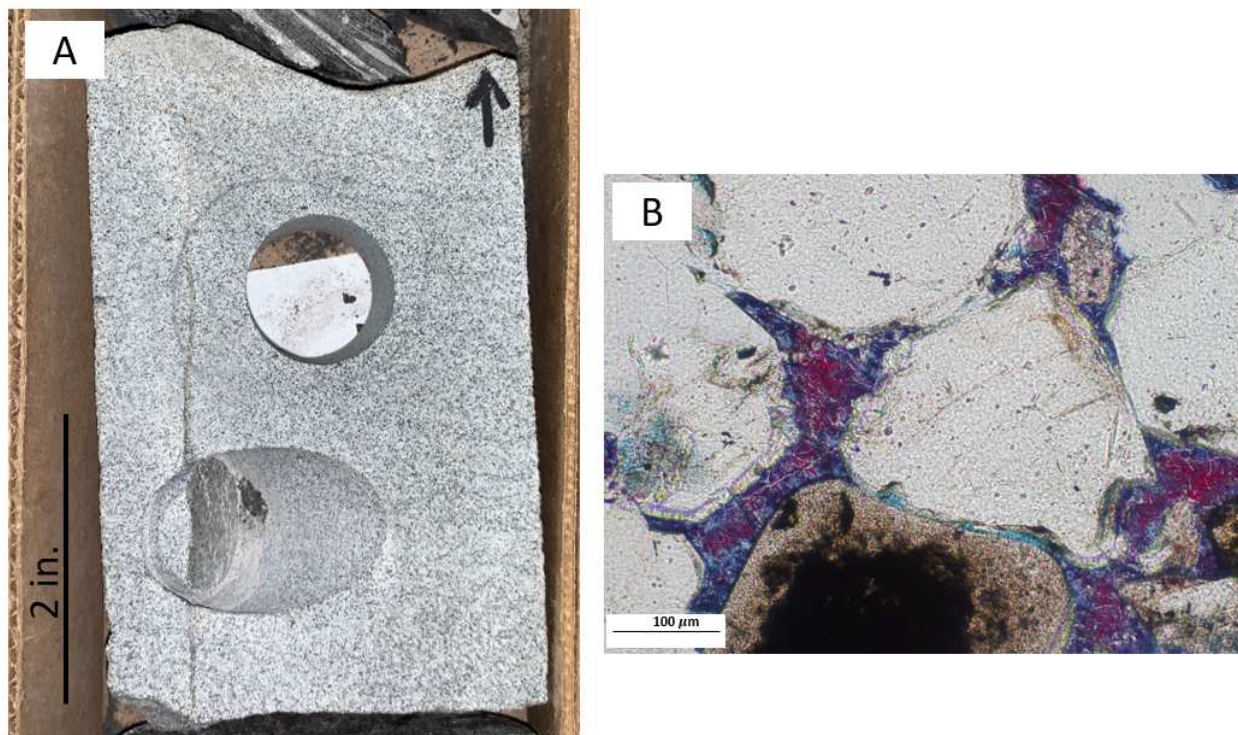


Figure 3.16: Facies 6: Medium-grained sandstone. A) shows a representative core photo of the sandstone facies. B) shows a representative photomicrograph of the facies in thin section at a depth at 5297 ft in the Colen 10-10 core.

### 3.4.7 Facies 7: Silty Argillaceous Mudstone

Facies 7 is a dark grey, silty, argillaceous mudstone (Figure 3.17). The mudstone beds are primarily composed of clay with an abundance of silt grains. In addition, the mudstone facies has several silt beds ranging from a few centimeters in size to two inches thick. This facies has minimal bioturbation, or a bioturbation index of 1, and no visible sedimentary structures. It mostly occurs 3-10 feet thick at the base of each flooding surface and marks the beginning of a new Turner depositional cycle after a rise in sea level. From core analysis, this facies has a porosity value of 10% and permeability value of 0.001 mD from one core based measurement. From these measurements, an average  $R_{35}$  of  $0.44 \mu\text{m}$  was calculated. Based upon the source rock analysis conducted on the Colen 10-10 core, this facies has a TOC value of 0.07 wt % from one core measurement. Although this facies has the lowest

porosity and permeability, it is interpreted to not act as a baffle for hydrocarbon migration or hydraulic stimulation.

From XRD it is composed of 58% clay and 38% quartz. The other 5% is composed of minor amounts of plagioclase, potassium feldspar, and other constituent minerals.

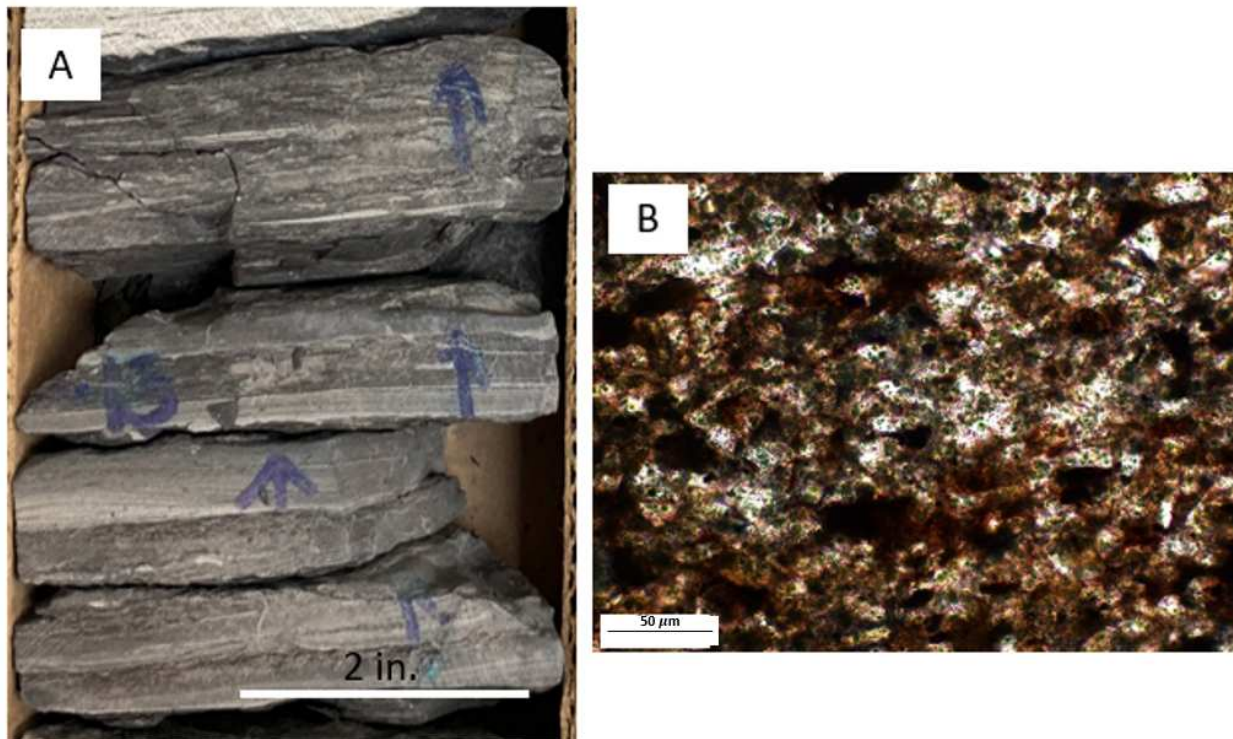


Figure 3.17: Facies 7: Argillaceous, silty mudstone. A) shows a representative photo of the mudstone facies. B) shows the facies in thin section at a depth at 4840 ft in the McTuillin Federal 1 core.

#### 3.4.8 Facies 8: Interbedded, Laminated, Sandstone, Siltstone, and Mudstone

Facies 8 is an interbedded, laminated, sandstone, siltstone, and mudstone (Figure 3.18). This facies occurs less frequently within the Turner interval, but is distinguished by its interbedded siltstones and sandstones. Planar laminations occur frequently within the sandstone beds in this facies. In addition to the lamina, flame structures were observed. The bioturbation index is small, BI=1, for this facies. From core analysis, this facies has a porosity value of 12% and permeability value of 0.05 mD from one core based measurement. From

these values an  $R_{35}$  value of  $0.43 \mu\text{m}$  was calculated for pore throat size radii. No source rock analysis was available for this facies, and only one data point was available for the mineralogy and rock properties of this facies.

From XRD, this facies is primarily composed of quartz and clay, 41% and 52% respectively. Also measured was 1% potassium feldspar, 2% plagioclase, and 1% calcite. The remaining 3% is made up of small amounts of other minerals such as pyrite and dolomite.

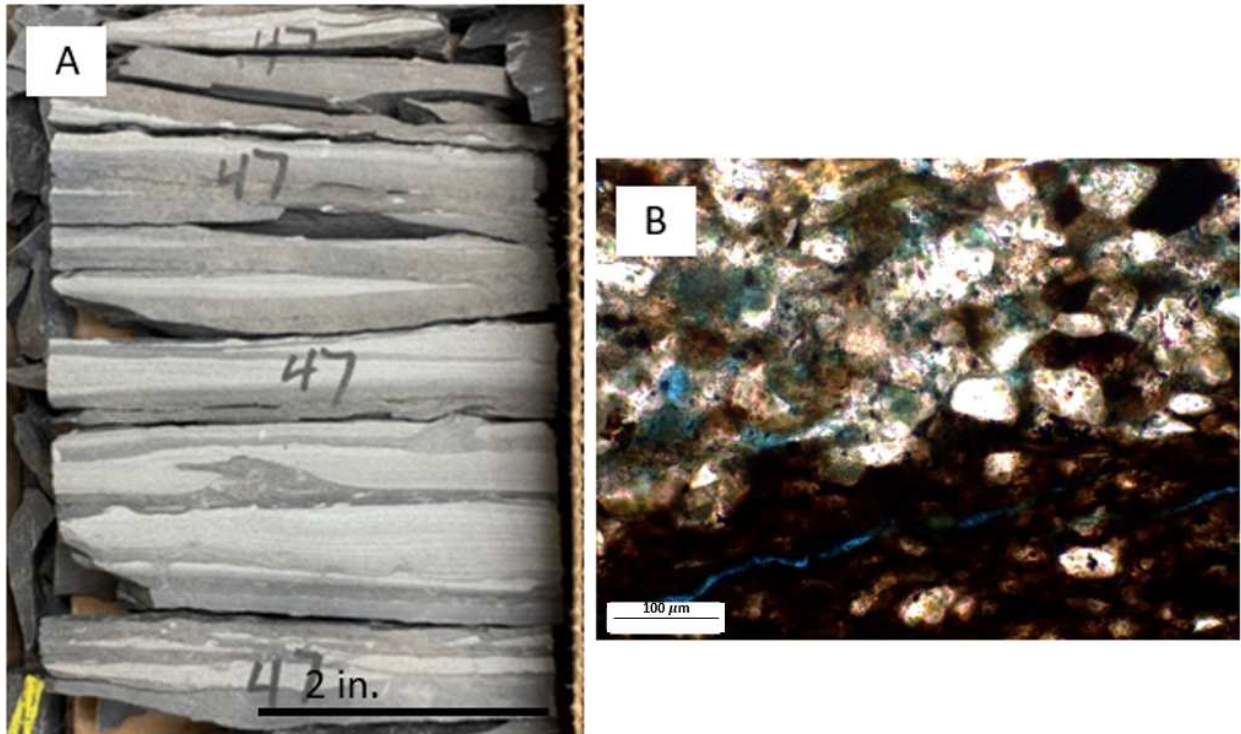


Figure 3.18: Facies 8: Interbedded, laminated, sandstone, siltstone, and mudstone. A) shows a representative core photo of the interbedded facies. B) shows a photomicrograph of the facies in thin section at a depth at 4838 ft in the McTuillin Federal 1 core.

### 3.5 Ichnology and Bioturbation

Bioturbation is present throughout the Turner stratigraphy in the Finn-Shurley Field cores with varying levels of bioturbation intensity and trace fossil types. Trace fossils and bioturbation intensity can give insight into the paleo-environment, sedimentation rates, paleo-topography, and overall energy levels. It is crucial to understand the distribution of bioturbation intensity and the type of trace fossils preserved within the rock to make interpretations and understand the type of environments these organisms were living in at the time of deposition.

For this study, a bioturbation index was assigned to each facies within the cores. Figure 3.19 shows the key for the bioturbation index used for this study, which is typically defined as a range between BI = 0, which shows no visible burrowing, BI = 3, shows moderate bioturbation, up to a BI = 6, which is complete bioturbation and homogenization of sediment (MachEachern and Bann, 2008). The trace fossils are coarse in scale and can be observed by the eye at the core scale rather than just at the microscopic level. A BI was assigned to each facies classified within this study and then related to depositional environment and even reservoir quality. The diversity, type, and abundance of trace fossils can be associated with different depositional environments, and by understanding the ichnofauna within each facies, assumptions can be made about the type of environment and changes in those environments during times of deposition (Figure 3.20)

Throughout the heterolithic Turner strata, the bioturbation index ranged from BI = 0-6 across the facies. Facies 1 (Bioturbation Index= 6), Facies 4 (Bioturbation Index= 4-5), and Facies 3 (Bioturbation Index= 3-4) had the highest intensity of bioturbation and contained the majority of the preserved trace fossils. Facies 1 is also interpreted to be a secondary reservoir facies having 14% porosity and greater than 0.1 mD permeability on average. Facies 4 is also interpreted to be a potential secondary reservoir facies having 14% porosity and greater than 0.15 mD permeability on average. Facies 1 and 4 also host the largest diversity of ichnofauna observed in the study area. Facies 3 is not interpreted to be

a potential reservoir facies for this study area. Although these three facies are all highly bioturbated, the trace fossils present within this facies and the intensity of bioturbation do not appear to always be detrimental to porosity or permeability. Typically, facies that have a higher diversity of trace fossils in the more intensely bioturbated intervals have preserved their primary porosity and permeability. In these intervals, the intensity has not diminished porosity and permeability significantly and have inhibited other diagenetic mechanisms from reducing it.

However, the largest control on trace fossil diversity is interpreted to be the flooding surfaces that correlate to changes in the Western Interior biozones such as the *Scaphites warreni* and the *Scaphites whitfieldi*. The most commonly observed trace fossils within the lower Turner one were *Skolithos* and *Planolites* suggesting overall a lower range of diversity (Figure 3.21). However, other trace fossils, such as *Asterosoma*, *Thalassinoides*, and *Teichichnus*, were observed in the lower Turner one, but not pervasive and occur locally in beds. The small range of diversity suggests a harsh sub-oxic to oxic, high energy environment, difficult for many organisms to survive in. Within the Turner two, the most commonly observed trace fossils were *Asterosoma*, *Thalassinoides*, and *Teichichnus* (Figure 3.21). Although those were the most commonly observed ichnofauna, *Skolithos* and *Planolites* were also identified within the Turner two zone (Figure 3.21). This suggests not only an overall higher intensity of bioturbation, but a much larger diversity of ichnofauna within the Turner two depositional cycle.




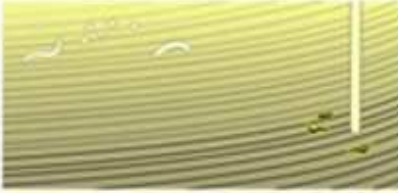

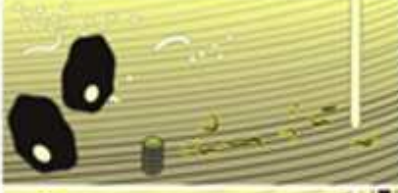


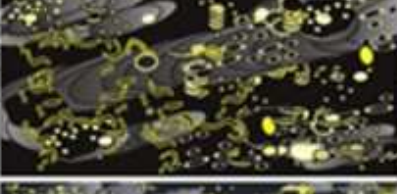



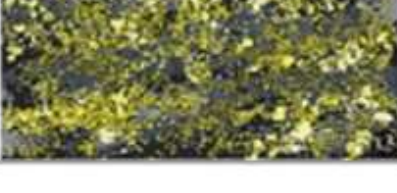

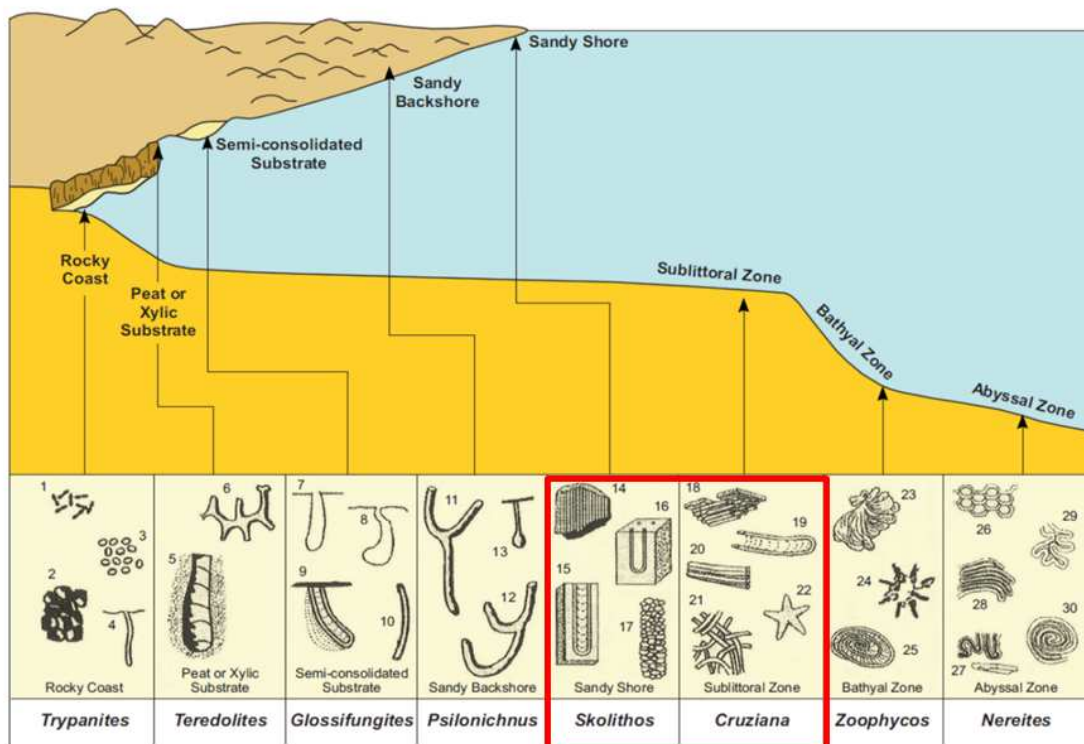
KEY TO BIOTURBATION INTENSITY			
BI	Characteristics	Mudstone Facies	Sandstone Facies
0	Bioturbation absent		
1	Sparse bioturbation, bedding distinct, few discrete traces		
2	Uncommon bioturbation, bedding distinct, low trace density		
3	Moderate bioturbation, bedding boundaries sharp, traces discrete, overlap rare		
4	Common bioturbation, bedding boundaries indistinct, high trace density with overlap common		
5	Abundant bioturbation, bedding completely disturbed (just visible)		
6	Complete bioturbation, total biogenic homogenization of sediment		

Figure 3.19: Bioturbation index key with a 0-6 scale. Modified from Reineck (1963), Taylor and Goldring (1993) and Taylor et al. (2003) by MacEachern and Bann (2008).





#### Distribution of Common Marine Ichnofacies

Typical trace fossils include: 1) *Caulostrepsis*; 2) *Entobia*; 3) echinoid borings; 4) *Trypanites*; 5) *Teredolites*; 6) *Thalassinoides*; 7, 8) *Gastrochaenolites* or related genera; 9) *Diplocraterion* (*Glossifungites*); 10) *Skolithos*; 11, 12) *Psilonichnus*; 13) *Macanopsis*; 14) *Skolithos*; 15) *Diplocraterion*; 16) *Arenicolites*; 17) *Ophiomorpha*; 18) *Phycodes*; 19) *Rhizocorallium*; 20) *Teichichnus*; 21) *Planolites*; 22) *Asteriacites*; 23) *Zoophycos*; 24) *Lorenzina*; 25) *Zoophycos*; 26) *Paleodictyon*; 27) *Taphrohelminthopsis*; 28) *Helminthoida*; 29) *Cosmorhaphis*; 30) *Spirorhaphis*.

Figure 3.20: Common marine ichnofacies. Modified from Seilacher (1954).

Overall, the dominant ichnofauna identified within the core are most typically associated with *Skolithos* and *Cruziana* ichnofacies, suggesting that at the time of deposition these organisms were living between the sandy upper to lower shoreface transitioning to the sublittoral zone. Seilacher (1954) interprets that the *Skolithos* ichnofacies is generally found in moderate to high energy environments, which makes it lower in diversity due to the inability for most organisms to survive in those kinds of environments. Seilacher (1954) also suggests that the *Cruziana* ichnofacies is characterized by much higher diversity, but lower energy environments. The majority of the *Skolithos* and *Planolites* ichnofauna occur within the lower Turner one, with the higher concentration of the *Cruziana* ichnofacies occurring within the lower Turner two cycle. These observations suggest that the first Turner depositional cycle

within Finn-Shurley was dominated by waning and waxing flows or tidal cycles, with alternating high, moderate, and low energy environments where only select organisms were able to burrow and thrive in these conditions. Following a major flooding surface and the end of a western interior biozone, this intermixed high and low energy environment shifted to a dominantly lower energy environment where diverse organisms could survive. In addition, the intensity of bioturbation is observed to increase as the section shallows upward within each depositional cycle. The facies with the highest intensity of bioturbation, Facies 1 and 4, occurs primarily at the top of each depositional cycle in all of the cores in the study area. This suggests that the environment is slowly transitioning from a highly stressful or high energy, yet oxic environment, to a less stressful, or lower energy, oxic environment. This could be indicative of the local sedimentation rates, progradation, changes in environment, or energy levels within each individual cycle.

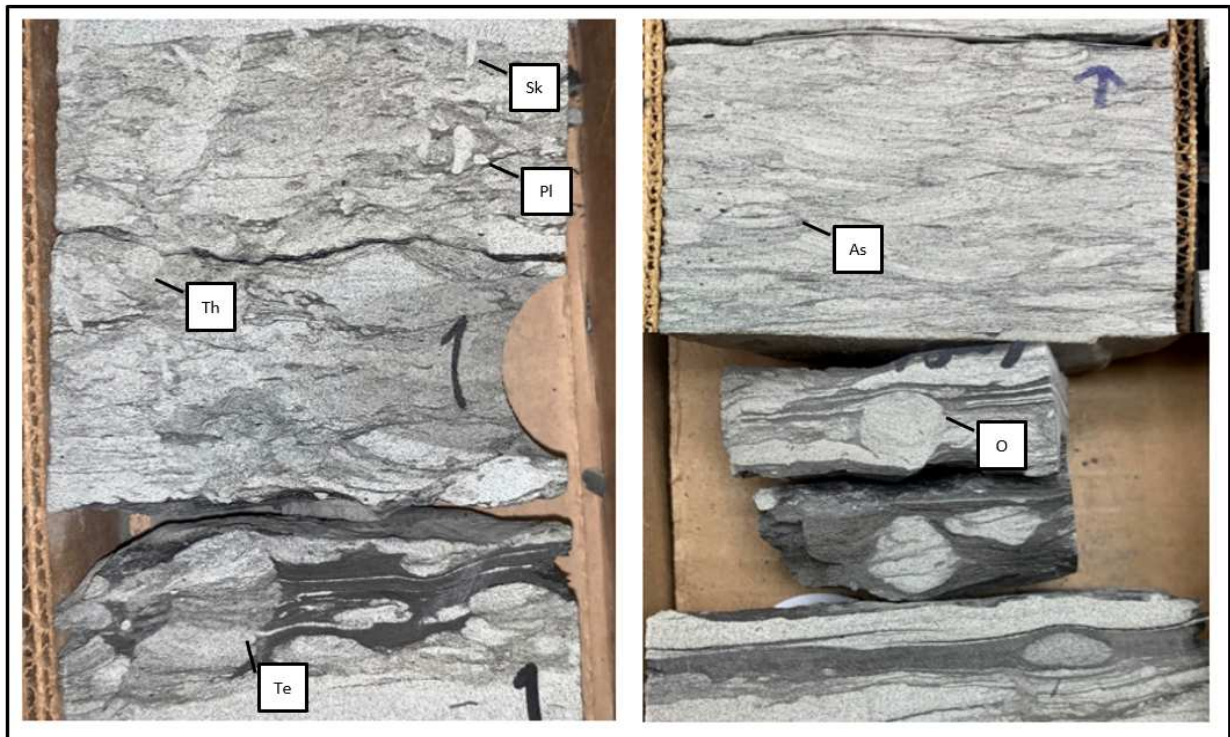


Figure 3.21: Core photos from the lower Turner two cycle. Most common trace fossils present include examples of *Skolithos*(Sk), *Planolites*(Pl), *Teichichnus*(Te), *Thalassinoides*(Th), *Asterosoma*(As), and *Ophiomorpha*(O).

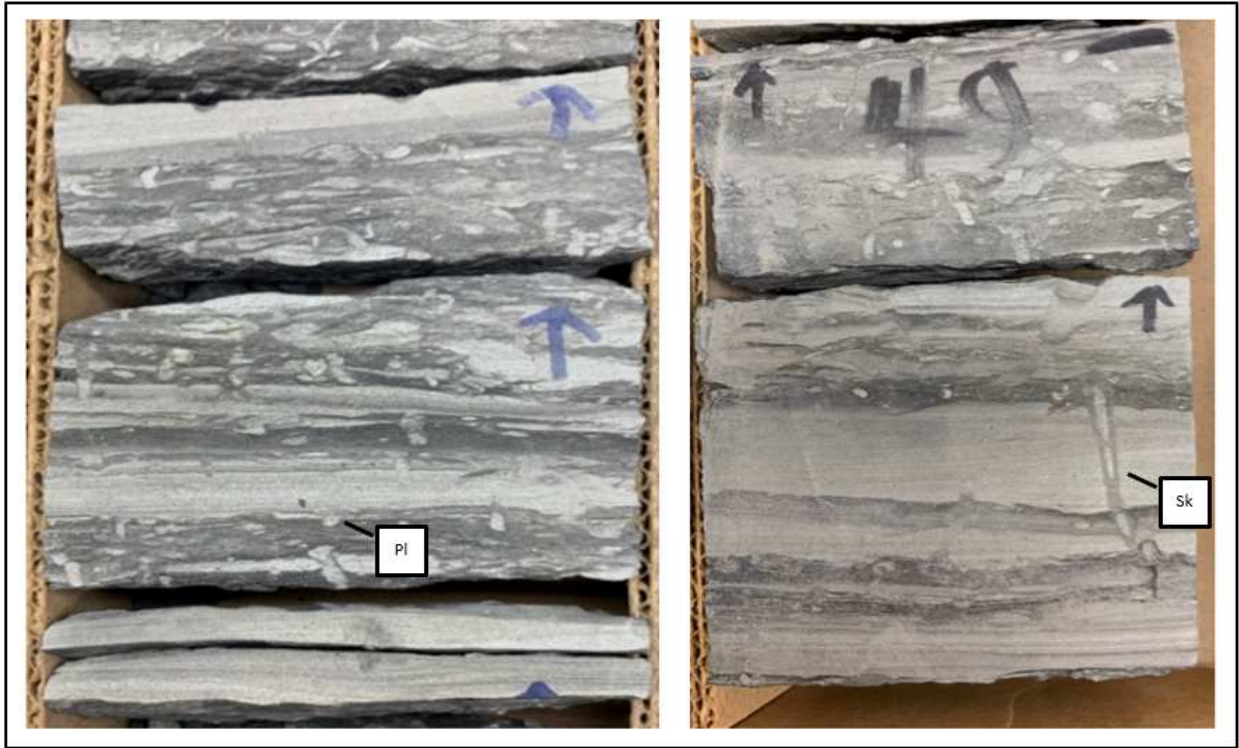


Figure 3.22: Core photos from the lower Turner one cycle. Most common trace fossils present include examples of *Skolithos*(Sk), and *Planolites*(Pl).

### 3.6 Sedimentary Structures

Sedimentary structure observations are critical for understanding the environment of deposition from interpreted depositional processes. The variety, consistency and preservation of sedimentary structures can give insight into the paleo-environment, energy levels, types of flow, and sedimentation rates. Within the Finn-Shurley cores in this study, several different types of sedimentary structures were present and preserved throughout the four cores, which aided in facies identification and depositional environment interpretations (Figure 3.23). Different depositional processes can result in various sedimentary structures. Some of the most common sedimentary structures observed in the four cores at Finn-Shurley include planar to low angle laminations, climbing and bi-directional ripples, hummocky or swaley cross stratification, wavy or flaser laminations, mud drapes, and mud rip-up clasts. The majority of the planar and wavy laminations as well as ripple and hummocky stratification were observed

in Facies 2 and Facies 5 in the cores. From the observed sedimentary structures, the main depositional processes responsible for sedimentary structures within the lower Turner sands are interpreted to include tides, storm events, and a lesser amount of hyperpynal flows.

Planar to low angle laminations are a result of high energy events or flows and can be interpreted to be associated with storm events within the Western Interior. As a result, laminations create thin scale, less than 1 cm, beds within the core (Figure 3.23d). Other sedimentary structures that are a result of storms are hummocky or swaley cross stratification (Figure 3.23f). Storm related structures were seen extensively throughout the core. In addition to storm structures, some of the other most common structures include wavy or flaser laminations, mud drapes, ripples, and bi-directional cross stratification (Figure 3.23). In general, these structures are associated with tidal processes or waning and waxing flows. Merewether (1980) observed in outcrop that the dominant paleocurrent direction from cross-beds and ripple marks was southeast.

It is also important to note that when any sedimentary structure in the Turner is preserved, they are amplified by the presence of thin mud laminations or mud drapes. Mud laminations occur less than a centimeter thick and cap laminated bed forms. This suggests either cyclicity with suspension settling, such a tides, or episodes of deposition with mud in the system. Mud beds also can occur up to 1-2 cm thick. When mud beds occur up to a few centimeters thick and are interstratified with fine sand beds, the mud is interpreted to have been deposited by dynamic deposition or hyperpynal flows along the shelf.

Rip-up clasts were also observed at the base of beds within the core. This suggests a high energy flow eroding semi-lithified mud beds as the suspended sediment moves basinward. In addition, the abundance of clean sandstones suggests that during the overall transgressive events, these sands were reworked by other processes such as tides and storms. The observed depositional processes across the Turner suggest that the Turner is a shallow shelf sand reworked by tidal processes and occurs below fair-weather wave base in order to account for the dominant storm event structures.

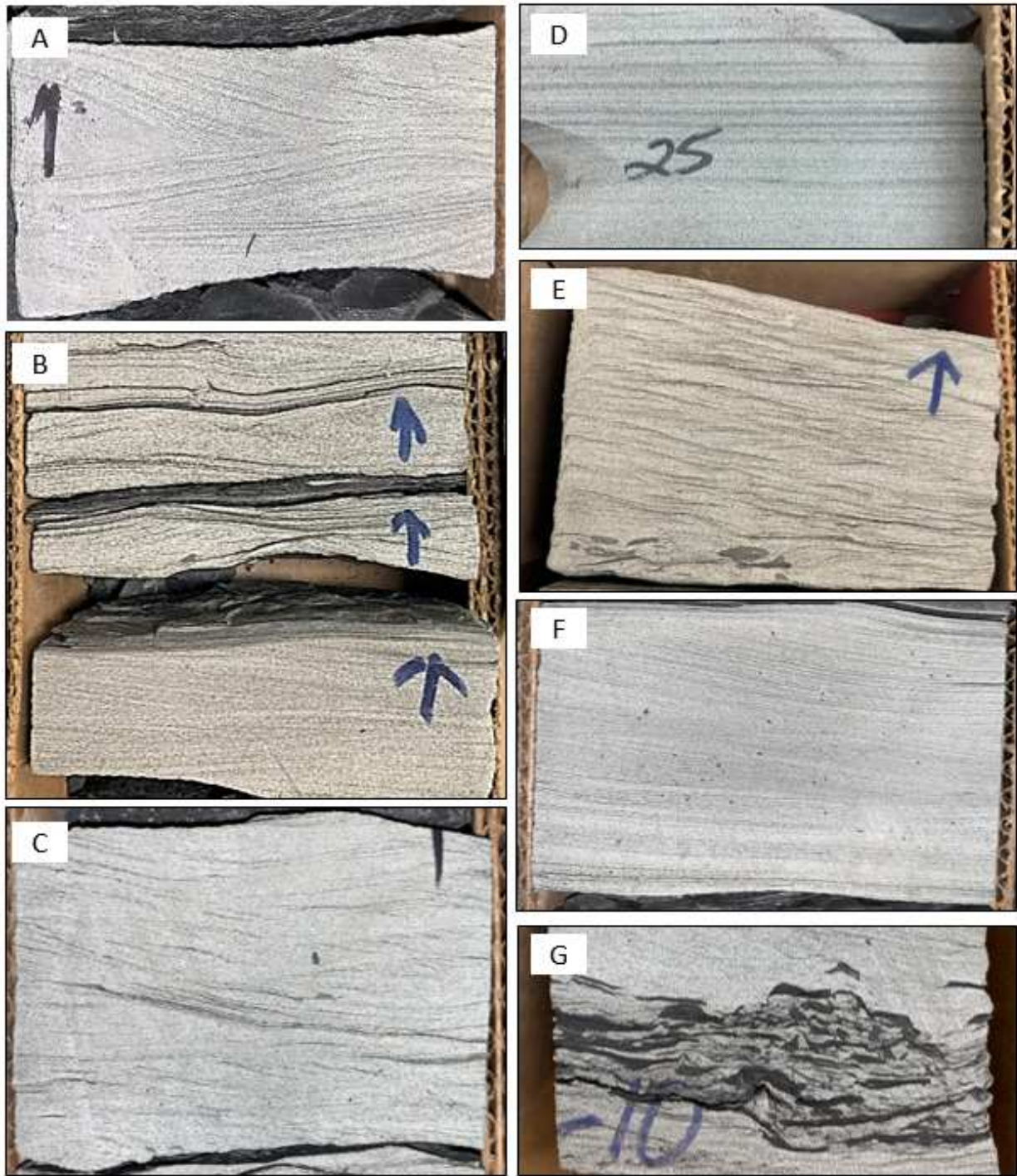


Figure 3.23: Observed sedimentary structures. A) bi-directional ripples B) wavy-flaser laminations C) ripple cross sets D) planar laminations E) climbing ripples F) hummocky or swaley cross stratification G) mud rip-up clasts.

### 3.7 Facies Distribution

Facies were identified and described in all cores in the study area for the Turner interval. All four wells were cored through some portion of the lower Turner stratigraphy, and the interpreted *S. warreni* flooding surface. Where the Perpetual Finn 8 was also cored through the interpreted contact between the upper and lower Turner, the *S. whitfieldi* flooding surface, and the Colen 10-10 was also cored through the contact with the underlying Poole Creek member, the Turonian unconformity.

Figures 3.24-3.26 shows the distribution of facies in the Colen 10-10, Perpetual Finn 8, Dreiling Federal 7, and the McTuillin Federal 1. Variability in facies distribution would suggest subtle changes in depositional environment across Finn-Shurley. Facies 1, 2, 3, 4, 5, and 7 are seen in all four of the wells ranging from 0.5 - 20 feet thick across the study area. Facies 6, and 8 only occur in two cores and range from 0.5 - 1 foot thick within their respective local section of the study area. Overall, the distribution of facies is relatively similar across the study area, where the subtle differences are likely due to the length of the cored interval, thickness of Turner in each core, and which depositional cycle was captured within the core. This suggests there is not significant lateral variability in facies distribution and this field at the time of deposition was a paleo-depocenter where sediment was deposited relatively uniform across the field. This paleo-depocenter could be a result of extra accommodation space from basement fault reactivation that occurs throughout the PRB. This lack of large lateral variability likely changes as we move further away from Finn-Shurley. Figure 3.24 shows the distribution of facies across the field north to south and east to west in each core. This figure is in the form of pie charts, which takes the total length of the core and shows the percentage of each facies within that cored interval. Figure 3.35 shows the distribution of the facies for the available cored interval of the lower Turner one zone and the lower Turner two zone (Figure 3.35). Figure 3.35 also illustrates the changes in facies assemblages across the *S. warreni* flooding surface.

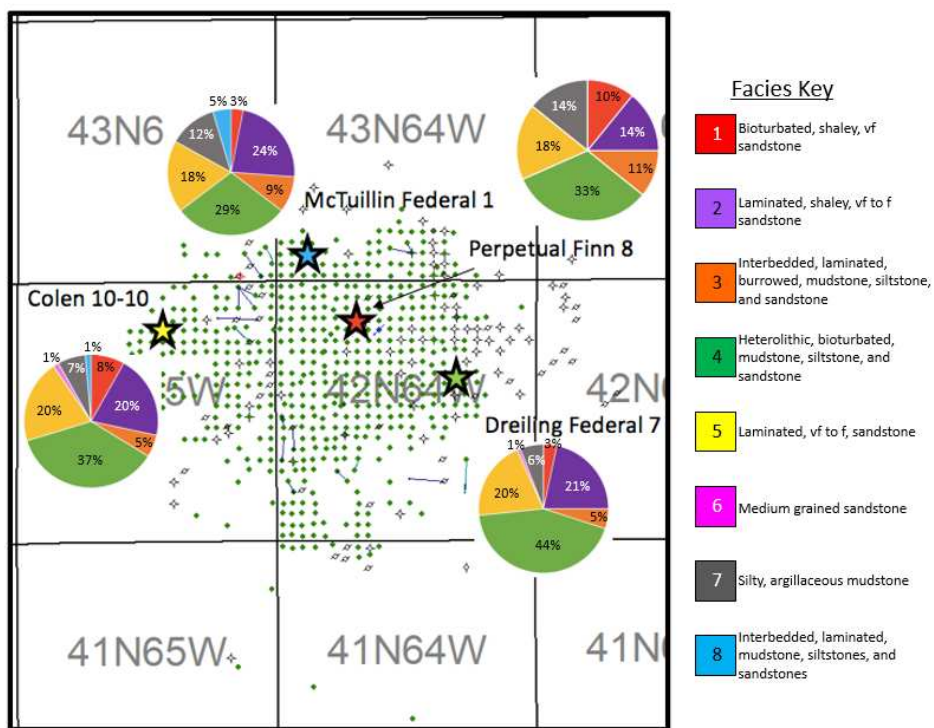


Figure 3.24: Pie distribution of facies in each core across Finn-Shurley.

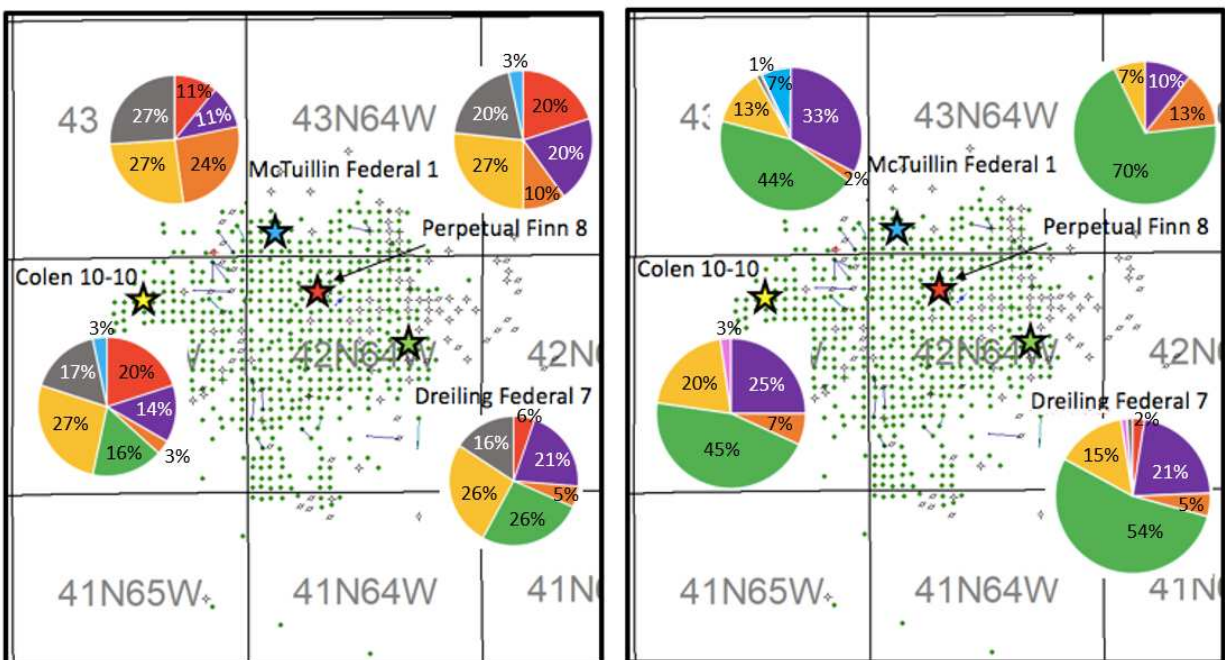


Figure 3.25: Distribution of facies across Finn-Shurley. Left shows the distribution of facies in the lower Turner two. Right shows the distribution of facies in the lower Turner one.

Figure 3.26 shows the lateral facies changes across the field and the vertical stacking trends of the described facies in all of the core. From four core descriptions, Facies 4, Facies 2, and facies 5 dominate the lower Turner one zone, and Facies 2, Facies 3, Facies 5, and Facies 1 dominate the lower Turner two zone. In general, the base of the cores are characterized by a significant section of Facies 2, a laminated, muddy, fine-grained sandstone with a small intensity of bioturbation, BI of 1-2. Moving up section, the stratigraphy is dominated by Facies 4, the heterolithic more heavily bioturbated, BI between 3-5, fine-grained sandstone, siltstone, and mudstone. This trend is pervasive through all four cores until approximately 10 feet below the *Scaphites warreni* flooding surface. At this point, the facies shift into a sandier and less bioturbated character with interbedded beds of either Facies 2, Facies 5, Facies 8, or Facies 3. This trend continues up until the *Scaphites warreni* flooding surface, or the top of the first major Turner depositional cycle. The beginning of the Turner two depositional cycle always begins with Facies 7, the argillaceous, silty mudstone that is anywhere from 3-10 feet thick. This cycle is then dominated by thin beds of intermixed facies, primarily Facies 5, Facies 3, and Facies 2, which are all facies where multiple preserved laminations with mud drapes occur. Again, a general increasing upward intensity of bioturbation is seen, with Facies 1, a heavily bioturbated (BI=6) facies, seen capping the tops of this cycle in the Perpetual Finn 8. These observations are summarized in Figure 3.25, these show the distribution of each facies of the cored interval in the lower Turner one and lower Turner two, respectively.



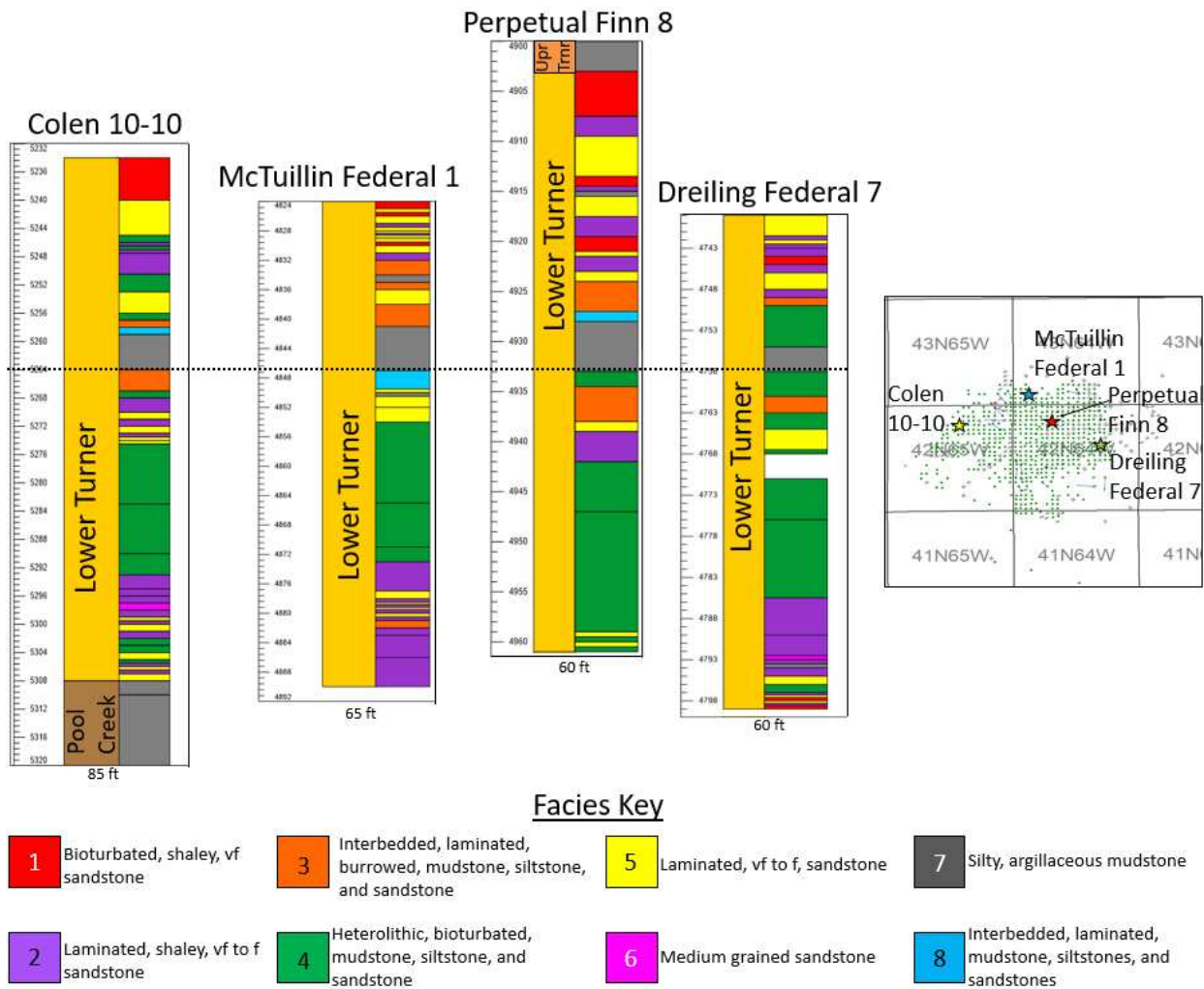


Figure 3.26: Vertical distribution of facies across Finn-Shurley. The black dashed line represents the *S. Warreni* flooding surface.

### 3.8 Subsurface Correlations

Nearly 750 wells were correlated across the study area using a suite of petrophysical well logs that included gamma ray, spontaneous potential, and resistivity. Figure 3.27 show a north to south stratigraphic cross section across the field that has been datumed on the top of the Turner. Figure 3.28 shows a east to west stratigraphic cross section across the field also datumed on the top of the Turner. The top of the Turner is marked by a decrease in gamma ray showing the transition into the sandstone beds from the overlying mudstones of

the Niobrara Formation. The base of the Turner is interpreted as a sharp increase in gamma ray where the Pool Creek member is interpreted to be present between the overlying Turner Sandy member, and the underlying Greenhorn Limestone bed. The Greenhorn Limestone is easily discerned on well logs as a 50 foot thick low gamma ray bed, making for an easy marker to pick across the study area. Overall, the Turner is approximately 130-150 feet thick across the study area, with a slight thickening in the central portion of the field. This suggests that this study area was a paleo-depocenter at the time of deposition. The Pool Creek member is the unit that experiences thinning moving across the study area. Mentioned previously, major flooding surfaces can be correlated in well logs throughout Finn-Shurley (Figures 3.27-3.29). Through the integration of core description, the *S. whitfieldi* and the *S. warreni* have been interpreted in well logs across the field. These were important surfaces to correlate to determine changes in rock quality and reservoir development across Finn-Shurley Field, and likely across the entire PRB. Minor flooding surfaces can be seen in the logs within the larger transgressive parasequences. However, these were not correlated across the basin as they are local events and do not appear to have any affect on fluid flow or variations in reservoir quality across these surfaces. In addition, the unconformity at the base of the Turner was interpreted across the field as it marks a change in stratigraphy at the base of the Turner and the top of the Pool Creek member.

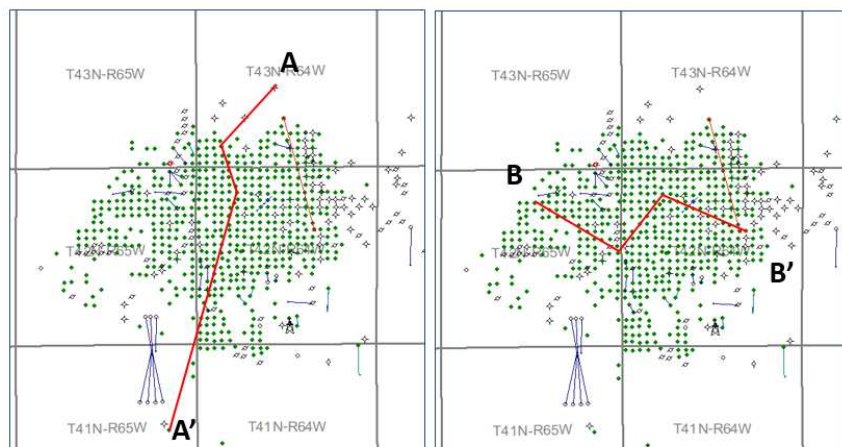


Figure 3.27: Surface map showing cross section A-A' and B-B'.

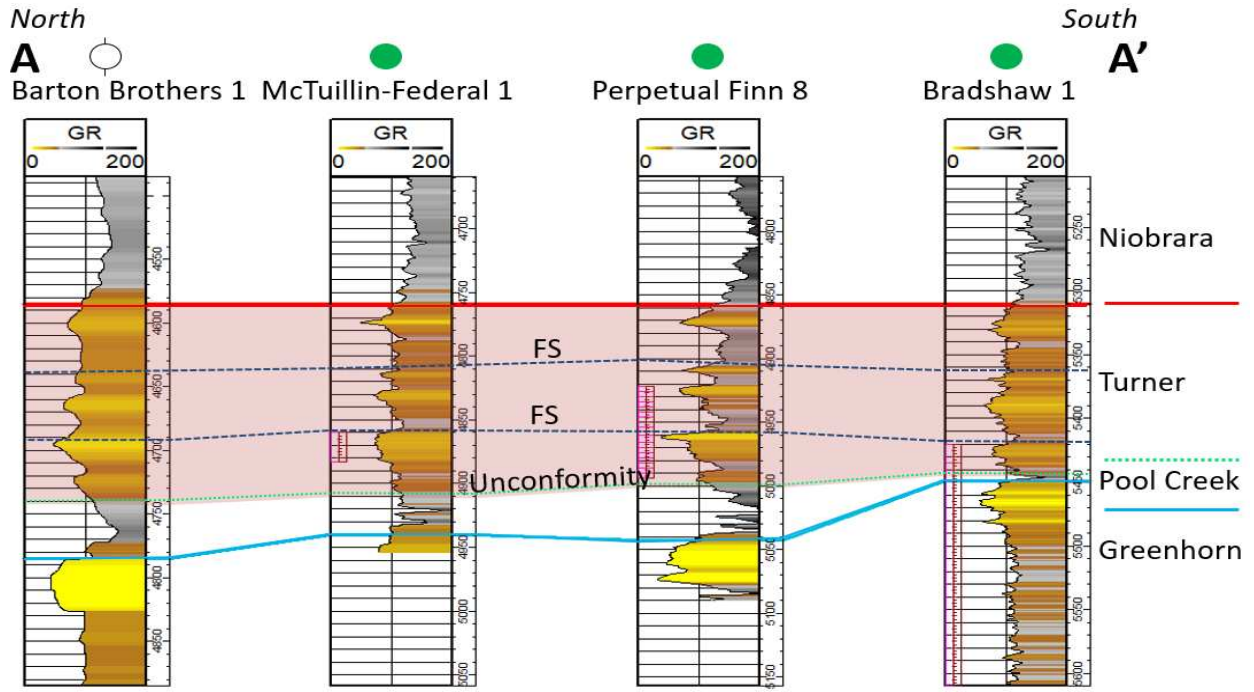


Figure 3.28: Subsurface stratigraphic correlation N-S across Finn-Shurley from A-A'. Flattened on the top of the Turner.

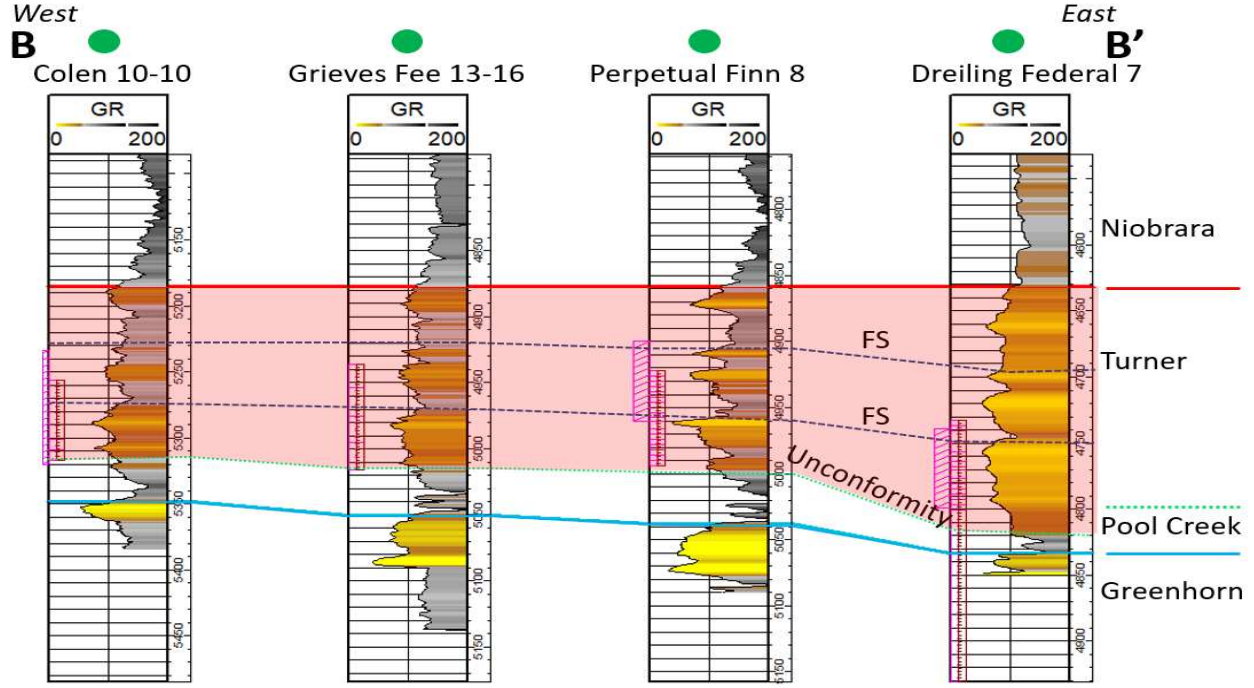


Figure 3.29: Subsurface stratigraphic correlation E-W across Finn-Shurley from B-B'. Flattened on the top of the Turner.

### 3.9 Elemental Geochemistry

In addition to core description, facies classification, XRD, and source rock analysis, elemental geochemistry can be an additional analysis to give insight into paleo-environment, mineralogy, and diagenetic character with the utilization of X-ray Fluorescence (XRF). This workflow is typically useful to discern fine scale detail of mudrocks to observe changes that are not able to be seen with a hand lens. However, due to the heterolithic nature of the Turner, it is an effective way to get a full elemental profile of the interstratified fine-grained sandstones, siltstones, and mudstones. By using elemental chemostratigraphy supplemented with XRD, indicators for not only various minerals, but environmental conditions, and element to mineral conversions can be integrated into the interpretations for the larger core data set and core based observations. XRD data points provide a basis to prove the validity of the XRF values for mineral conversion, which in turn allows for XRF to be used to interpolate between XRD data points once proven that the elements convert to minerals successfully.

Mineral indicators mean that XRF can be used in diagnosing carbonate and detrital systems. Observing intervals of elevated elemental indicators can suggest times of higher deposition rates, increased sediment supply, or intervals more affected by diagenetic processes. Carbonate system indicators include calcium (Ca), strontium (Sr), and manganese (Mn). These elements are unique to carbonate systems and are used to identify depositional carbonate processes and subsequent diagenetic processes. Detrital elemental indicators suggest influx of terrestrially derived sediments, these include aluminum (Al), potassium (K), titanium (Ti) and silicon (Si). K is found in potassium feldspars sourced from weathering of felsic igneous rocks. Zr is found in zircons and are detrital in nature. Ti is found as the major elemental constituent of rutile and sphene derived from terrestrial systems (Sage and Lyons, 2009). Not only can individual elements tell a depositional story, but the utilization of ratios of certain elements can be used to determine changes in provenance. The use of ratios, rather than individual elements, is preferred, as these are less likely to be influenced by changes in

grain size. Elements and ratios that are best for chemostratigraphic studies are those that are almost exclusively concentrated in heavy minerals and are largely unaffected by post depositional weathering and diagenesis (Craigie, 2018). P/Ti and related ratios can provide indications of provenance changes throughout deposition. In addition, observing high K/Al ratios suggest that K is predominantly linked with potassium feldspar. Furthermore, K/Rb ratios are higher in potassium feldspar than in illite and mica, so this parameter can be used to model the proportion of potassium feldspar to illite (Craigie, 2018). Other ratios that show changes in provenance and that were utilized in this study include Zr/Ti and Nb/Th.

In addition to using individual elements and ratios as a proxy for depositional systems, a mineral model can be created by converting XRF values to minerals by the use of element to mineral conversions summarized by Nance and Rowe (2015). This is done by using the overly simplified relationship that calcium is 40% of calcite, potassium is 6% of illite (Weaver, 1965), silicon averages 25% of illite, which has to be subtracted from total silicon before quartz is calculated (Mermut and Cano, 2001), and consequently silicon is 47% of quartz. These simple relationships allow for a comprehensive mineral model of clay, calcite, and quartz to be computed for the Turner using XRF data.

### **3.9.1 Colen 10-10 Chemostratigraphy**

For this study, 78 feet of the Colen 10-10 well was sampled at the USGS with a handheld XRF gun every 3 inches for 180 seconds, unless the core was missing, pucked, or broken where a reliable data point could not be recorded. The 78 feet of core that was sampled included 4 feet of Pool Creek, 44 feet of lower Turner one unit, and 30 feet of lower Turner two unit.

Figure 3.30 shows a plot of all the terrestrial indicators, Si, Al, Ti, K, and Ti/Al with the core description for the Colen 10-10. This plot shows the high amount of terrestrial input into the system during the entirety of the Turner deposition. The high values of elements in ppm suggest that there were significant amounts of terrestrial clays and quartz being deposited into the system. Figure 3.31 shows a plot of all the carbonate indicators, Ca, Sr,

and Mn with the core description for the Colen 10-10. The only spikes that occur in these elements are in areas where there are confirmed and interpreted as calcite cements, such as in Facies 6, the medium-grained sandstone. Areas of higher calcite suggest zones where diagenesis has affected initial porosity and permeability in the reservoir.

Figure 3.32 shows provenance indicators used in this study with the core description for the Colen 10-10. These include Nb/Th, K/Rb, Zr/Ti, K/Al, and P/Ti. Both the K/Al and K/Rb curves show areas of higher potassium feldspar, as higher values for this ratio suggest that the potassium is linked to feldspar rather than clays. Whereas lower values for this ratio show areas that are higher in clay. In general, it is observed that bulk changes in these ratios occur at boundaries of flooding surfaces, both minor and major. This suggests slight changes in provenance across these boundaries and could also be linked to changes in rock quality and facies successions.

Figure 3.33 shows the mineral model generated from XRF. This was computed by taking XRF elemental data and converting them to minerals based upon known mineral formulas for the three main constituent minerals, quartz, clay and calcite. The facies and lithology logs for the Colen 10-10 are available for comparison with the combined mineral model and the three curves separated out. The individual mineral curves are shown and compared to XRD data points to show the validity of the computed mineral percentage values. It shows that in general the XRF values closely correspond to the calculated values from XRD, and it is interpreted that the variation is likely due to the simplistic assumptions made in the calculation. In addition to element to mineral conversions, the XRF data was used to create a pseudo gamma ray log to compare to the petrophysical gamma ray. This means that in general, the simple assumptions create the ability to develop a full modeled mineralogical profile throughout the Colen 10-10 core and a pseudo gamma ray that closely resemble the XRD data and the petrophysical gamma ray log. However, a more detailed mineral model can be created utilizing oxides and more detail from the mineral formulas of different clay types.

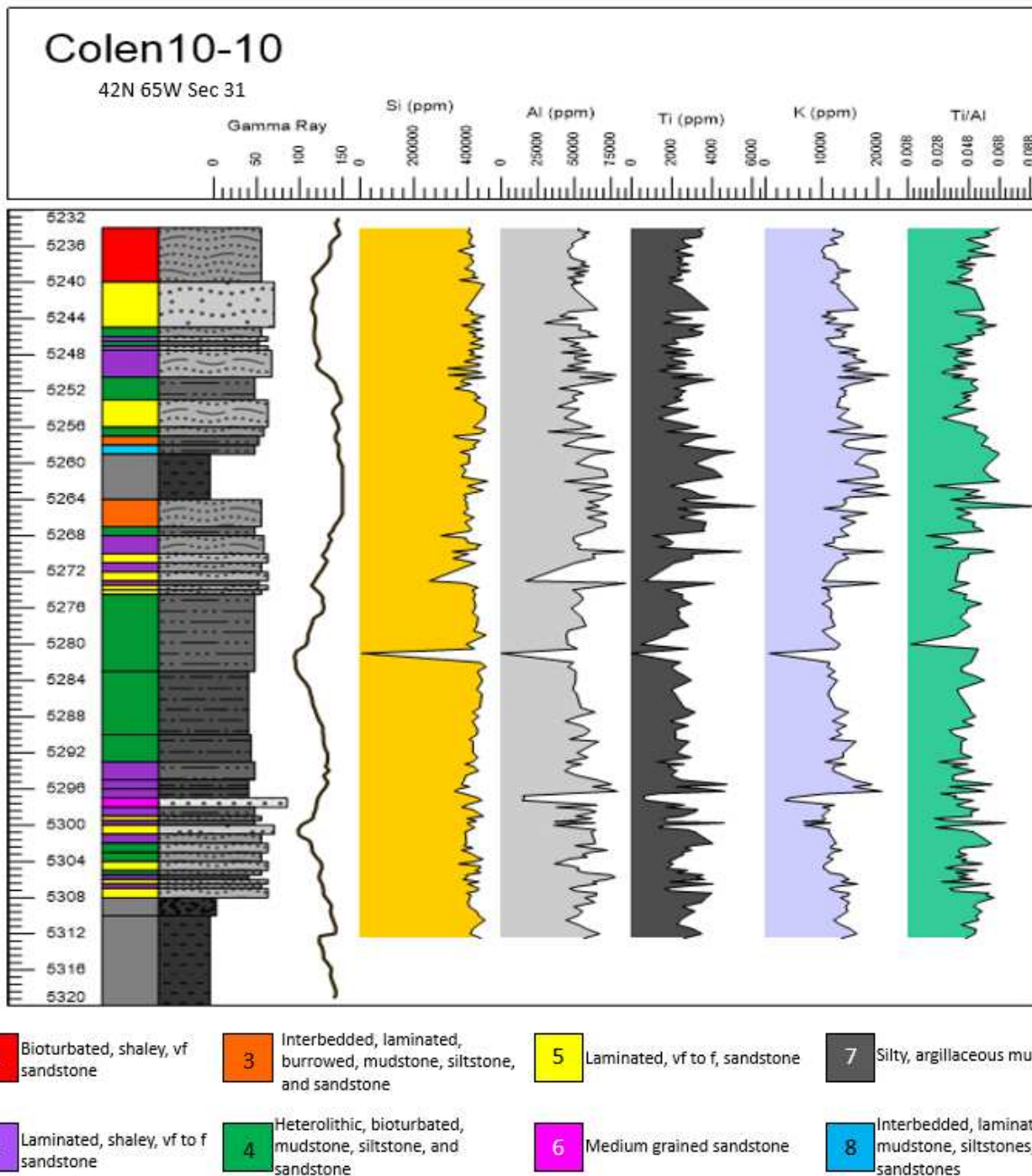
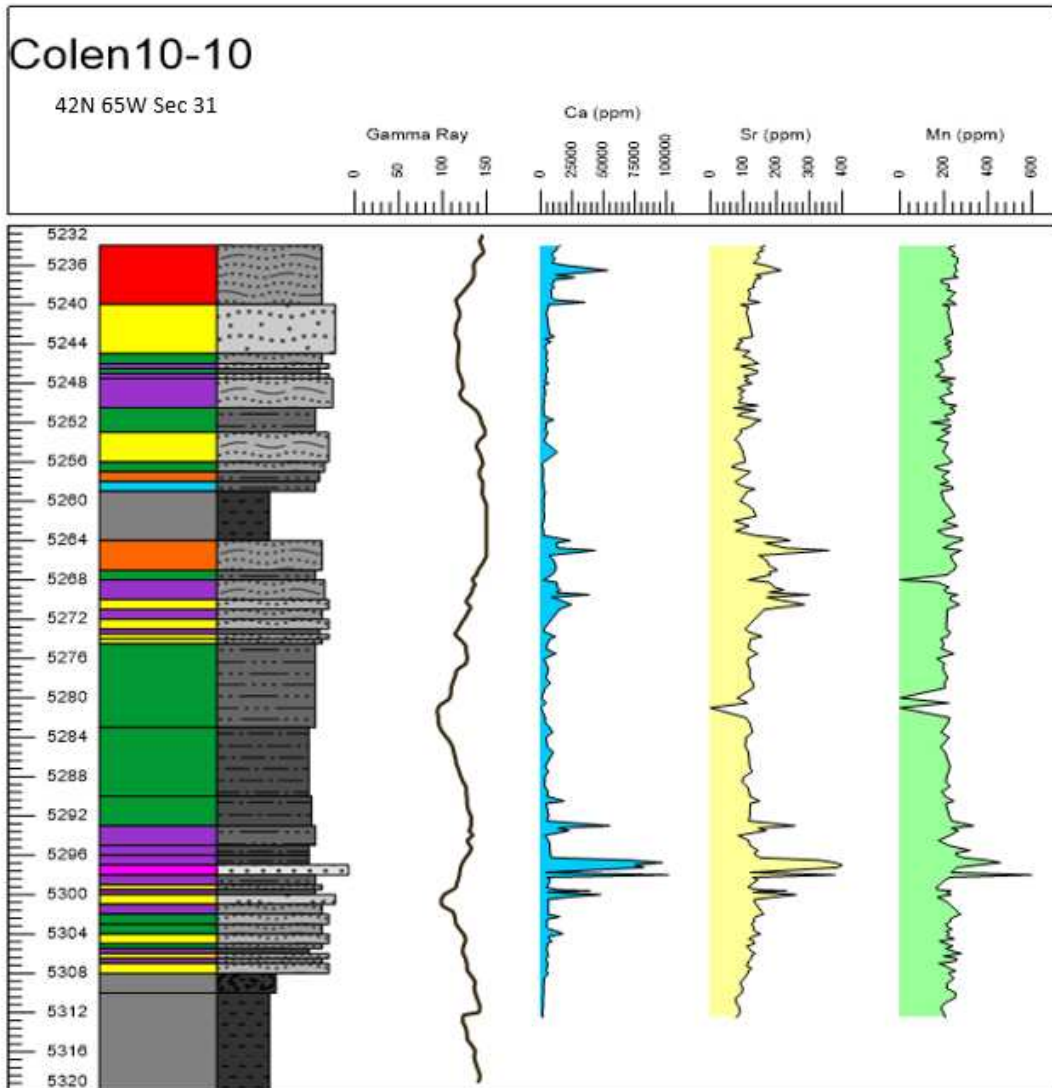


Figure 3.30: Detrital elemental indicators from XRF for the Colen 10-10 core. Included is a core facies log, a lithology log, a gamma ray curve, and curves for Si (ppm), Al (ppm), Ti (ppm), K(ppm), and a Ti/Al ratio.



- |  |  |   |  |
|--|--|---|--|
| <p><b>1</b> Bioturbated, shaley, vf sandstone</p>    | <p><b>3</b> Interbedded, laminated, burrowed, mudstone, siltstone, and sandstone</p> | <p><b>5</b> Laminated, vf to f, sandstone</p> | <p><b>7</b> Silty, argillaceous mudstone</p>                                 |
| <p><b>2</b> Laminated, shaley, vf to f sandstone</p> | <p><b>4</b> Heterolithic, bioturbated, mudstone, siltstone, and sandstone</p>        | <p><b>6</b> Medium grained sandstone</p>      | <p><b>8</b> Interbedded, laminated, mudstone, siltstones, and sandstones</p> |

Figure 3.31: Carbonate elemental indicators from XRF for the Colen 10-10 core. Included is a core facies log, a lithology log, a gamma ray log, and curves for Ca (ppm), Sr (ppm), and Mn (ppm).



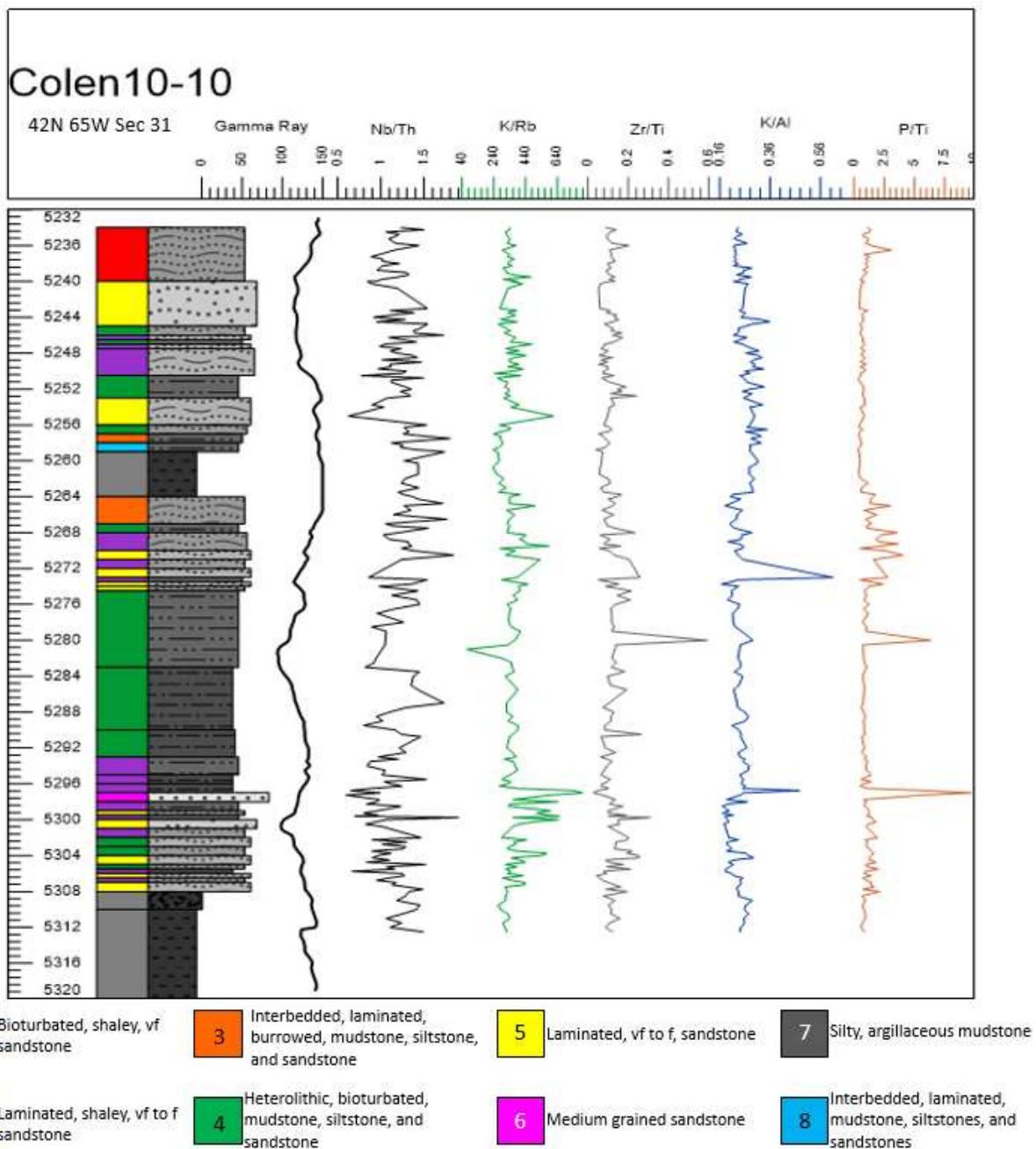


Figure 3.32: Provenance elemental ratios from XRF for the Colen 10-10 core. Included is a core facies log, a lithology log, a gamma ray log, and ratio curves for Nb/Th, K/Rb, Zr/Ti, K/Al, and P/Ti.

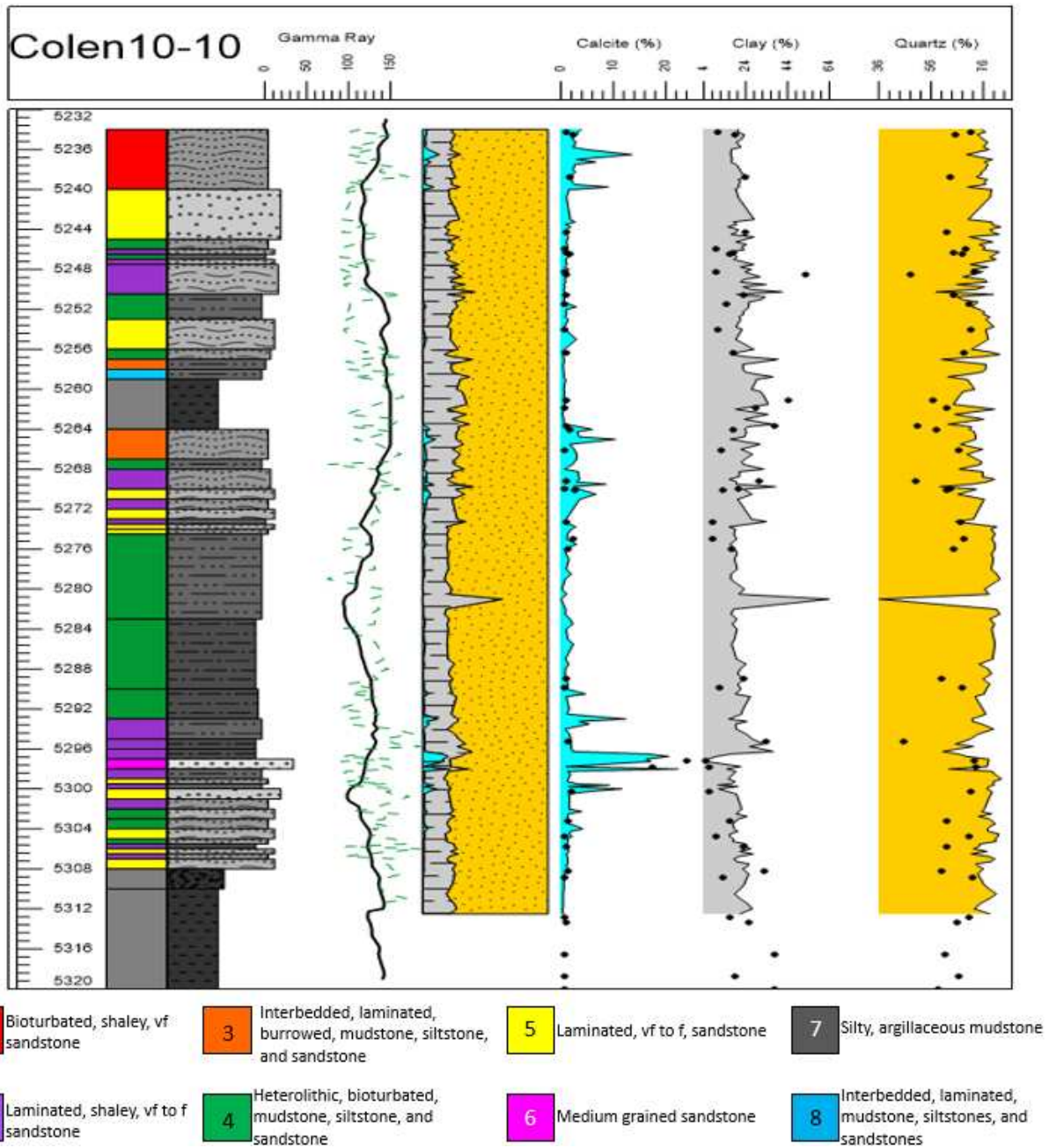


Figure 3.33: Comprehensive mineral model in weight percent generated from XRF for the Colen 10-10. Included is a core facies log, a lithology log, a petrophysical and pseudo gamma ray log, and mineralogy curves for calcite, clay, and quartz. Each individual mineralogy curve is then compared to XRD data points (black dots) for each mineral profile. A pseudo gamma ray log (green dashed line) is also calculated from K, U, and Th and superimposed on the petrophysical gamma ray log (black solid line).

### 3.9.2 Colen 10-10 Chemofacies Classification

Elemental geochemistry is a beneficial way to collect large quantities of data both quickly and inexpensively. XRF elemental profiles are a simple and effective way to determine trends and make conclusions based upon individual elements and elemental ratios. However, XRF data collection can be utilized and integrated in a way that provides insight into larger elemental trends as a collection of chemofacies. Chemofacies show much more detail and small scale variability in elemental enrichment's and depletion's through the vertical section than single element profiles. The application of these chemofacies can then be later tied to various reservoir properties such as porosity, TOC, mechanical strength, etc., if correlations can be found and proven. This study was a preliminary way to create a chemofacies workflow for sandstones from XRF data, meaning it was not integrated with reservoir properties as mentioned previously or similar to how it is typically used in mudrocks. This was considered outside the scope of this study and is included in further recommendations. However, this chemofacies study was compared to depositional facies classified from core to see if chemofacie had ties to core defined reservoir facies. This study agrees with Ramkumar (2015) in the definition of a chemofacies or chemozone as "the unique rock record defined by chemostratigraphic indices and recognizable through unique geochemical signature(s) which in turn helps distinction of a designated rock record from other rock records and also correlation with applicable analogs at appropriate/applicable spatiotemporal scale". Where chemofacies and chemozones are used synonymously in this study.

Due to the fact that the Turner is neither a mudrock nor self-sourcing, typical workflows for developing chemofacies in mudrocks do not work for this interval. Such as partitioning organophillic indicator elements or redox indicator elements for high TOC intervals. This study will attempt to develop a simple workflow that will create chemofacies based upon K-means clustering to understand the nature of the elemental relationships in the vertical section. K-means clustering is a method used widely in data analysis that partitions data based upon a notion of similarity (Wagstaff et al., 2001). Further information on the

mathematics and applications of K-means clustering analysis can be found in MacQueen (1967). The XRF data collected was loaded into a Python programming language platform and put through a dimensionality reduction, in order to compare all the elements at the same scale. This was important because there are a large range of ppm values across the data set that vary significantly between elements. Using a silhouette analysis, a method which visualizes similarity, the optimal number of clusters, where a cluster is a collection of data points aggregated together due to certain similarities, was concluded to be four. The amount of clusters will determine the number of chemofacies that will be generated and can be edited based upon an iterative processes for an individual dataset. This was supplemented with a principal component analysis (PCA) done in the Unistat software program for the dataset. Figure 3.34 shows an image from the PCA showing the determined cluster of elements that appear to have similar relationships. From this figure it appears that Si and the group of Ca, Sr, and Cl appear to have little to no relationship with the majority of the other elements, but are considered critical elements in this lithology. In general, four groupings of elements emerge from this image, which supplements the silhouette analysis conducted. During the K-means clustering analysis, the goal was to create a set number of chemofacies that vary in enriched and depleted elements in order to best see lithologic trends. Figure 3.35 shows a vertical log plot of every individual elements measured from the XRF, the calculated euclidean distance, the generated chemofacies log, and the depositional facies log. The euclidean distance measures the distance of each element from the cluster center as a means to compare similarity. Large changes in the euclidean distance value then generates different chemofacies. This creates four chemofacies that have different enrichment and depletion values for each element measured from XRF.

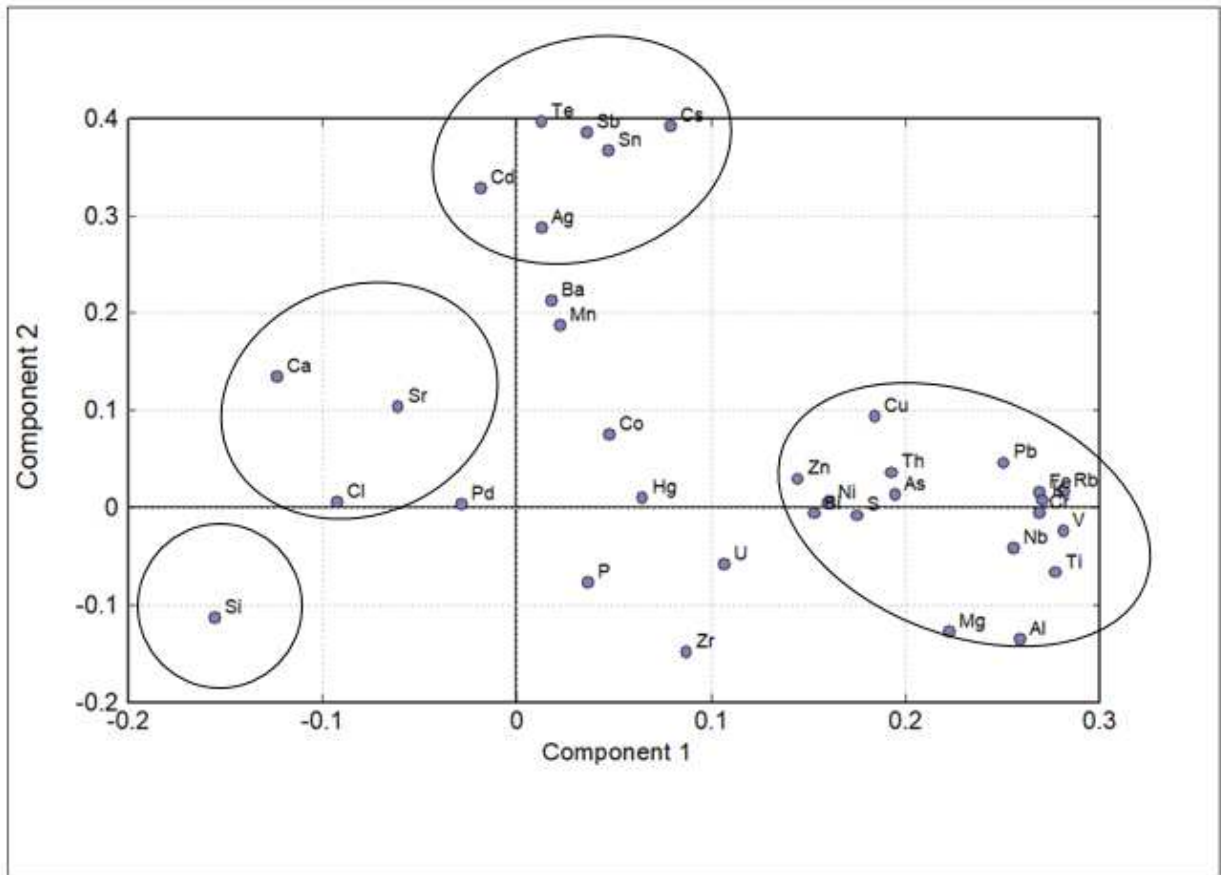


Figure 3.34: PCA analysis image showing the interpreted general clusters and trends of elements in two dimensions.

Once the four chemofacies have been created from the K-means analysis, the elemental signatures that make each chemofacies unique, the enrichment and depletion of each element, is the next critical part to understand. Figure 3.36 is a bar graph of each classified chemofacies that shows enrichment in green, and depletion in red. Enrichment or depletion of an element is based upon how much that value for the individual element varies from the median data point. Each chemofacies is defined based upon the specific set of elements whose concentration in ppm appear higher or lower than the average ppm value for that cluster. This allows for classification of chemofacies to make assumptions and interpretations about the lithology from a chemostratigraphic framework. Chemofacies 1 is enriched in Ca and slightly in W and depleted in Mg, Si, P, Al, S, K, Ti, Fe, and Zr. Suggesting

this chemofacies will occur where there is an elevated amount of calcium in the rock, likely as detrital calcite or diagenetic calcite cements in the fine-grained sandstone. Chemofacies 2 is enriched in Si, Cl, and Ca and depleted in Fe, Ti, K, S, Al, P, and Mg. This suggests this chemofacies will occur in areas that correspond to slightly silty and muddy, fine-grained sandstones in the core. Chemofacies 3 is extremely depleted in Si and Ca, and enriched in Zn, Ni, Co, Fe, Mn, Cr, V, Ti, K, S, Ba, Al, P, and Mg. It is most extremely enriched in Al, Fe, Mg, Ti, K, and S, and extremely depleted in Si. This suggests these facies are dominantly mudstone or clay rich intervals. Chemofacies 4 is extremely enriched in Si, and some Ca and is depleted in Mg, P, Al, S, K, Ti, and Fe. This suggests this chemofacies is a response of the cleanest sandstone facies where it is dominantly silica and suggests micro-crystalline authigenic quartz grain coats contributing to the high silica concentration. Based upon these observations, chemofacies 2 and 4 would align best with the characteristics of the better reservoir facies and would likely make for better target zones. Figure 3.35 shows the distribution of the chemofacies defined in Figure 3.36 compared to the core defined facies, where the best reservoir facies are colored in yellow, purple, green, and red. In general, the highest concentration of the best core reservoir facies occur below the *S. warreni* flooding surface. Chemofacies 2 and 4 are interpreted to coincide with the best reservoir facies, and agrees with the observation that the highest concentration of these facies occur in the lower Turner one.

Chemostratigraphy as a correlation technique is a powerful tool to analyze small scale changes in elemental data that can be tied to larger depositional, mineralogical, and diagenetic trends. This understanding can be integrated into reservoir targeting with the correct application. Although this workflow is preliminary and requires even more iterative work, the workflow is successful in generating chemofacies based upon a statistical analysis. With further understanding of elemental relationships in the Turner, this workflow can be refined to then tie to reservoir properties such as diagenetic signatures, high porosity zones, and even mechanical properties to the chemofacies for enhanced targeting and reservoir understanding.

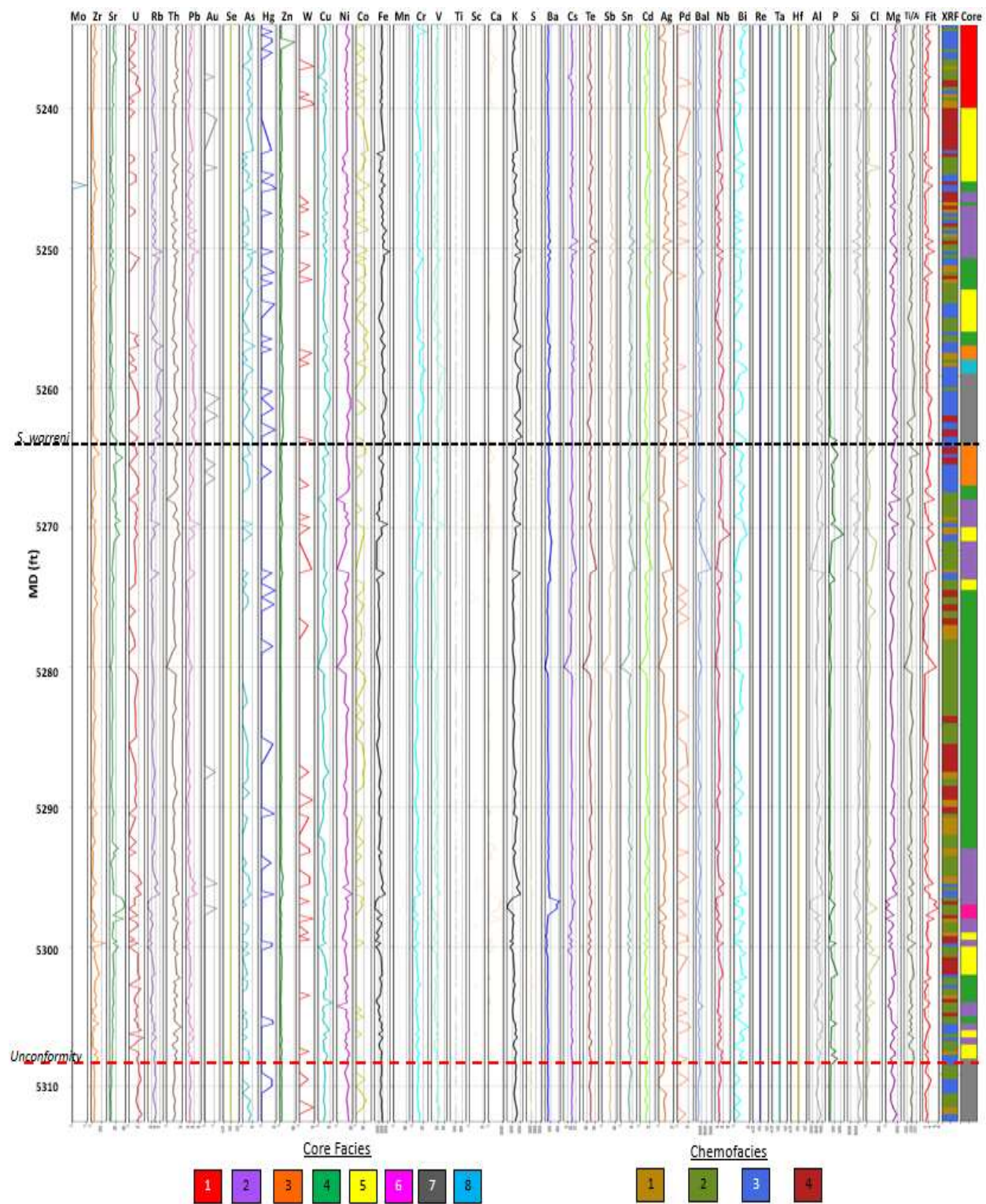


Figure 3.35: Log plot of raw XRF data in ppm for each element through the vertical succession of the Colen 10-10 core. Also included is the euclidean distance from data average (FIT), vertical chemofacies log (XRF), and core description facies log (CORE).

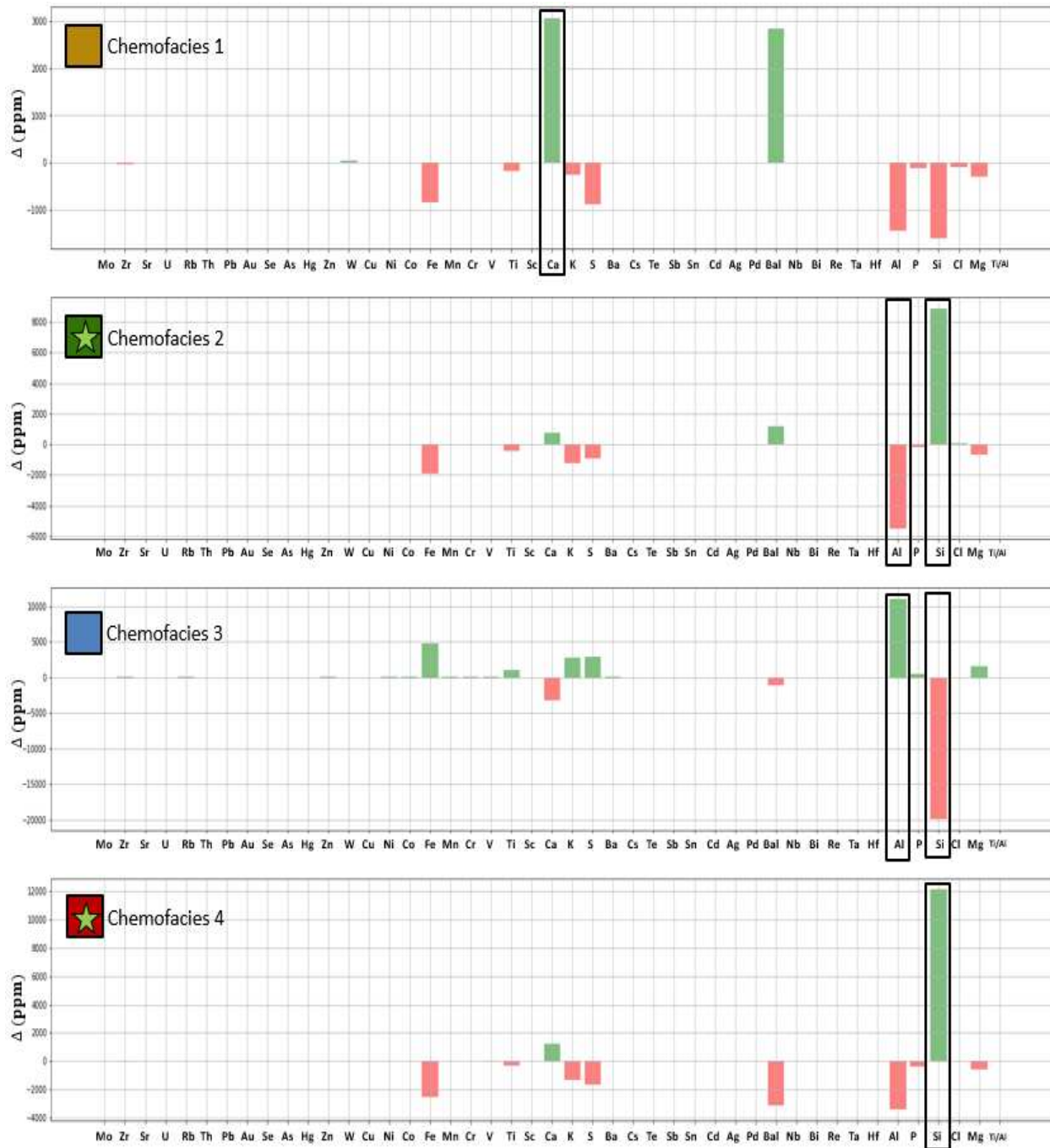


Figure 3.36: Bar graph that shows the enrichment or depletion of each element for each defined chemofacies for the Colen 10-10. Enriched elements are in green, depleted elements are in red. Elements in black bars was the largest enrichment or depletion used to classify chemofacies. Chemofacies 2 and 4 are enriched in Si, with lower concentrations of Ca and Al, which correlate with better reservoir quality facies (green star).



## CHAPTER 4

### PETROGRAPHIC ANALYSIS

#### 4.1 Petrographic Analysis Overview

This chapter focuses on the investigation of the Turner Sandy member at the microscopic scale to best understand mineralogical and diagenetic controls on the mechanical and reservoir quality at Finn-Shurley field. Through the utilization and integration of thin section and Field Emission Scanning Microscopy (FE-SEM) analysis, a thorough and detailed investigation of the framework and matrix mineralogy will be conducted. FE-SEM photomicrographs include backscatter images, secondary electron images, EDS mineral maps, and cathodoluminescence images. This analysis requires observing grain size, textures, and morphologies in order to document the extensive diagenetic history for the Turner interval. The pore network of the rock, including pore types, geometry, and size, can be best captured at this scale to understand the controls on hydrocarbon production in the reservoir. It is also important to note that although source rock properties were measured for the Colen 10-10 core, including total organic carbon content (TOC), S1, S2, S3, and Tmax, the petrographic analysis discussed in this chapter is primarily focused on investigating the reservoir and mechanical properties, such as mineralogy, diagenesis, and porosity. Even though there is a potential for organic matter to occur within the Turner, this interval is not believed to be self sourcing and is primarily sourced from both the Mowry and the Niobrara Formations. The Turner source rock will be discussed in more detail in Chapter 5 which covers reservoir characterization.

Although a few petrographic studies have been conducted in the chronostratigraphic equivalent Wall Creek Member of the Frontier Formation in the Western PRB, little has been published about the petrography of the Turner Sandy member of the Carlile Shale. This chapter will help piece together the diagenetic history of the Turner in Finn-Shurley

Field through the integration of previous work, thin section photomicrographs, and FE-SEM analysis. Merewether (1980) made some observations in the Turner near Osage, Wyoming, approximately 30 miles outside of Finn-Shurley Field. From SEM observations, authigenic minerals such as quartz, feldspar, kaolinite, chlorite, and pyrite were present in the Turner. From thin section observations, Merewether (1980) reported angular to sub-rounded grains of quartz, chert, and feldspar, where the more angular grains are due to later replacement of clay and calcite. Almon and Tillman (1979) conducted an extensive study that analyzed the petrography of reservoir and non reservoir facies within the Wall Creek member of the Frontier Formation in Spearhead Ranch Field. From this study, a paragenetic sequence was created that summarizes the diagenetic history of the Wall Creek member (Figure 4.1). The diagenetic stages that make up the reservoir and non-reservoir facies of the Wall Creek member began with early chlorite coating of framework grains and continued chronologically with quartz cementation from secondary overgrowths, feldspar leaching, illite/smectite development, late calcite cements, and concluded with hydrocarbon emplacement in the reservoir facies.

Due to the fact that the Wall Creek member is a time equivalent formation to the Turner Sandy member, the study by Almon and Tillman (1979) was used as an analog when researching the regional background and previously studied diagenetic stages that occur within the mid Turonian sediments in the PRB. These analog studies can give insight into the regional effects the environment can have on the diagenetic stages that occur during compaction and burial. However, variations from the Frontier petrographic studies were expected to be observed and documented, but by being aware of the diagenetic stages of time equivalent stratigraphy, diagenetic textures and cements can be properly timed and interpreted.

Through the integration of thin section and FE-SEM photomicrograph observations, the major diagenetic features documented for the Turner interval include early framework grain coating of both chlorite clays and authigenic microcrystalline quartz, dissolution of

feldspars and quartz by pressure solution, large quartz overgrowths, authigenic clay growth, and late calcite cementation of available pore space. Microscopic observations suggest that these occurred at various stages throughout the rocks burial history, which have aided in generating a comprehensive paragenetic sequence for the diagenetic history of the Turner.

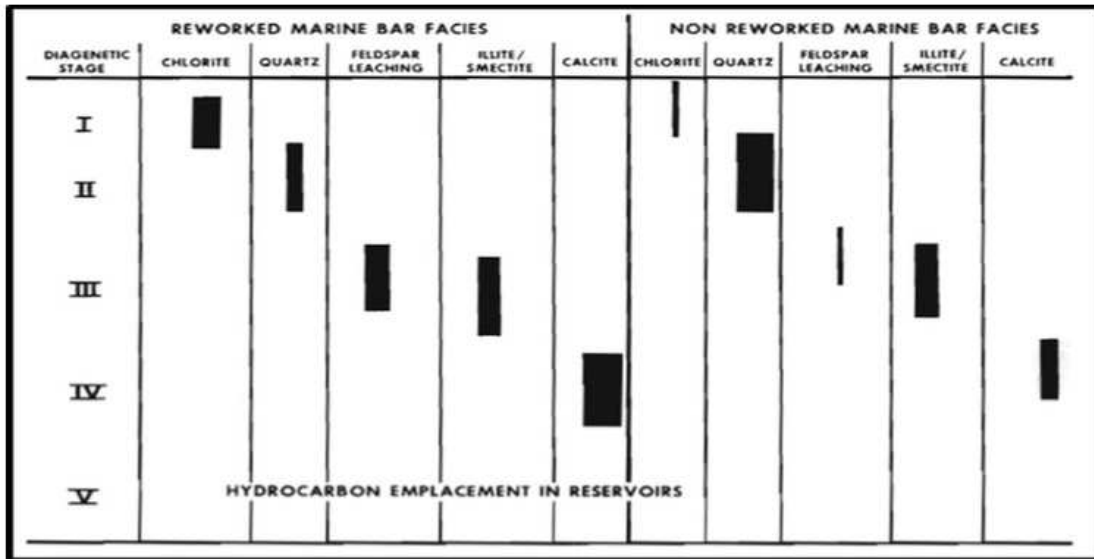


Figure 4.1: Paragenetic sequence of the Wall Creek member of the Frontier Formation from Almon and Tillmon (1979).

## 4.2 Thin Section Analysis

Forty-eight thin sections were made available from the USGS CRC for the purpose of this study. The vintage and preparation process of these samples is unknown. Of these thin sections, 28 sampled depths were from the McTuillin-Federal 1 core, and 20 sampled depths were from the Colen 10-10 core. Statistically, 48 sampled depths can give a fairly detailed microscopic profile throughout the lower Turner. However, due to the heterolithic nature of the stratigraphy, more thin sections were necessary for the overall characterization. Therefore, an additional six thin sections were made, three from the Colen 10-10 core, and three from the McTuillin-Federal 1 core, to give a better profile of specific reservoir and non-reservoir facies. These reservoir and non-reservoir facies were selected to further

investigate the ability to see porosity and diagenetic features in thin section. By creating new thin sections, better observations can be made about any visible porosity in the rock, with the introduction of a yellow-fluorescent dye to the thin sections during preparation. This preparation process enhances pore size and shape within the rock matrix that allows fluid flow by the addition of a yellow dye which fluoresce brightly under UV light. The suite of thin sections available for this study can help integrate the mineralogy and the rock fabric to the reservoir quality, as well as investigate diagenetic effects and determine the paragenetic sequence.

Thin section analysis was vital to this study, due to the fine-grained nature of the Turner. Much of the information that is necessary to understand the Turner was too small to be observed at the core scale. By documenting the framework and matrix mineralogy, including textures, fabrics, and diagenetic indicators, assumptions can be made about the microscopic scale controls on reservoir quality. Depending on the size and measurability of each control factor, it can then be scaled up to be measured at the core scale. Major observed diagenetic features in these rock examples contain chlorite coatings of silica grains, quartz overgrowths, calcite cements, feldspar dissolution, and quartz dissolution due to pressure solution. From petrographic observation, chlorite grain coats precede quartz overgrowths, which are only visible in the cleaner and coarser sand intervals and facies. Figure 4.2 displays high porosity from a lack of quartz overgrowths due to the abundance of early chlorite grain coatings. From XRD, a higher percentage of chlorite is observed in the cleaner, sandier, less muddy facies where more porosity is observed. Clay coatings are interpreted to occur during early diagenesis, before 80-100 degrees C. The chlorite occurs early in the diagenetic paragenesis and is known to inhibit the growth of pore-filling syntaxial quartz overgrowths, which decrease porosity (Cecil and Heald, 1971). From thin section analysis, the chlorite appears to form rims around quartz grains which look like a green/brown rim between the quartz grain and the pore filled with blue epoxy (Figure 4.3). Figure 4.4 shows quartz cements occurring in what appears to be initial pore space, suggesting the grain coats did not cover the entire

surface of the grain, allowing for secondary quartz overgrowths to grow in the pore space.

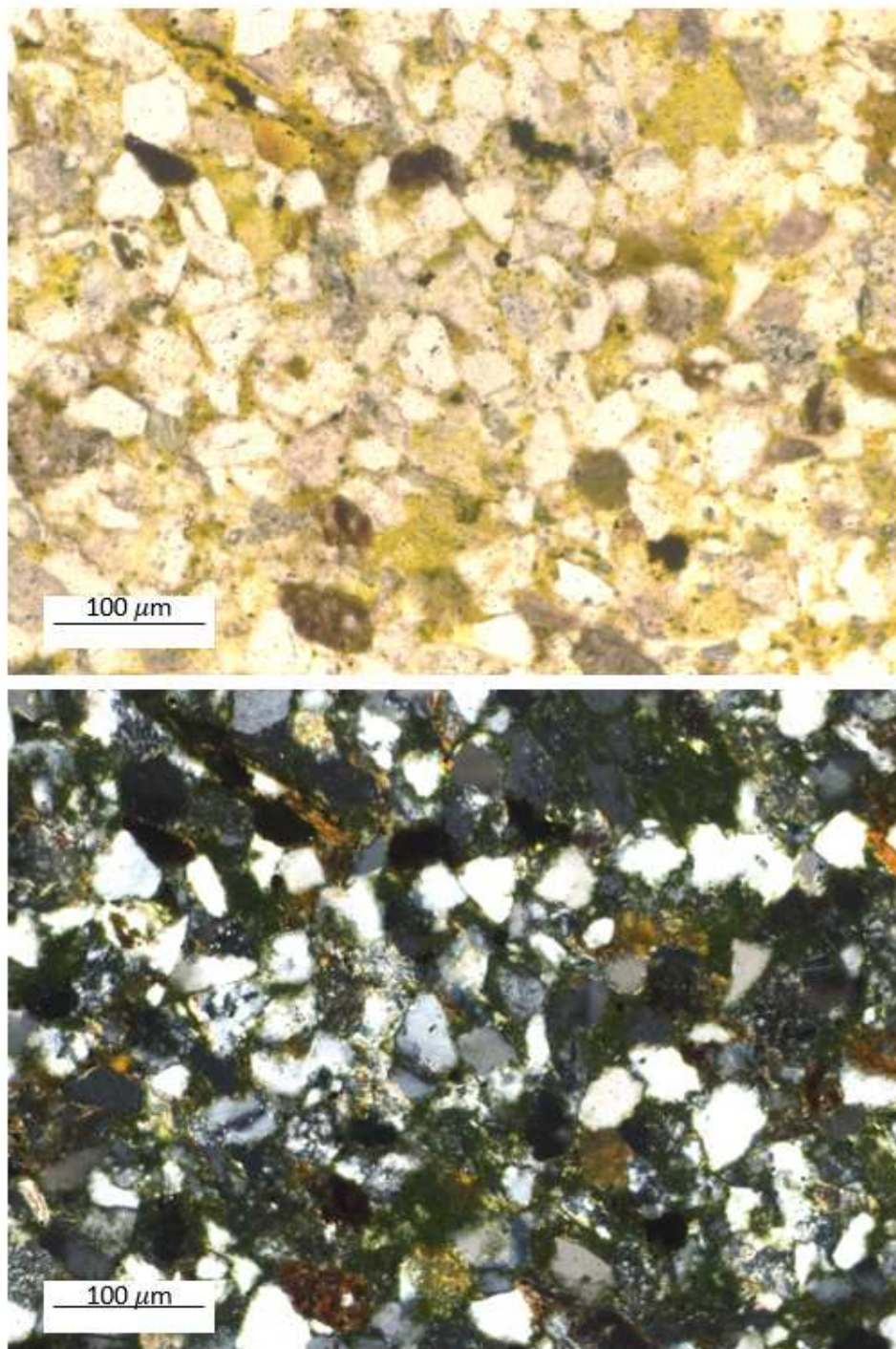


Figure 4.2: Thin section photomicrograph in plane light (top) and cross polar light (bottom) from the Colen 10-10 at a core depth of 5275 ft. Photomicrograph displays epifluorescent yellow dye highlighting primary porosity and possible secondary porosity with observed chert grains. Porosity from core is 16% and permeability from core is 0.38 mD at this depth.

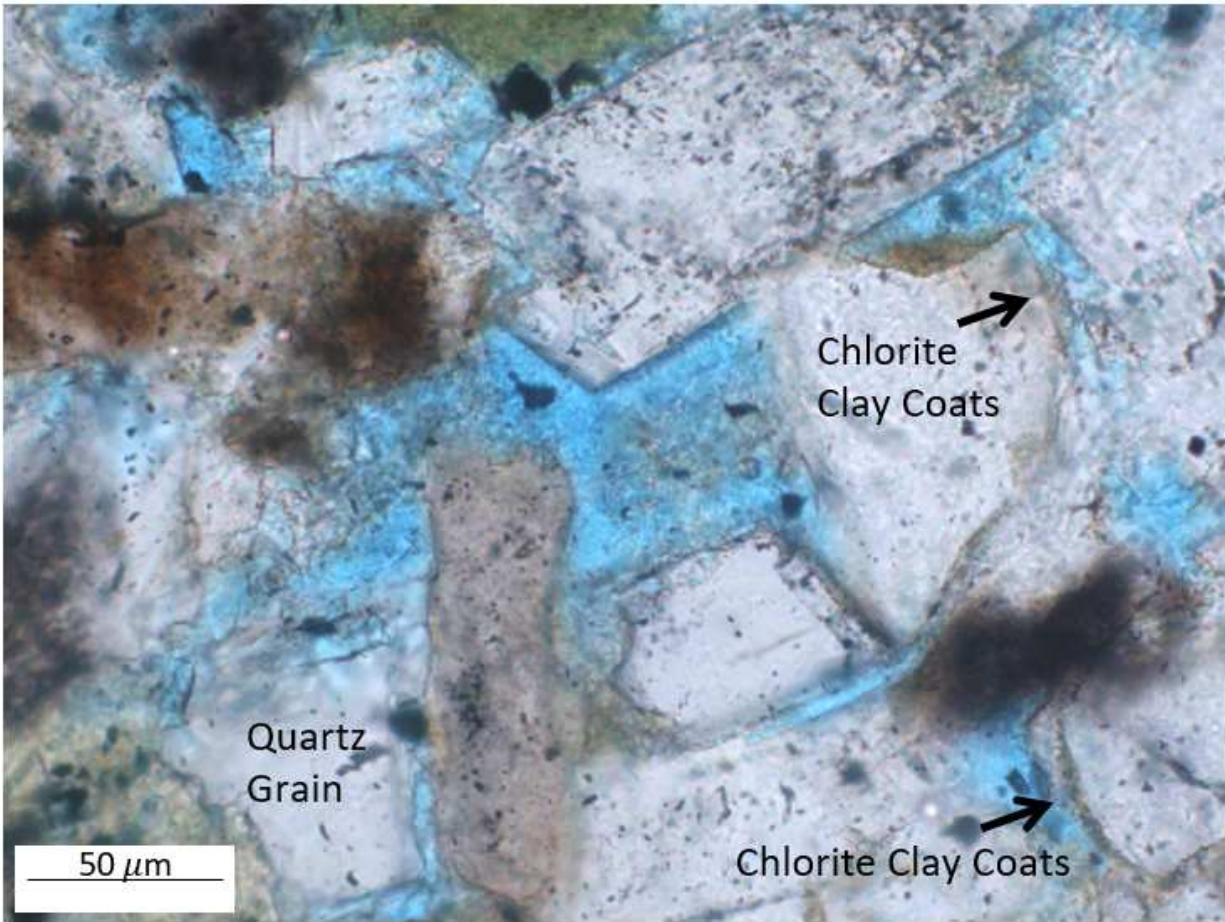


Figure 4.3: Thin section photomicrograph in plane light from the McTuillin Federal 1 at a core depth of 4851 ft. Photomicrograph displays chlorite coating of grains observed as partial green/brown dust rims around quartz grains with visible intergranular porosity. Porosity from core is 15.5% and permeability from core is 0.33 mD at this depth.

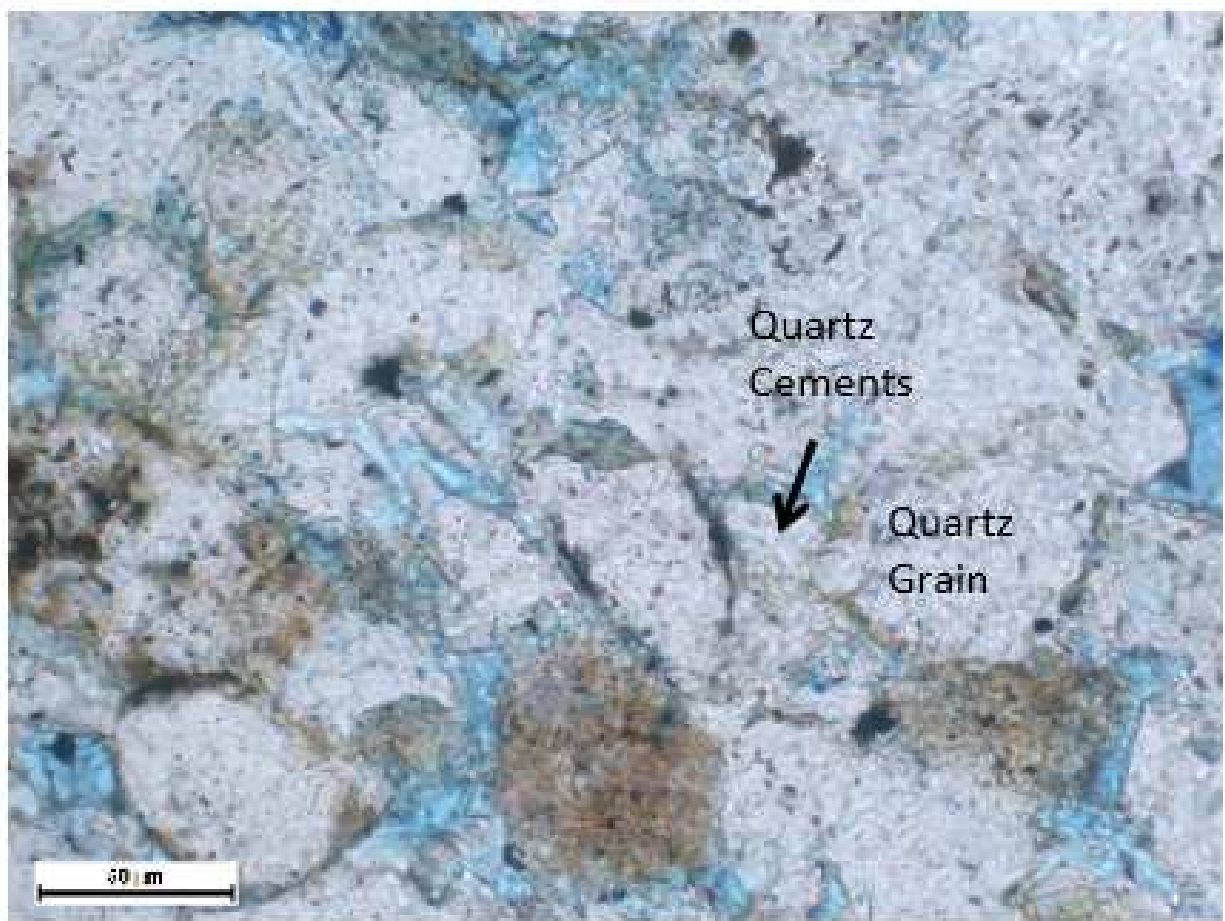


Figure 4.4: Thin section photomicrograph in plane light from the McTuillin Federal 1 at a core depth of 4876 ft. Photomicrograph displays quartz overgrowths as quartz cements interpreted to have grown in the initial pore space.

Also observed in thin section is the dissolution of feldspar (Figure 4.5) and quartz as a result of pressure solution (Figure 4.5). Figure 4.5 shows the dissolution of feldspar illustrating secondary porosity in the sample where the feldspar is no longer present. Also seen is an example of quartz dissolution due to pressure solution at the grain to grain contact. It shows that quartz dissolution does not give secondary porosity but rather quartz cement near or at the grain contact.

In the medium-grained facies, calcite cements are present as shown by the alizarin red stain. Any sediment that occurs finer than medium-grained and with higher mud content, less than 10% do not appear to have any large calcite cement precipitation. Figure 4.5

also displays calcite cementation in addition to all previously discussed diagenetic processes. Suggesting this was the last stage that occurred and was detrimental to the porosity and permeability of this facies, which was expected to be much higher prior to cementation. From core analysis, this facies has a porosity of 13% and permeability of 0.003 mD.

Compaction of the Turner occurred throughout the diagenetic process, with the finer-grained and muddier facies appearing to have seen a larger effect. The cleaner sandstones intervals with higher percentage of silica were able to hold a stronger framework and preserve intervals of higher porosity and permeability for hydrocarbon accumulation.

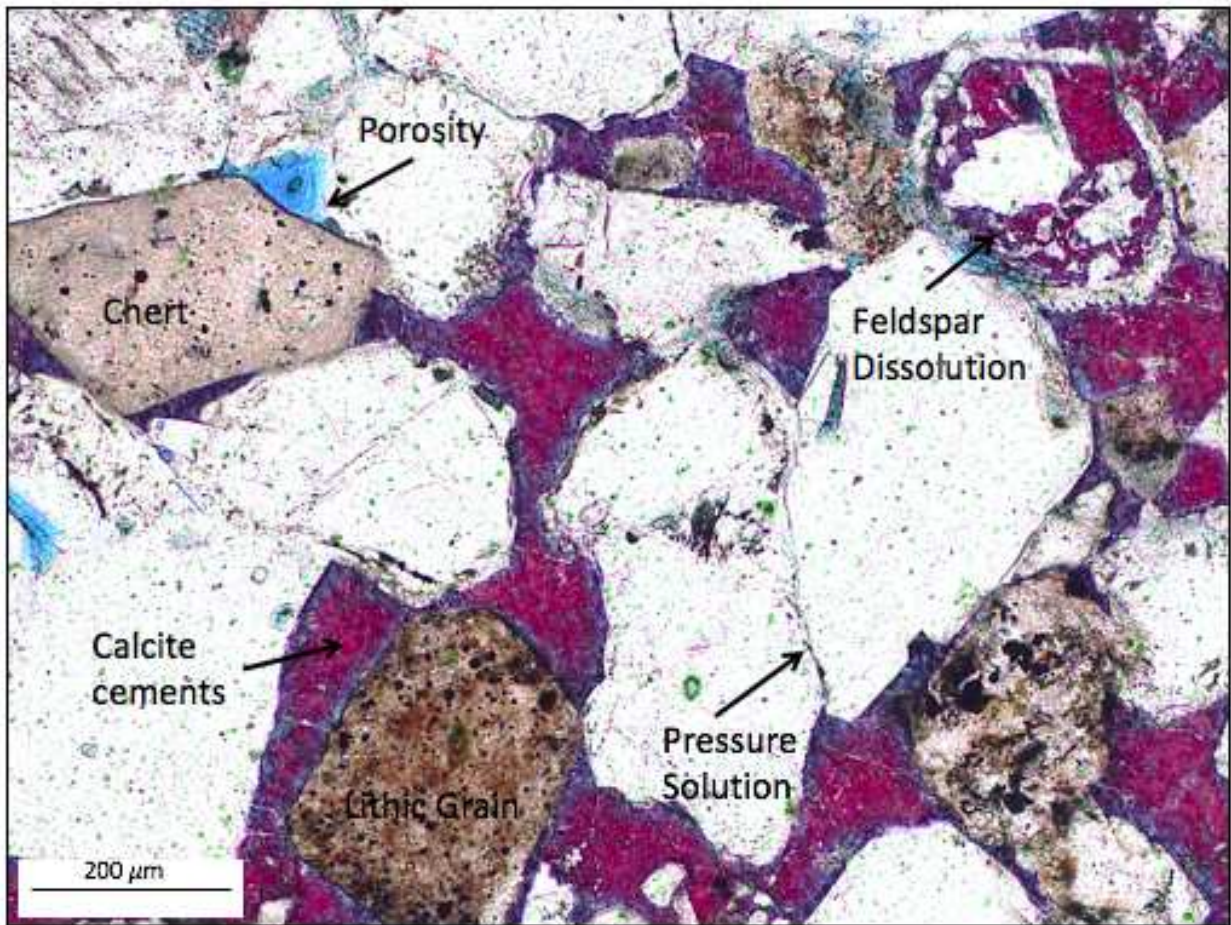


Figure 4.5: Thin section photomicrograph in plane light from the Colen 10-10 at a core depth of 5297 ft. The photomicrograph displays late calcite cements that have destroyed most of the initial porosity. Also displays partial feldspar dissolution, pressure solution, and quartz overgrowths.



### 4.3 FE-SEM Analysis

A substantial portion of this research was dedicated to investigating and understanding the microscopic scale effects on reservoir quality. This included taking 18 rock samples from 18 different depths and 6 different facies, Facies 1, 2, 3, 5, 6 and 7, prepared for imaging under the Field Emission-Scanning Microscope (FE-SEM) at the Colorado School of Mines (CSM). These facies were chosen because 1, 2, and 5 are the best reservoir facies, and 3, 6, and 7 are the lowest quality reservoir facies. In hopes that observing and comparing the diagenetic textures and features in the good and poor reservoir intervals, variations in the composition, framework, and pore networks, would highlight diagenetic controls on the quality of the rock to be a good reservoir. These samples were prepared by breaking rock samples from the McTuillin-Federal 1 and the Colen 10-10 cores to create a broken surface, the best method to discern surface textures, which were gold coated for 2-3 minutes per sample to achieve the best imaging.

Two types of images were acquired for each sample, a backscatter electron (BSE) image and a secondary electron (SE) image. BSE images are ideal for identifying compositional differences of minerals and zonation of minerals. These images highlight variations in the atomic number of the elements that compose the mineral, where elements with higher atomic numbers appear brighter. SE images are best for discerning pore shape, sizes, and types. These images have a high signal strength, resulting in topography contrasts in the sample. Overall, the combination of these images are ideal for investigating porosity, pore networks, and framework mineral and matrix mineral textures. In addition to the BSE and SE images, energy dispersive spectroscopy (EDS) mineral mapping was performed on these samples to show the distribution and concentration of elements within the field of view. Using either a BSE or SE image, elemental maps were made using X-ray energy dispersive spectroscopy to generate a mineral map on top of either a BSE or SE image as a base. Keeping in mind the dominant lithology of quartz, feldspar, plagioclase, clays, and calcite, the primary elements that were mapped in color include silicon (Si), aluminum (Al), magnesium (Mg),

calcium (Ca), iron (Fe), potassium (K), and sodium (Na). In addition, two thin sections from the Colen 10-10 core were polished and carbon coated and investigated under the SEM using the cathodoluminescence (CL) and the SE beam, also available at the CSM lab. The luminescence of all detrital and diagenetic minerals such as quartz, feldspar, phyllosilicates, carbonates, etc can be quantitatively characterized by spectroscopy (Richter et al., 2003). One of the most important minerals in sandstones is quartz, however, the origin of quartz can vary significantly. CL can discriminate detrital grains from cements and provide evidence for the replacement of other minerals based upon their luminescence (Sippel, 1968). Common CL colors include red, the best color for discerning quartz, green, and blue wavelengths, which were all investigated using the FE-SEM cathodoluminescence beam at CSM.

The primary goal was to compare the diagenetic textures and processes in the best reservoir rock with the textures and processes in the poorest reservoir rock. This means that the poorest reservoir rock samples gave the most insight on the full diagenetic history, and provided the best images to convey the history of the study area. Observations from several samples suggest that early grain coating of major framework grains plays a crucial role in preserving initial porosity within the Turner stratigraphy. Figure 4.6 shows a BSE image from a Colen 10-10 sample in the fine-grained sandstone facies where both microcrystalline quartz and chlorite blades appear to coat a framework quartz grain. In terms of timing, it is interpreted that the microcrystalline authigenic quartz grain coats precedes the coating of the chlorite clay blades. This is largely due to the appearance of chlorite blades that form on top of the microcrystalline authigenic quartz and act as a secondary grain coat after the initial coating. This early grain coating prevents the nucleation of quartz overgrowths forming on the framework grain and growing in the pore space later during diagenesis. This process results in the preservation of porosity. However, in the finer grained sediments, this coating does not occur everywhere and the result is that more pervasive large euhedral quartz overgrowths grow in the pore space (Figures 4.7-4.8).

Secondary quartz overgrowths occur throughout the Turner as large euhedral grains in the pore space of regions where no early chlorite or microcrystalline authigenic quartz grain coatings have occurred. This quartz growth occurs between 80-100 degrees °C burial depth where the growth can nucleate on a quartz surface and grow outward into the pore space. Figures 4.7 and 4.8 show examples of these secondary overgrowths in two different samples, where the size of the overgrowths appear to correlate to the amount of pore space and the size of quartz nucleation surface available for growth. This typically is observed in coarser grained sediments, which have larger pore space and quartz framework grains, resulting in larger overgrowths. Another analysis looking at size, morphology, and shape of quartz overgrowths is by using thin sections and CL imaging. Figures 4.9-4.10 show a typical suite of images to best observe overgrowths. Figure 4.9a and 4.9d shows a SE image of the thin section where the size and shape of the grain can be observed. Figures 4.9b and 4.9e shows a combination image of the red, blue, and green wavelengths. Figures 4.9c and 4.9f show an image of just the red wavelength, the dominant light to discern quartz grains and secondary growths. Figure 4.10 shows the same image suite at a different core depth in the medium-grained facies. These CL images begin to separate out the origin of the grain where later growth can be seen as contrast variations in these images. In CL, detrital grains will luminesce brighter compared to authigenic minerals. Although there are ways to interpret secondary quartz growth in thin section, CL imaging combined with SE images of thin section samples best show how extensive secondary growth is and to what size these are to interpret initial porosity and clearly shows the effects of these growths on the porosity of the reservoir.

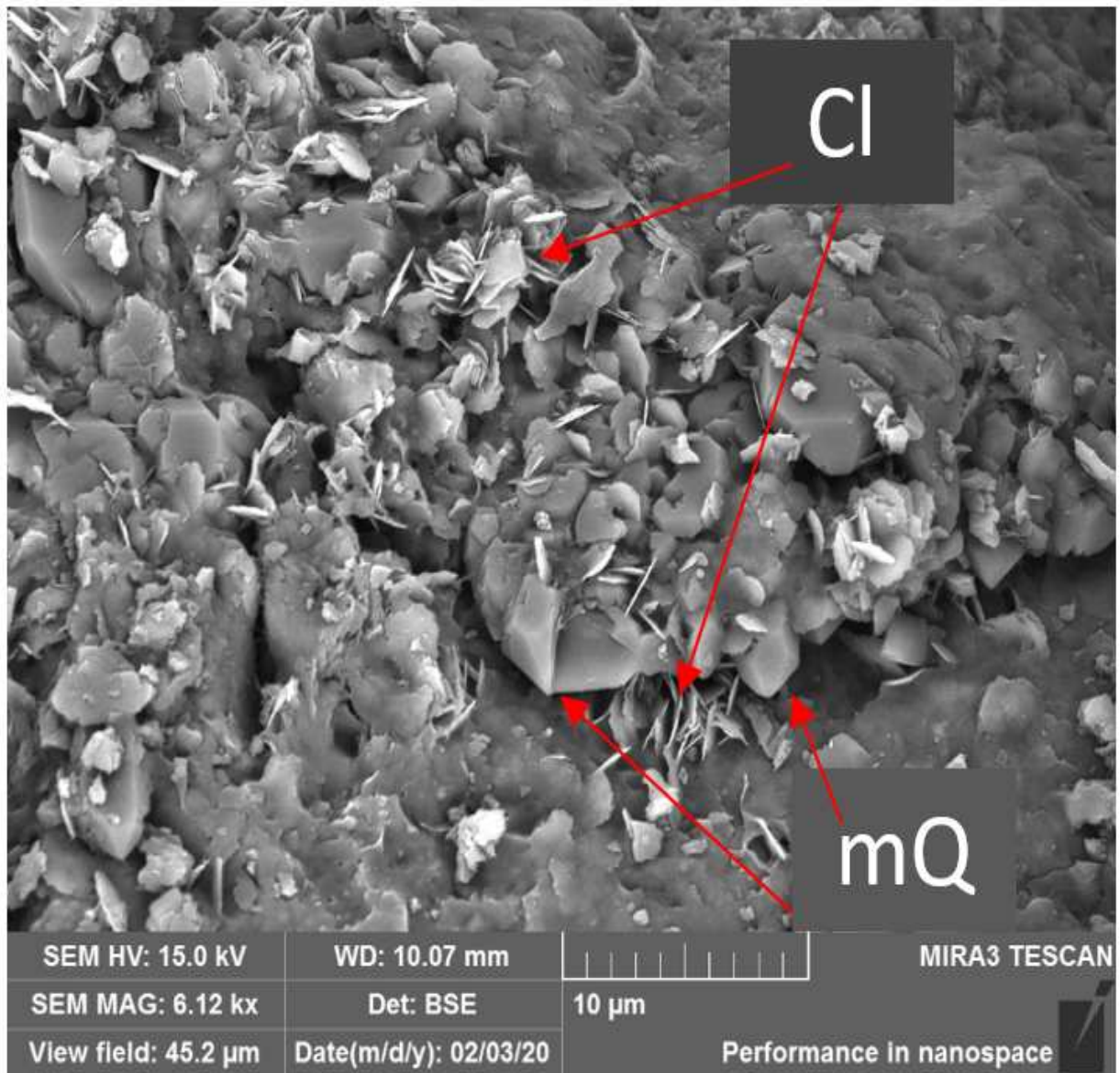


Figure 4.6: FE-SEM BSE image from the Colen 10-10 core at 5300 ft. core depth. BSE image shows a early microcrystalline authigenic quartz grain coat (mQ) and a later secondary authigenic chlorite (Cl) grain coating on a framework grain.



Figure 4.7: FE-SEM BSE image from the Colen 10-10 core at 5300 ft. core depth. BSE image shows a large euhedral quartz overgrowth (Q) in the pore space.

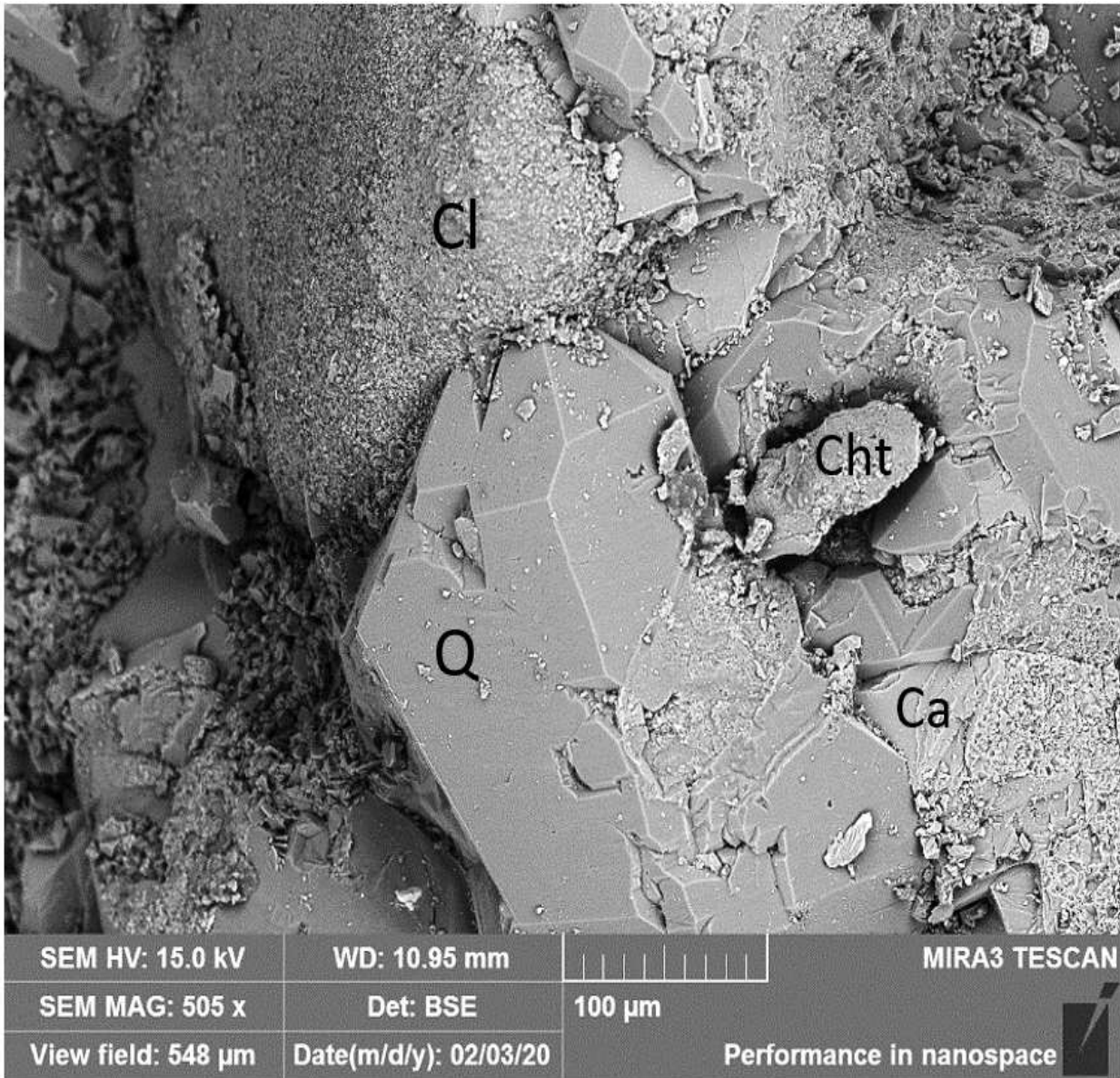


Figure 4.8: FE-SEM BSE image from the Colen 10-10 core at 5297 ft. core depth. BSE image shows another large euhedral quartz (Q) overgrowth in the pore space. Also seen in the image is an interpreted detrital chert grain (Cht), a framework grain with authigenic chlorite grain coat (Cl), and an authigenic calcite grain (Ca).

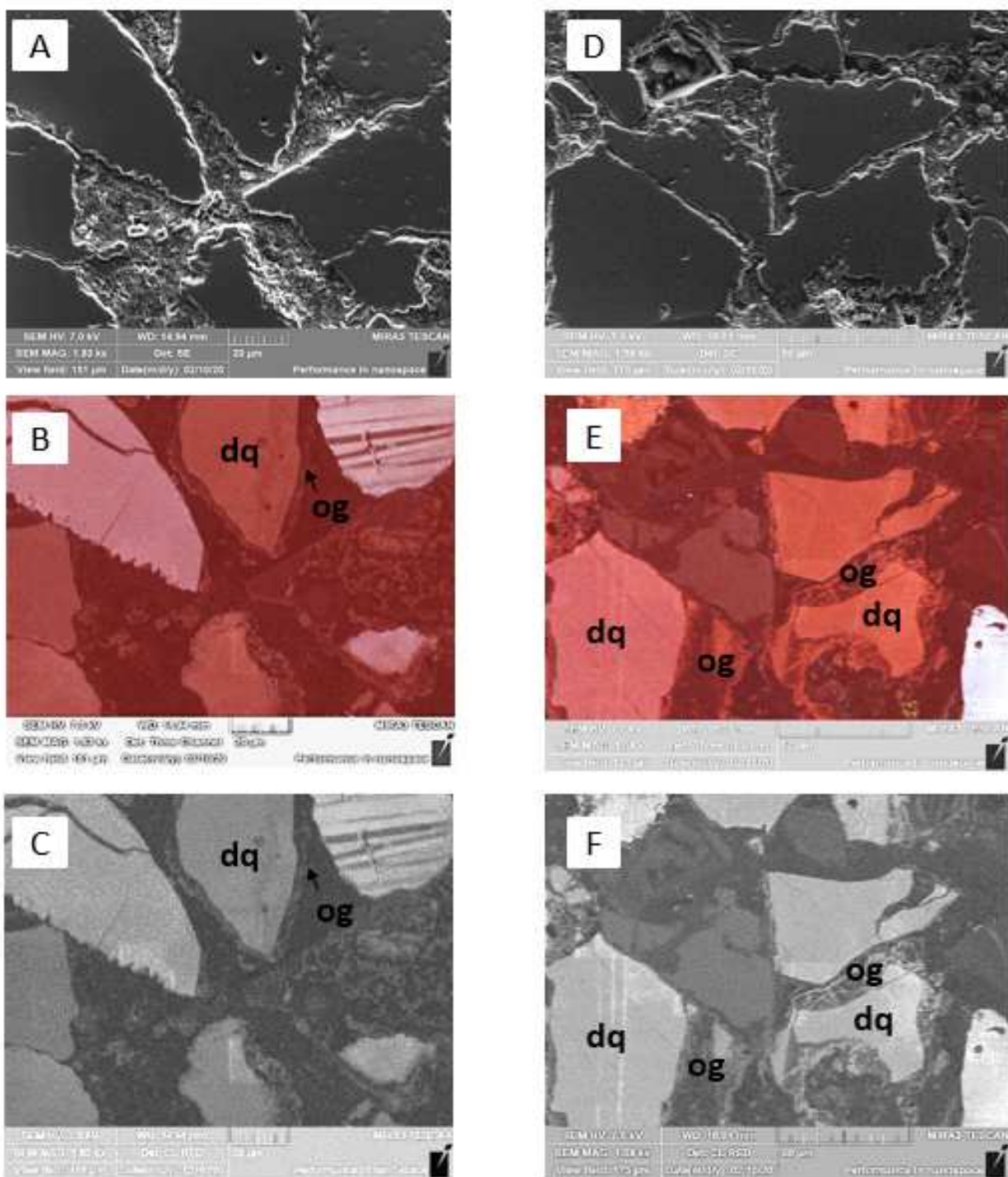


Figure 4.9: FE-SEM CL image from the Colen 10-10 core at 5275 ft. core depth. A/D) shows SE image of thin section. B/E) shows combined red, blue, and green CL image. C/F) shows red CL image. Detrital quartz grain (dq) displays bright luminescence in contrast to the dull luminescence of the authigenic quartz overgrowth (og).

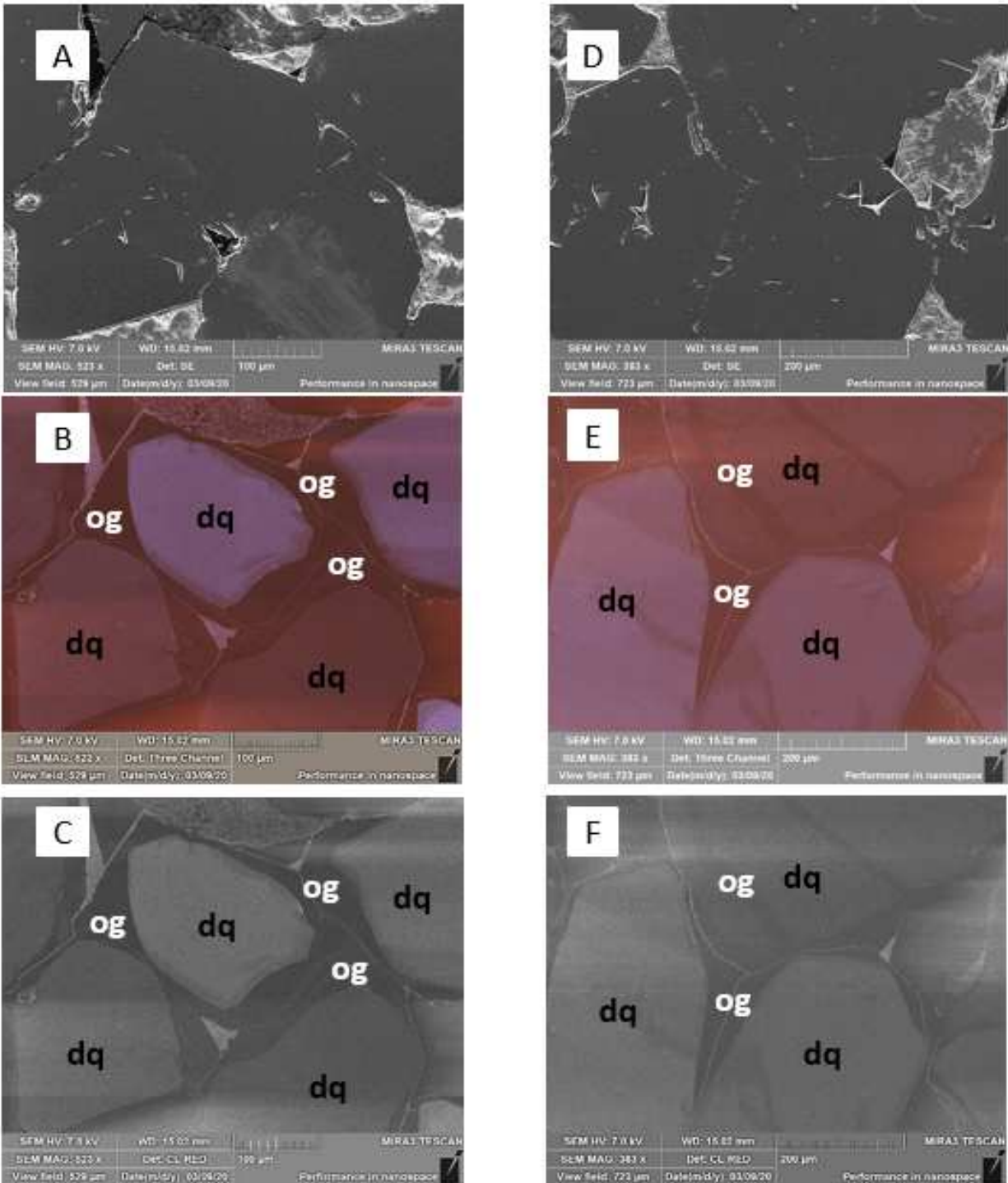


Figure 4.10: FE-SEM CL image from the Colen 10-10 core at 5297.2 ft. core depth. A/D) shows SE image of thin section. B/E) shows combined red, blue, and green CL image. C/F) shows red CL image. Detrital quartz grain (dq) displays bright luminescence in contrast to the dull luminescence of the authigenic quartz overgrowth (og).



Figure 4.11 shows an example of small euhedral quartz grains appearing to grow out from a microcrystalline quartz grains. However, the interpretation is that this is a chert grain, seen extensively in cross polarized light with the petrographic microscope, in the Turner. This suggests these polycrystalline quartz are not authigenic and instead detrital as lithic fragments sourced from the Sevier Highlands during deposition. The observed polycrystalline quartz in this image is not an early grain coating and can be a nucleation source for microcrystalline quartz growth. The nucleation site is much smaller due to the inherent size of the detrital chert, which is why there does not appear to be extensive quartz growth on these grains.

Four diagenetic processes were observed as potential silica sources for secondary quartz overgrowths: 1) pressure solution, 2) feldspar dissolution, 3) illite to smectite conversion, 4) chert dissolution. Quartz cements from pressure solution is another observed stage of diagenesis. This can cause quartz dissolution, although seen more pervasive in thin section, further evidence in FE-SEM was observed. Figure 4.12 shows a framework quartz grain with conchoidal fractures, interpreted to be a result of pressures and stresses. In addition to quartz dissolution, possible evidence for feldspar dissolution was seen in FE-SEM by dissolution textures later filled with diagenetic cements. However, this stage in the burial history was investigated more in thin section by evidence of secondary porosity. The third process observed that could be a potential source of silica for secondary overgrowth is authigenic clay growth from the conversion of smectite to illite during later burial. This process is interpreted to occur as one of the last events prior to secondary quartz overgrowth. When temperatures reach 80-100 °C during burial, detrital clays can become unstable and they are replaced with mixed layer clay minerals and illite. Figure 4.13 shows an example of well developed kaolinite books that have grown within the pore space. From XRD, the Turner shows a elevated percentage of clay content, both illite-smectite and kaolinite within the finer grained sandstones and siltstones. Facies 7 and 8 have high mudstone content with over 50% clay, Facies 1 and 3 have between 30-40% clay content, and the remaining facies

are all less than 15% clay.

The last stage of observed diagenesis in the Turner is late calcite cements precipitating in the pore space. This appears to occur most extensively in the medium-grained sediments as a result of the excess pore space for the calcite to precipitate. These cements are interpreted to occur last because in the sediments that they occur, all previously mentioned diagenetic stages were observed, indicating that calcite cements were the last stage to occur in the Turner.

Integrating FE-SEM observations, BSE, CL, and SE images with EDS maps is a key tool when summarizing the diagenetic history. Figure 4.14 shows an EDS map of a sample from the Colen 10-10 core where authigenic microcrystalline quartz has been identified in red for silicon, chlorite has been identified in yellow for an iron-rich aluminosilicate clay, kaolinite has been identified in green for an aluminosilicate clay, and calcite has been identified in blue for calcium. In Figure 4.14a, the red and yellow colors representing microcrystalline authigenic quartz and chlorite blades coating a framework grain in the left section of the image. Moving to Figure 4.14b, the field of view has been shifted to the pore space of the framework grain where the blue and green colors representing calcite and kaolinite are seen filling the pore space of the grain. By utilizing EDS mapping, patterns, timing, and minerals that are not easily discerned in simply BSE or SE images become apparent. For example, the chlorite grain coating appears to occur on top of the microcrystalline authigenic quartz, suggesting that the quartz grain coat precedes the chlorite grain coat. In addition, the texture of the calcite in this pore space makes it hard to separate from the well developed kaolinite books. Without the use of EDS mapping, the calcite could easily have been missed and depicts how the calcite filled in the remaining pore space that was not occupied by authigenic kaolinite.

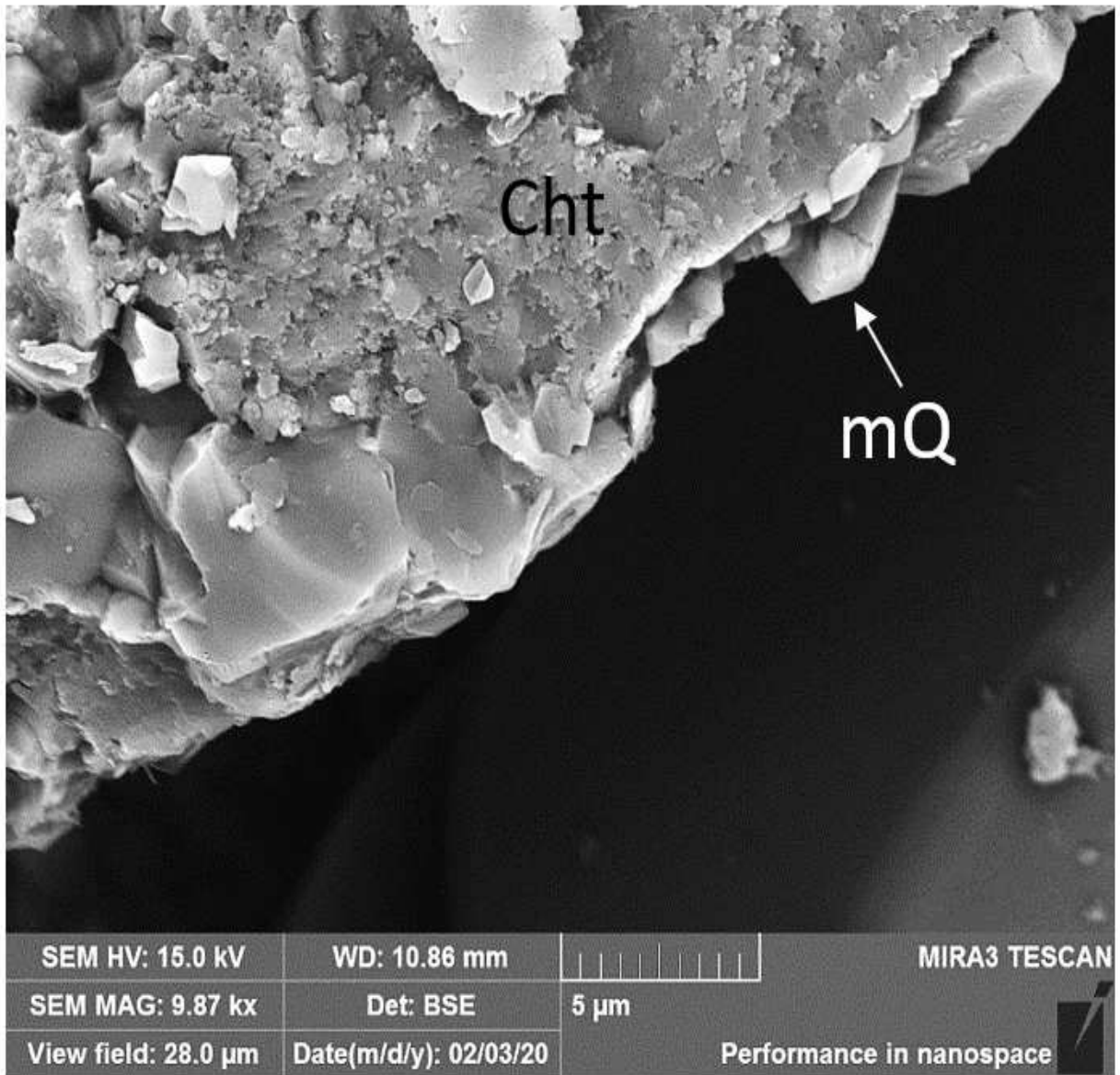


Figure 4.11: FE-SEM BSE image from the Colen 10-10 core at 5297 ft. core depth. BSE image shows a close up of a detrital chert grain. Authigenic microcrystalline quartz (mQ) is interpreted to be using the detrital chert as a nucleation site.

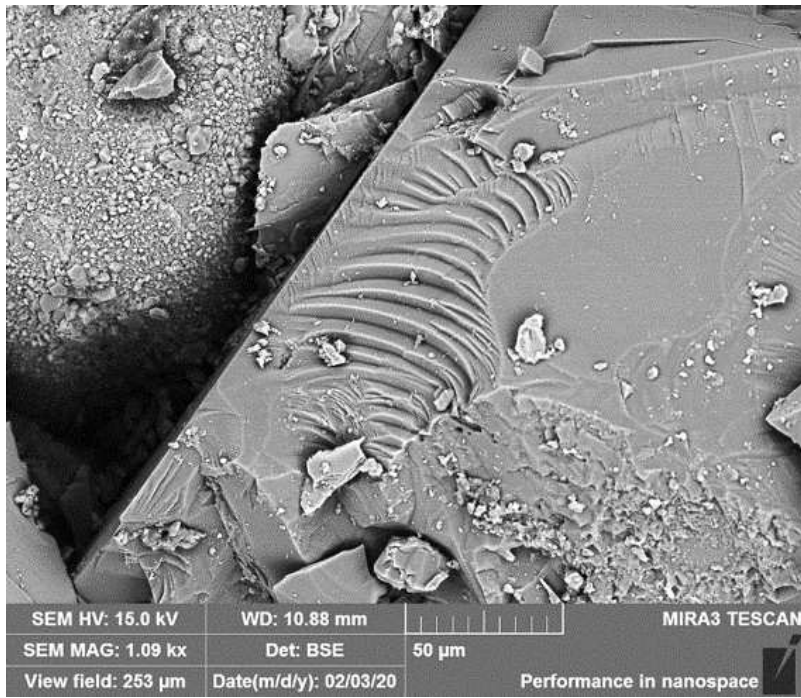


Figure 4.12: FE-SEM BSE image from the Colen 10-10 core at 5273.6 ft. core depth. BSE image shows conchoidal fractures as a result of rock breakage.

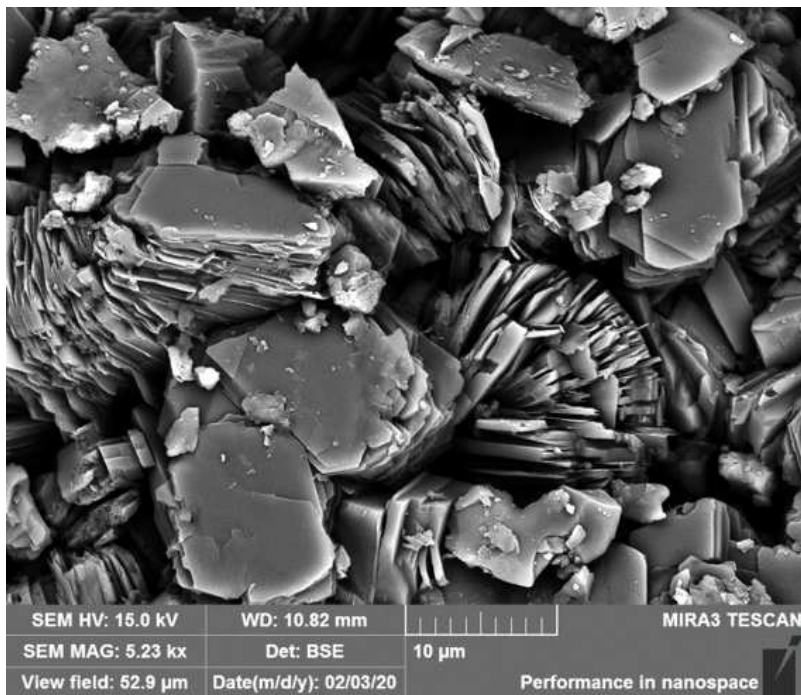


Figure 4.13: FE-SEM BSE image from the Colen 10-10 core at 5297 ft. core depth. BSE image shows authigenic kaolinite (classic "book" morphology) growing in the pore space.



Figure 4.14: FE-SEM BSE image with EDS map from the Colen 10-10 core at 5297 ft. core depth. Authigenic microcrystalline quartz grain coat is shown in red, chlorite grain coat is seen in yellow, pore filling calcite cement is seen in blue, and pore filling authigenic kaolinite books are seen in green.

### 4.3.1 Diagenesis Summary

The diagenetic imprint on the varying lithologies within the Turner have created a unique history for this Turonian aged prolific reservoir in the PRB. The specific depocenter and environment during Turner deposition at Finn-Shurley gave a unique opportunity for various diagenetic mechanisms and processes to alter the lithology. These mechanisms affected all of the sediment of the Turner to some degree, with the coarser grain sediments appearing to have the greatest magnitude of alteration occurring when compared to the finer grained and muddier sediments of the Turner.

Microcrystalline authigenic quartz grain coatings and chlorite grain coatings are the first stages of diagenesis to occur early in the rocks burial history. These two coating processes are interpreted to have preserved initial porosity and permeability of the Turner. The source of silica for early grain coating is undetermined. However, chert grains are observed in both thin section and FE-SEM and are interpreted as detrital. This suggests that the weathering of these detrital chert grains during transport and deposition could be a source for silica early in the burial history. Sources for the early chlorite grain coatings are likely a result of weathering of ferroan metamorphic minerals, low temperature metamorphic volcanic rocks fragments, alteration of feldspars during transport and burial, or as a hydrothermal alteration product (Deer et al., 2013a). In areas where grain coating is less prevalent, secondary quartz overgrowths are more pervasive as the early grain coating inhibits the nucleation and growth of secondary quartz cements in the pore space, thus decreasing initial porosity and permeability. In the event that there is minimal to no early grain coating, a source of siliceous material must be present in order to promote secondary quartz overgrowths. For the Turner, this excess source of silica is interpreted to be from three different diagenetic processes. The first observed potential source of silica is quartz dissolution from pressure solution. Increasing pressures and temperatures can initiate dissolution of quartz at the grain to grain contact, releasing excess silica into the system to promote secondary overgrowths. The second observed potential source of silica is weathering and dissolution of feldspars and

other silicates to release silica into the system. The final observed potential source of silica is the illite to smectite conversion. Again at high temperatures and pressures, smectite becomes unstable and converts to illite or mixed layer clays. These processes can also be expedited with the introduction of saturated pore waters into the system during burial. Without much more extensive petrographic work, which of these potential sources is the main source of silica is indeterminable. With observations of all three processes, each is interpreted to have an effect on the source of silica for the purpose of this study. The final diagenetic process that was observed is late calcite cementation that occurs primarily only in the medium-grained sand intervals. Figure 4.15 shows a chronological paragenetic sequence generated for the Turner during burial from these thin section and FE-SEM observations.

In conclusion, the processes that are interpreted to have the largest effect on porosity and permeability are early microcrystalline authigenic quartz and chlorite grain coats, secondary quartz overgrowths, and late calcite cements. The initial grain coatings occurred early in diagenesis and aided in preserving initial porosity as it prevented later quartz overgrowths. In areas of absent or patchy grain coatings, overgrowths are prevalent and appear to have decreased initial porosity and permeability by filling the pore space with quartz cements. The final stage that affected porosity and permeability was late calcite cements. In the medium grained sand where this was observed, much of the pore space is filled with calcite and has been detrimental to initial porosity and permeability. Although the dissolution of quartz and feldspars can provide secondary porosity, if there is poor grain coating, quartz overgrowths are likely to occur and still adversely affect porosity and permeability. In conclusion, the best reservoir facies with the highest preserved porosity and permeability have extensive early grain coating of both microcrystalline authigenic quartz and chlorite, and are fine-grained with less than 15% mud in order to avoid secondary quartz overgrowths and the precipitation of calcite cements.

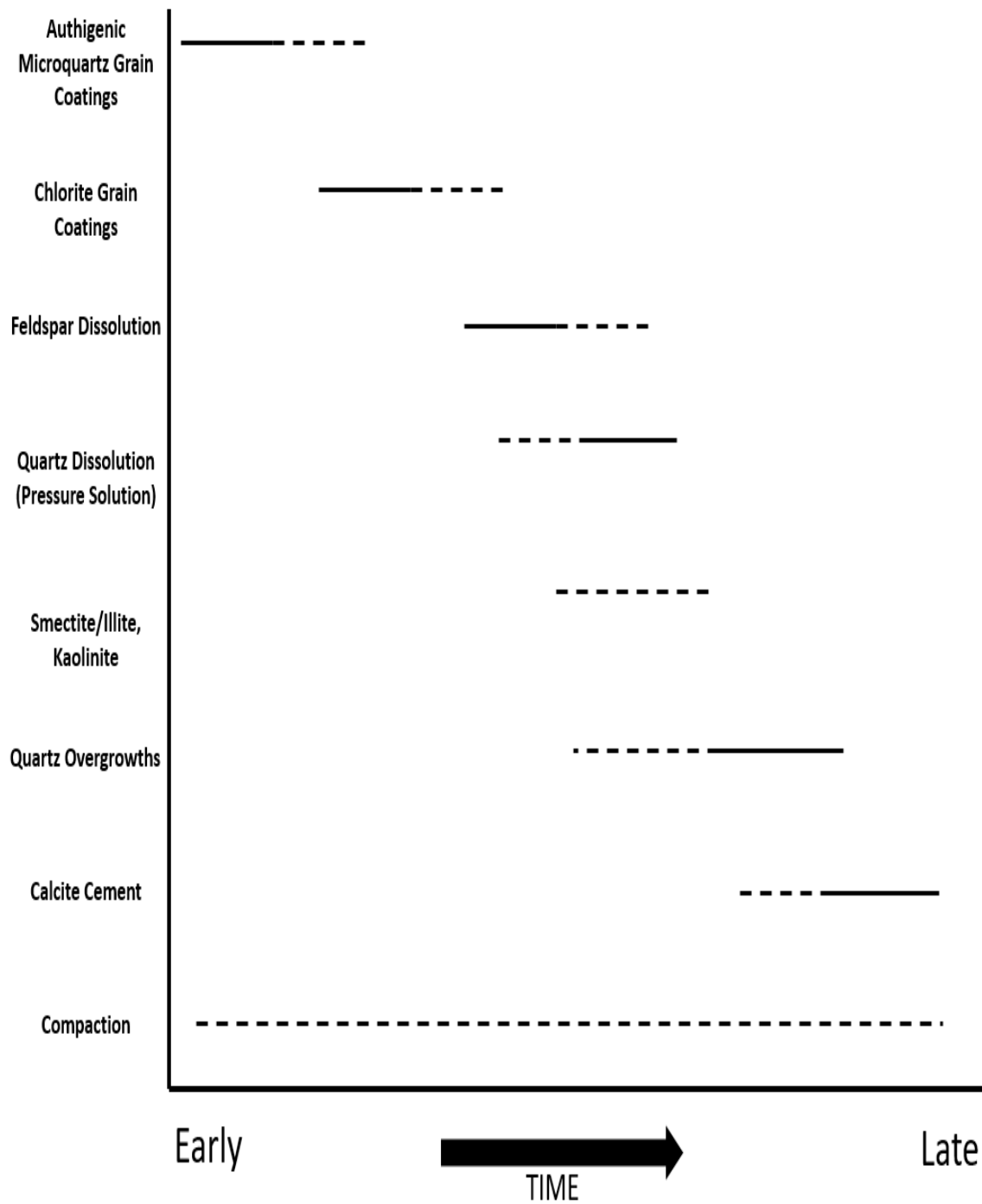


Figure 4.15: Paragenetic sequence of the Turner Sandy member created from thin section and FE-SEM analysis and interpretations.



## CHAPTER 5

### RESERVOIR CHARACTERIZATION

#### 5.1 Reservoir Characterization Overview

This chapter will discuss the integrated approach taken to characterize the reservoir intervals in Finn-Shurley Field, in order to understand how oil and gas can accumulate in the Turner. By utilizing and integrating routine core analysis (RCA), core description, XRD, XRF, petrographic observations, and petrophysical well logs, potential reservoir intervals based on the best rock and mechanical properties can be identified. By understanding the diagenetic history and depositional environments discussed in the previous two chapters, zones that developed and preserved the best porosity and permeability can be highlighted. Inferring zones in the reservoir interval to choose as horizontal drilling targets can lead to successful and economical production of hydrocarbons.

#### 5.2 Porosity and Permeability

In fine-grained sandstone reservoirs, porosity and permeability measurements from core are critical for classifying reservoir facies. By identifying intervals and facies with the highest porosity and permeability values, the intervals where there is the most amount of storage space and flow capacity for hydrocarbon migration and production are highlighted. Variations in porosity and permeability can be affected by mineralogy, diagenesis, bioturbation, depositional processes, or some combination of all these factors. Core measured porosity and permeability data was provided for all four cores, with each classified core facies having at least one data point available to make assumptions about reservoir capability. One density porosity log that covered the entire Turner interval was provided for the Perpetual Finn 8 core that showed the porosity profile throughout the interval. However, individual facies cannot be discerned on logs, meaning the core derived porosity measurements were the primary values used to interpolate porosity and permeability values to the described core

facies. The total number of core measured porosity and permeability data points for this study was 46. Porosity in these four wells ranges from 9.13% - 16.62%. Facies 1, 2, 4, and 5 are determined to be reservoir facies based upon core derived porosity and permeability values. Facies 3, 6, 7, and 8 were determined to not be reservoir facies using the criteria of a porosity cutoff of 12% and a permeability cutoff of 0.1 mD. Facies 1 has three data points available to calculate an average porosity value of 14% and permeability of 0.12 mD. Facies 2 has nine data points available to calculate an average porosity value of 13% and permeability of 2 mD. Facies 4 is the most abundant facies, and has nineteen data points available to calculate an average porosity value of 14% and permeability of 0.16 mD. The final reservoir facies, Facies 5 has seven available data points available to calculate an average porosity of 14% and permeability of 0.31 mD. In general, these reservoir facies are cleaner, less muddy, fine-grained sandstone intervals with preserved laminations, with Facies 1 and 4 as exceptions. Facies 1 and 4 facies are heavily bioturbated and laminations are not observed, but still meet the porosity and permeability criteria. Although, Facies 6 is medium-grained and cryptically bioturbated, the pore space experienced late calcite cements, greatly diminishing initial porosity and permeability.

From petrographic work and XRD, all reservoir facies have anywhere from 1-5% of volume from chlorite clays, except for Facies 1. This indicates early grain coats of chlorite and microcrystalline quartz, which are known to preserve porosity and permeability by inhibiting secondary quartz growth during burial. Porosity and permeability appear to be highly affected by diagenesis, as discussed in the previous chapter. Intervals of slightly higher clay content were more affected by compaction after deposition compared to the relatively cleaner, less muddy, fine-grained sandstone intervals. It is interpreted that the preservation of initial porosity and permeability in Facies 1 is due to the high intensity of bioturbation, which has appeared to inhibit mechanisms that destroy reservoir quality in this facies. Figure 5.1 shows a plot of porosity versus permeability values from the McTuillin-Federal 1 core and is colored by facies. The Turner is dominated by sub-micro, micro, and meso pore

throat sizes due to its fine-grained, mud-rich nature, and extensive diagenetic history. Facies defined as primary and secondary reservoir facies plot as some of the highest porosity and permeability values in the dataset, suggesting the potential for production from mesopores and micropores. Observations from FE-SEM and thin section photomicrographs suggest that porosity is dominated by intergranular or interparticle pore networks (Figure 5.2) and some fracture porosity. The introduction of an epifluorescent dye to the thin sections during preparation, aided in determining available pore space and what form it is present within the rock.

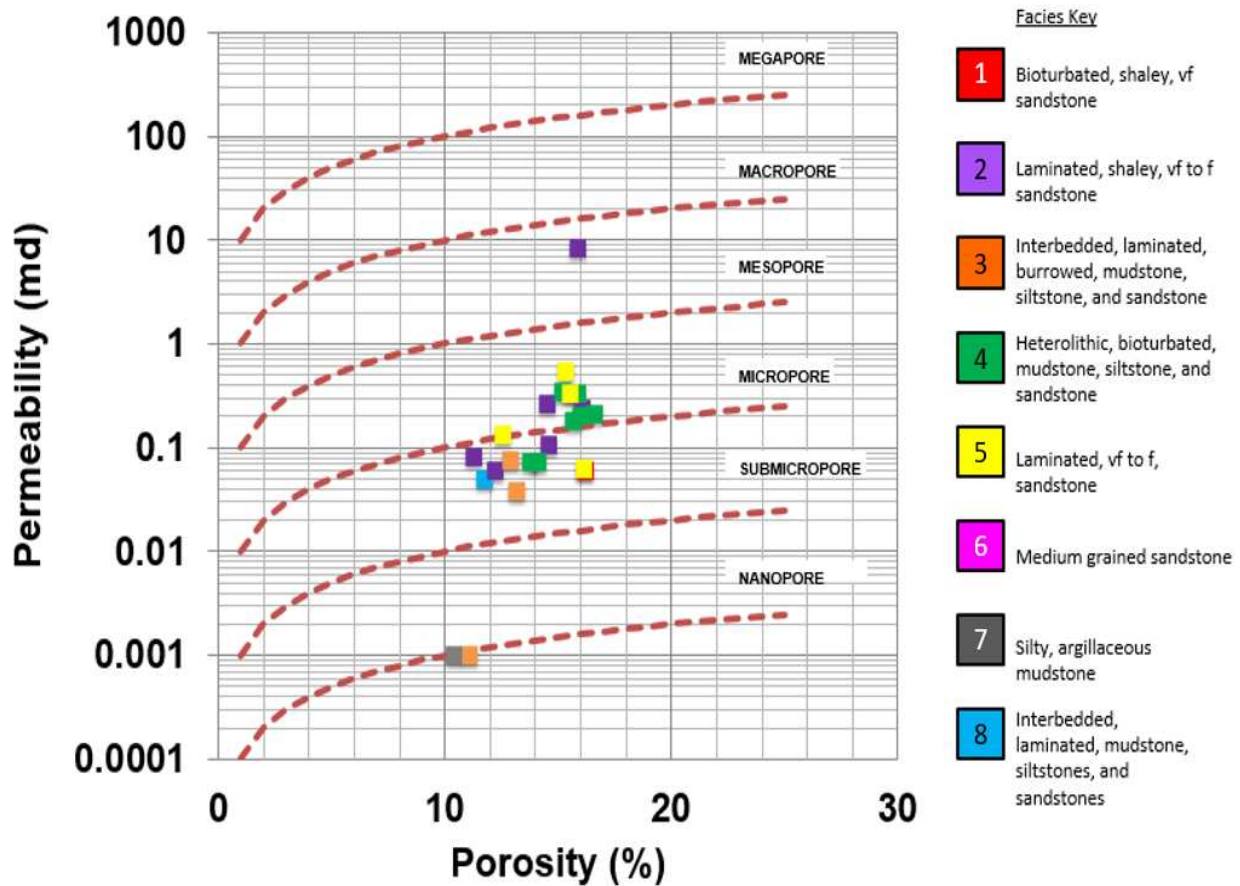


Figure 5.1: Porosity versus permeability plot of the McTuillin Federal 1 core colored by facies. Where the red, purple, green, and yellow squares are representative of reservoir facies. Dashed lines show the separation of pore throat sizes interpreted from  $R_{35}$  calculation from Hartmann and Beaumont (1999).

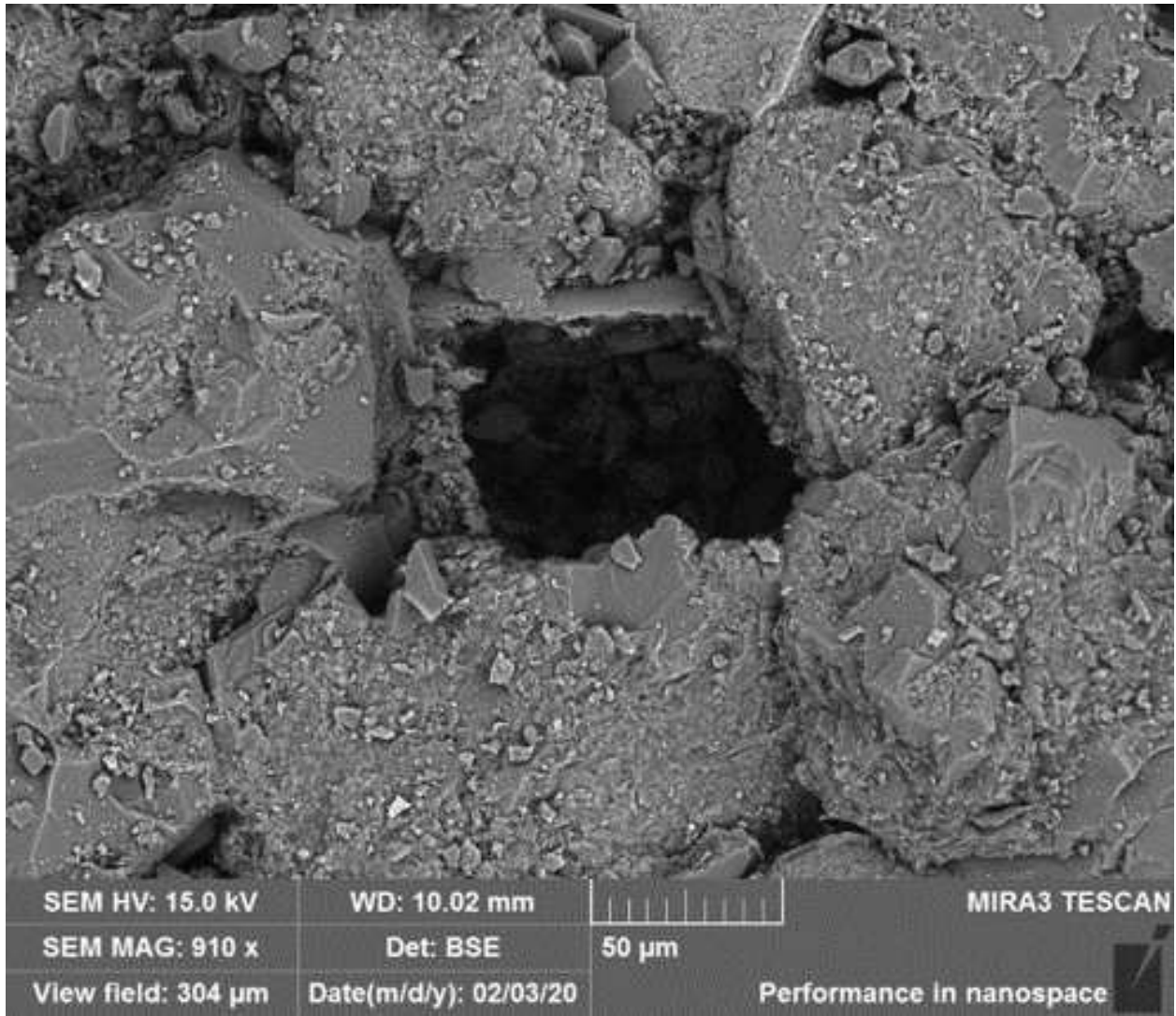


Figure 5.2: FE-SEM BSE image of an intergranular pore in a rock sample from Facies 5. This sample was from the Colen 10-10 core at a core depth of 5300 ft.

### 5.3 Source Rock

A key element to the success of Turner production at Finn-Shurley is the commercial size accumulation of migrated hydrocarbons from a organic-rich source that occurs in the PRB. For the Turner interval, the underlying Mowry Formation and the overlying Niobrara Formation are believed to represent the main source of accumulated hydrocarbons for this field. Figure 5.3 shows an Ro map of the Mowry Formation in the study area, which shows

the Mowry Formation located in Finn-Shurley, lying just on the edge of the early oil window, or having Ro values around 0.6 (Modica and Lapierre, 2012). Stratigraphically, the Mowry Formation lies below the Turner and is a proven world class source rock in the PRB. However, the high gravity oil that is produced from Finn-Shurley, 43°API, suggests that the source is well within the peak maturity window for hydrocarbon expulsion. This means that the oil would have had to have migrated from a region of higher maturity, likely in the central portion of the basin, updip, and become trapped in the Turner reservoir in Finn-Shurley.

To confirm this interpretation of a migrated oil accumulation, a one-dimension basin model was created using the software BasinMod from Platte River Associates. This model was created for the Dixon Smith 3 well, located just outside the study area to the northwest in sec 27 43N 65W (Figure 5.3). Figure 5.4 shows a burial history plot modeled for the well in BasinMod. The model displays historical tectonic and structural events as well as periods of non-deposition that shape the modern day PRB. The extensive tectonic history of the basin also allowed for hydrocarbon expulsion of known source rocks. Geochemical data was then integrated to the model to constrain the time when the Mowry Formation entered in the oil window in the study area. As seen in Figure 5.4, the Mowry Formation near Finn-Shurley is right on the edge of entering the mid mature window from the early mature window. Plotting as right in the transition between yellow, which denotes early mature, and green, which denotes mid mature, in the burial history plot (Figure 5.4). In addition, Finn Shurley Field is normal to sub pressured at 0.43 psi/ft (Toner, 2019). Higher gravity produced oils, 41-43 °API, measured by the Wyoming Geological Society (WGA) in Finn-Shurley Field are inconsistent with in-situ low maturity levels from source rock analysis and the 1D basin model. This confirms the interpretation of a long-distance migrated oil accumulation at Finn-Shurley.

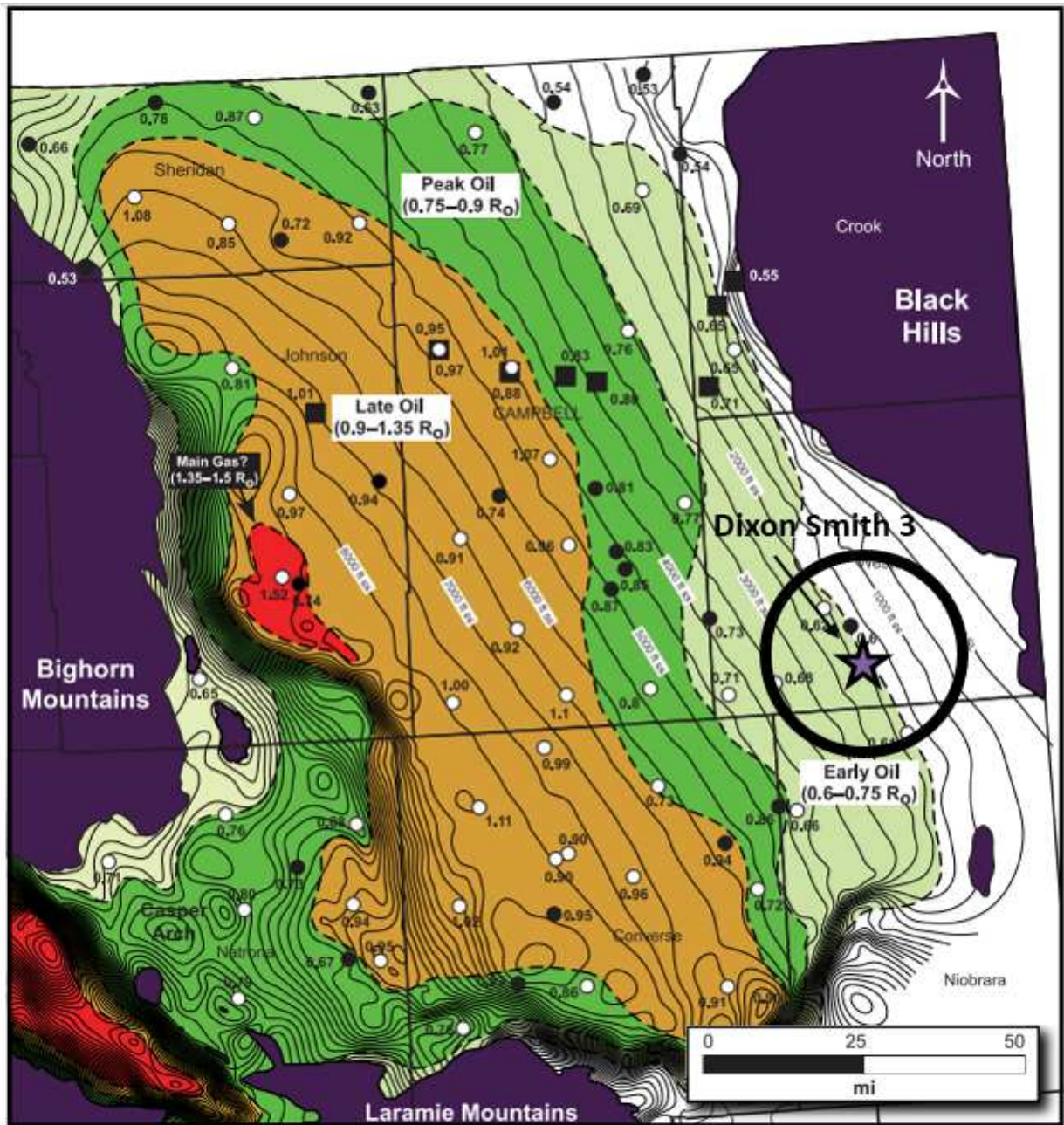


Figure 5.3: Maturity map of the Mowry Shale in the PRB. The black circle represents the study area and the purple star represents the well used for a 1D basin model. Modified from Modica and Lapierre (2012).

The Turner is typically associated with Niobrara petroleum system. In Finn-Shurley, the Niobrara Formation is in the early maturity window, according to the burial history model, and beginning to generate hydrocarbons, which happens around  $0.5 R_o$  (Anna, 2009). How-

ever, similar to the Mowry Formation, these Ro values are inconsistent with the level of maturity that is measured in the produced oil from Finn-Shurley Field. Because the hydrocarbons that charge Finn-Shurley are likely a result of migration from a region of peak maturity in the central portion of the basin, it is potentially being charged by both the underlying Mowry Formation and the overlying Niobrara Formation. Due to the structural complexity and extensive lineaments in the PRB, migration could occur updip by fault pathways for both the Mowry and Niobrara formations. However, further geochemical analysis is necessary to confirm this interpretation. This does support the idea that the Turner does not need to occur in an area where the source rock is mature if there is an ability or mechanism for oil to migrate into the reservoir interval and become trapped.

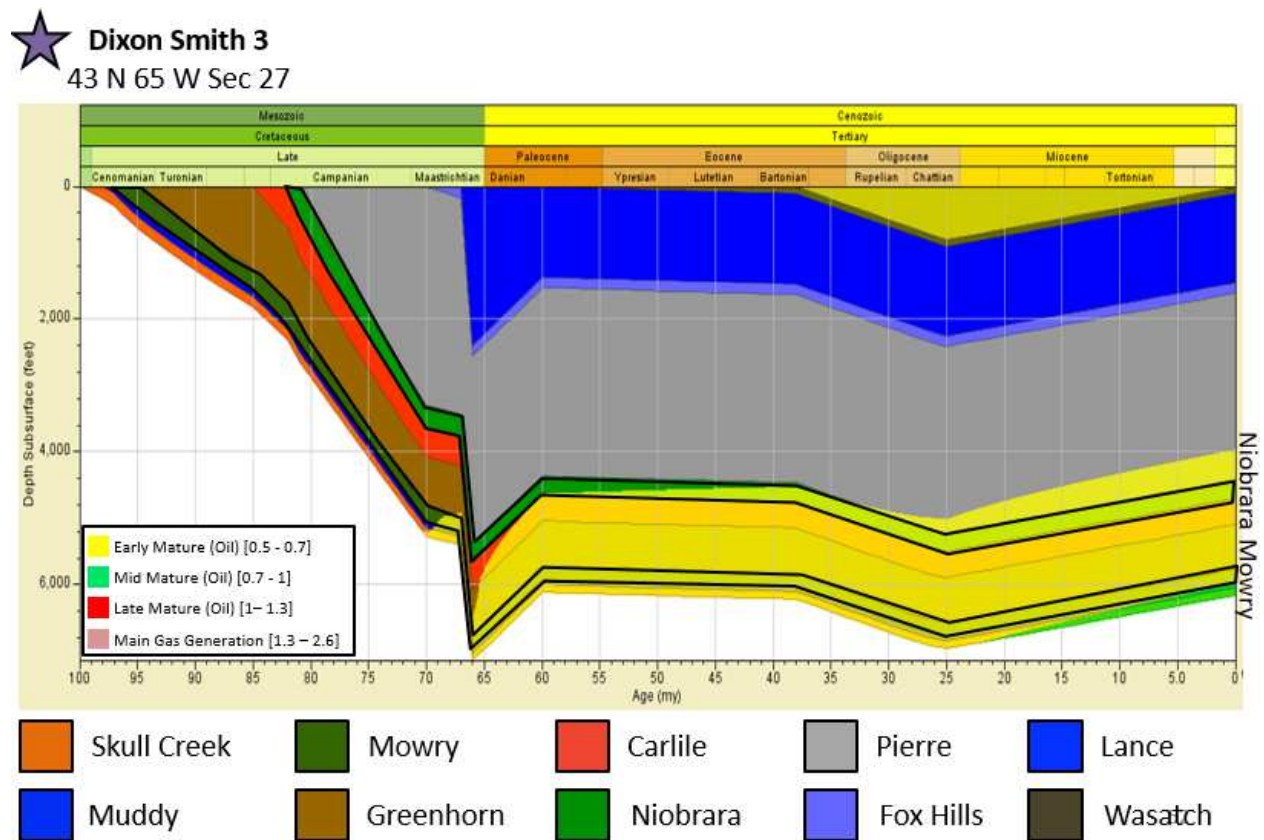


Figure 5.4: Basin Model created for the Dixon Smith 3 well just outside of the study area with maturity windows. Black line highlights the burial history of the Mowry Formation.

## 5.4 Reservoir Targets

One of the primary goals of this study was to identify potential reservoir targets in each well through the integration of core analysis, petrographic analysis, and petrophysical analysis. By integrating core descriptions, XRD, XRF, thin sections, FE-SEM analysis, and routine core analysis, a holistic view of the target intervals can be determined. Prospective targets for the lower Turner, including both the Turner one and two zones, were identified based upon highly porous and permeable zones in addition to high concentration of reservoir facies, and resistivity increases. Due to the high amount of clay content in the Turner, the resistivity values are lower than typically expected for hydrocarbon saturation. Based upon petrophysical logs, hydrocarbon saturation looks to be pervasive throughout the lower Turner interval and only occurs at the very shallowest sand interval in the upper Turner. The Perpetual Finn 8 well was the only well in the cored dataset with a density porosity (DPHI) log provided. The DPHI log was a valuable tool when available to highlight zones of higher porosity and indicate better reservoir quality intervals. Figure 5.5 shows the gamma ray, resistivity with a cutoff of 5 ohm-m, and a porosity log with a cutoff of 12% for all the Turner zones in the Perpetual Finn 8. While there are resistivity spikes and high porosity pay all throughout the lower Turner one, resistivity and net porosity pay begin to subdue in the lower Turner two. In the upper Turner, the majority of the porosity and resistivity is lost, except for the upper most sand that caps the top of the Turner interval where there could be potential pay. Internal flooding surfaces are interpreted to not act as barriers to hydrocarbon migration and rather convey a transition from the best developed reservoir rock to moderate reservoir rock quality moving up section.

In order to assess the mechanical stratigraphy of the Turner, XRD was utilized to calculate a mineralogy-based brittleness index. A mineralogy based brittleness index (BI) calculation can help predict areas that would be ideal targets for hydraulic fracturing. Using XRD mineralogy to evaluate brittleness or mechanical strength of the rock is comparable to a log-based dynamic elastic brittleness index (Jarvie et al., 2007). Equation 5.1 is a modified



approach of Jarvie by Xu and Sonnenberg (2016) that was used for this study of the Turner.

$$BI = \frac{(Qz + Kspar + Plag + Ca + Dol + Pyr)}{(Qz + Kspar + Plag + Ca + Dol + Pyr + Cly + TOC)} \quad (5.1)$$

Where  $Qz$  is the weight fractional quartz content,  $Kspar$  is the weight fractional potassium feldspar content,  $Plag$  is the weight fractional plagioclase content,  $Ca$  is the weight fractional calcite content,  $Dol$  is the weight fractional dolomite content,  $Pyr$  is the weight fractional pyrite content,  $Cly$  is the weight fractional potassium feldspar content, and  $TOC$  is the total organic carbon content. This methodology compares the sum of the brittle minerals and divides it by the sum of the brittle and ductile minerals. XRD was only available for the Colen 10-10 core and the McTuillin-Federal 1 core to compute these curves. Integrating mechanical stratigraphy with reservoir quality, targeting can be refined to include intervals with the most porous and permeable zones while still being brittle for successful completions and increase well production.

Figure 5.6 shows prospective target intervals for the Colen 10-10 well. The target intervals are those where high concentration of reservoir Facies, 1, 2, 4, and 5 stack, with the highest zones of porosity, permeability and resistivity. In addition, a high brittleness index is calculated in these zones. It is critical to integrate the data, as some zones of high resistivity and brittleness index can be a result of calcite cements and would be expected to have low porosity and permeability. This can be seen in core in the medium-grained sandstone of Facies 6 at a core depth of 5297 feet. These 15-25 foot targets are optimal thickness for drilling assuming that hydraulic stimulation would be able to propagate in both directions without the interference of fracture barriers. There are no fracture barriers inferred in the Turner since the mudstones have a high percentage of silt, making them not highly ductile, and are only 6-10 feet thick. With this observation, primary targets were chosen in the section to be considered the lower Turners "sweet spot". These "sweet spots" are identified as zones

of high porosity, high permeability, high resistivity, a high brittleness index, and in a zone primarily composed of Facies 1, 2, 4, and/or 5. Due to the lack of data and coverage in the lower Turner two zone, and based on the available core and log data, the primary targets were chosen for the lower Turner one zone where rock quality appears best. However, from petrophysical logs and core description, the lower Turner two zone shows potential pay and targets are considered secondary due to a lack of available data.

Figure 5.7 is an integrated image of the prospective reservoir targets determined for the McTuillin-Federal 1 well. Ideal targets are areas of the highest porosity, permeability, brittleness index, and resistivity in the lower Turner one zone. Which correspond to the highest concentration of the reservoir Facies 2, 4, and 5. There also appears to be a pay zone in the lower Turner two zone in a section of high porosity, permeability and brittleness, with resistivity greater than 5 ohm-m in the upper laminated and bioturbated sands.

Figure 5.8 illustrates the prospective reservoir targets determined for the Dreiling-Federal 7 well. Ideal targets are areas of high porosity, permeability, and resistivity in the lower Turner one zone. These zones correspond to the highest concentration of reservoir facies. A lower Turner two target was chosen as well that has a thick interval of reservoir facies. The Dreiling-Federal 7 well has the lowest variability of facies changes moving up the core, where thick successions of reservoir Facies 2, 4, and 5 occur in the strata above the MnFS above the medium-grained sandstone of Facies 6. The resistivity kick at a core depth of 4783 feet is interpreted to be an increase in calcite cements in the lower Turner one.

Figure 5.9 shows chosen intervals of prospective reservoir targets determined for the Perpetual Finn 8 well. Ideal targets are areas of the highest porosity, permeability, and resistivity in the lower Turner one and two zones, which correspond to the highest concentration of reservoir facies. The lower Turner one target zone is a 15 foot interval of predominantly reservoir facies and a high porosity, permeability, and resistivity zone. The lower Turner two prospective target is a 20 foot interval of laminated and bioturbated sands with high porosity, resistivity, and permeability.

●  
Perpetual Finn 8

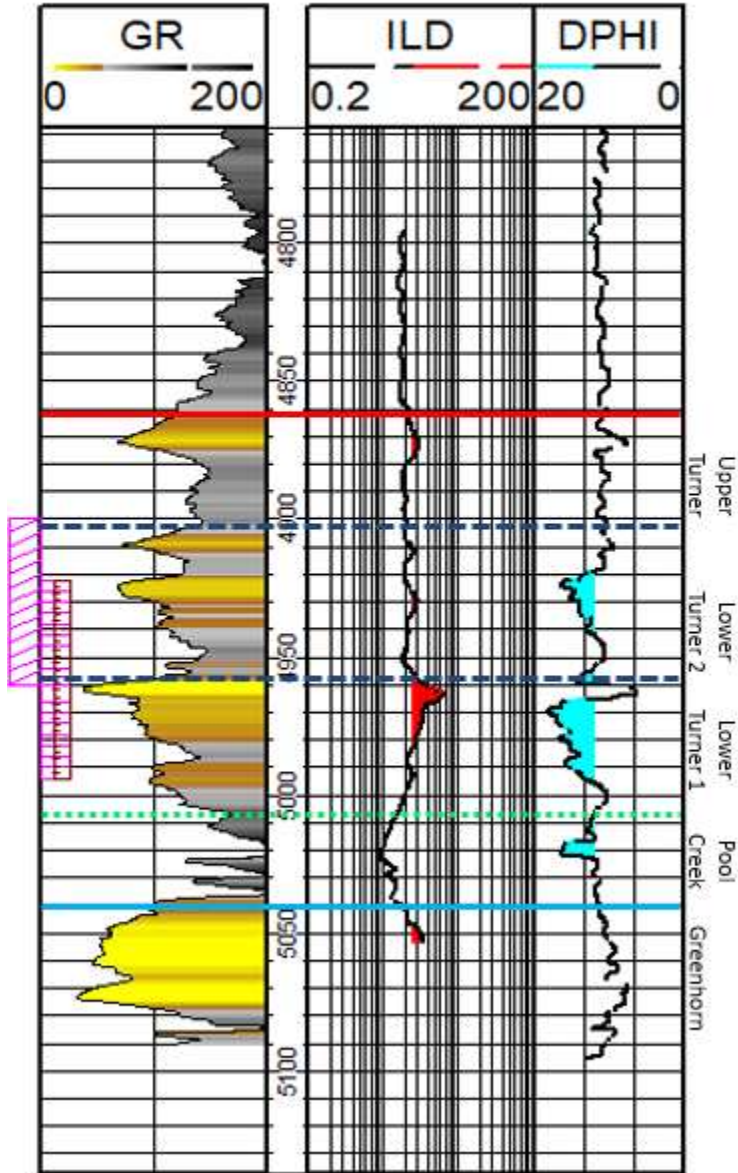


Figure 5.5: Type log section for the Perpetual Finn 8 that shows the gamma ray, resistivity, and density porosity profile through the Turner. Pink stippled bar shows cored interval and pink dashed bar shows perforated interval. Resistivity is filled in red where  $ILD > 5$  Ohm-m, and porosity is filled in blue where  $DPHI > 12\%$ . Net productive pay intervals are indicated by zones where both these cutoffs are met.

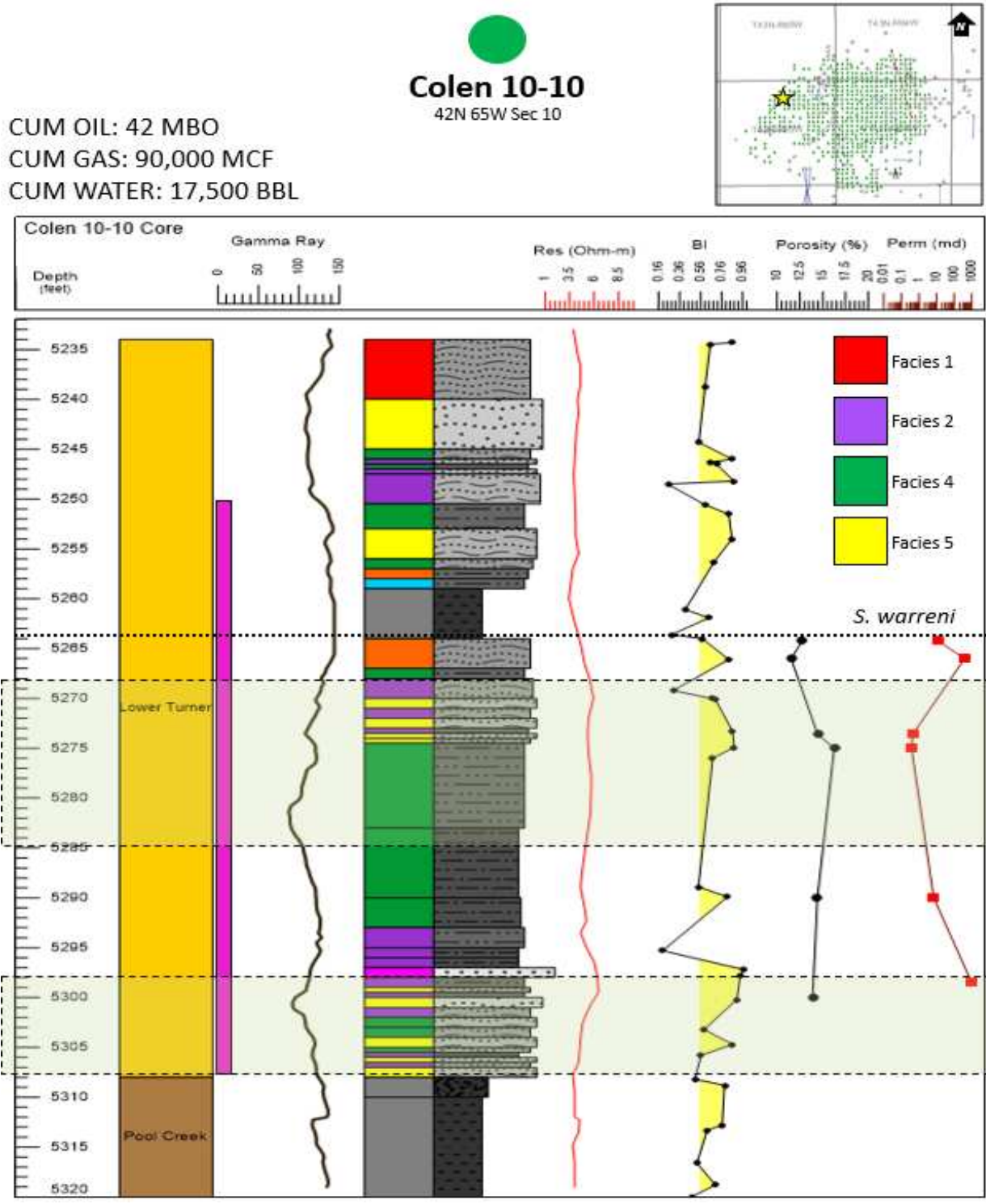


Figure 5.6: Chosen reservoir targets (green shaded intervals) for the Colen 10-10 well based upon facies classification, gamma ray signature, a resistivity cutoff, an arbitrary brittleness index cutoff of 0.55, high porosity values, and high permeability values. Well location is shown on the map in the right corner, and current production information is on the right corner where the perforated interval is shown in pink.

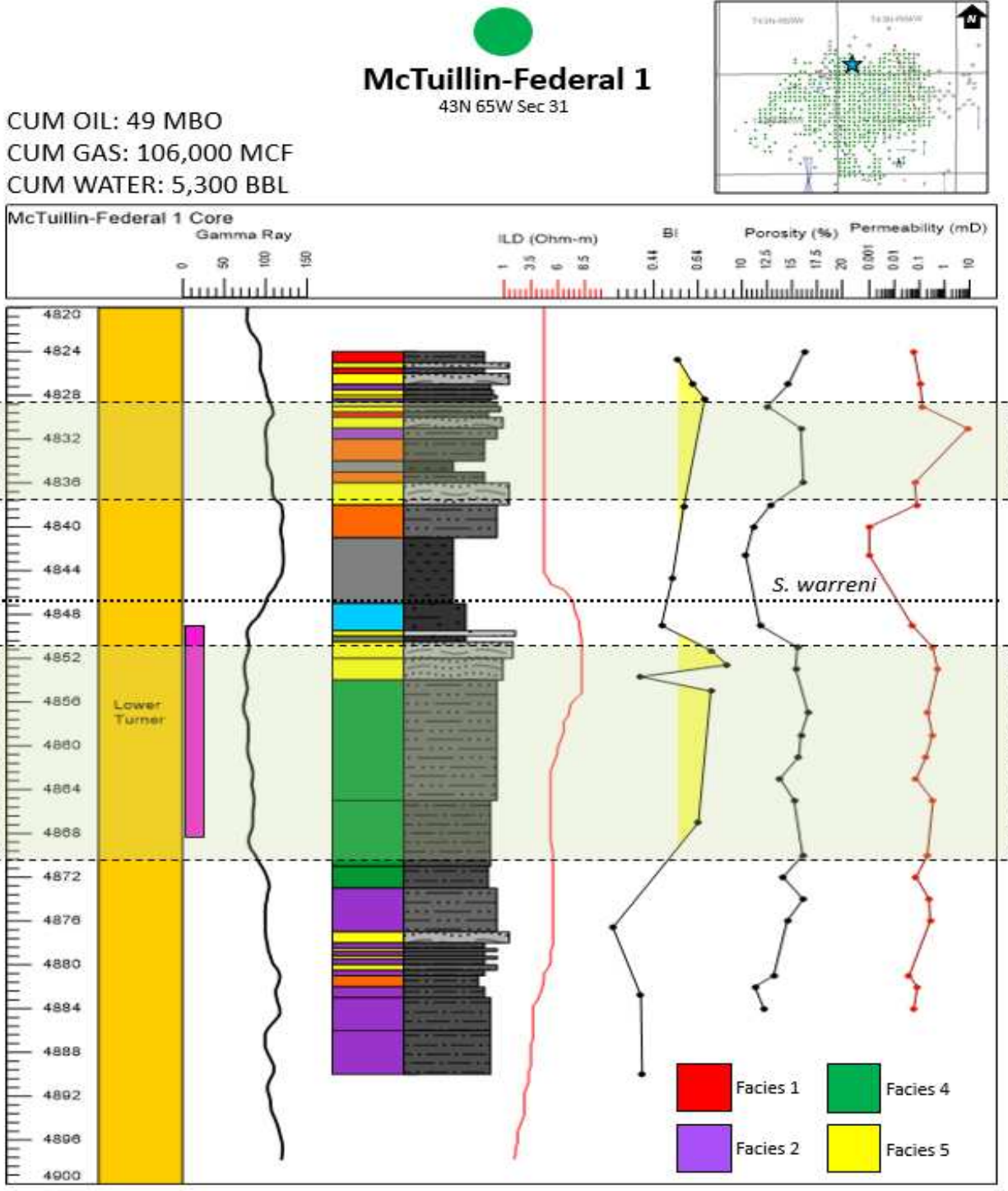


Figure 5.7: Chosen reservoir targets (green shaded intervals) for the McTuillin-Federal 1 well based upon facies classification, gamma ray signature, a resistivity cutoff, an arbitrary brittleness index cutoff of 0.55, high porosity values, and high permeability values. Well location is shown on the map in the right corner, and current production information is on the right corner where the perforated interval is shown in pink.

CUM OIL: 36 MBO  
 CUM GAS: 68,000 MCF  
 CUM WATER: 4,800 BBL

**Dreiling-Federal 7**  
 42N 64W Sec 15

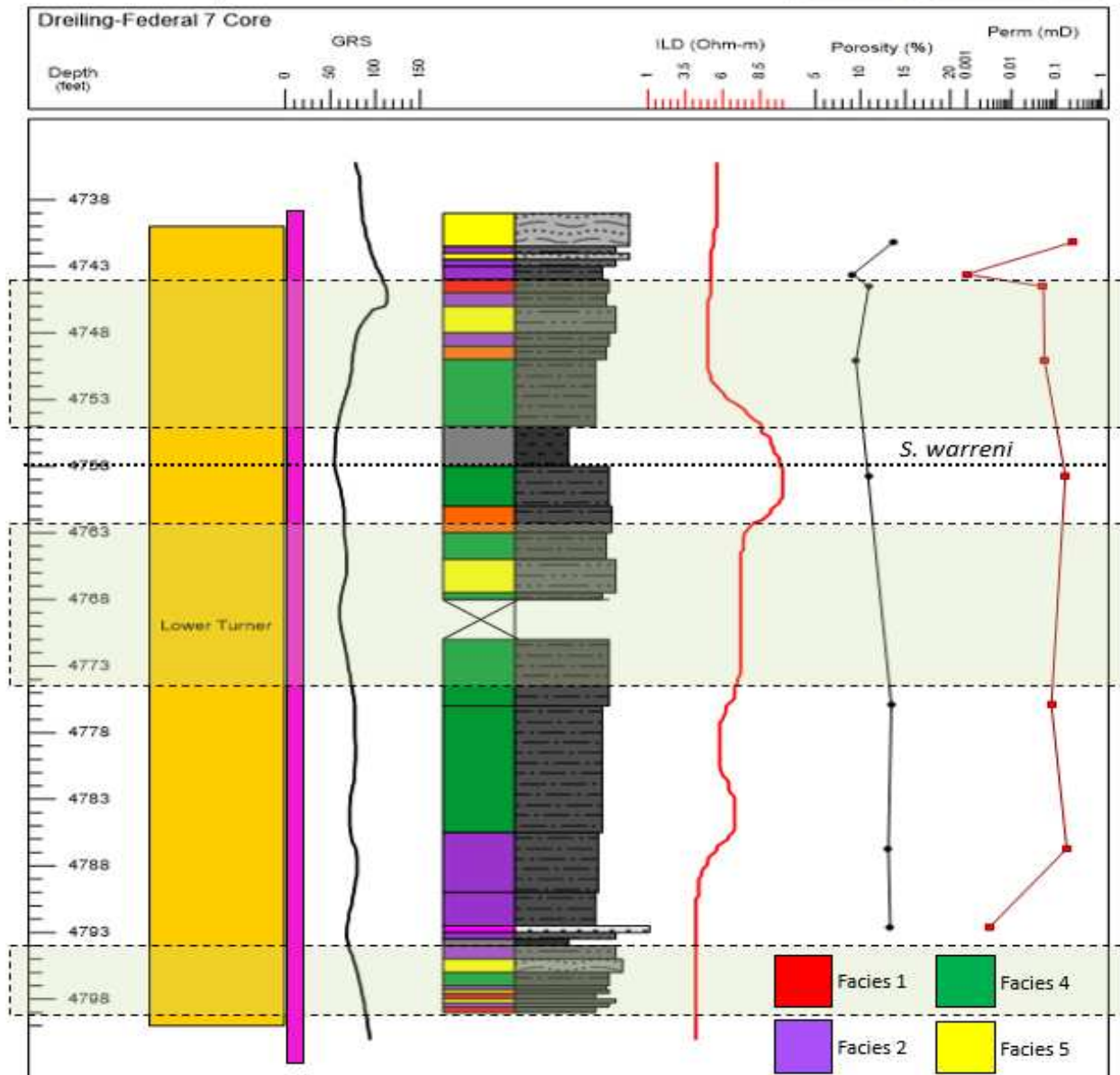


Figure 5.8: Chosen reservoir targets (green shaded intervals) for the Dreiling-Federal 7 well based upon facies classification, gamma ray signature, a resistivity cutoff, high porosity values, and high permeability values. Well location is shown on the map in the right corner, and current production information is on the right corner where the perforated interval is shown in pink.

CUM OIL: 56 MBO  
 CUM GAS: 96,000 MCF  
 CUM WATER: 30,000 BBL

**Perpetual Finn 8**  
 42N 64W Sec 5

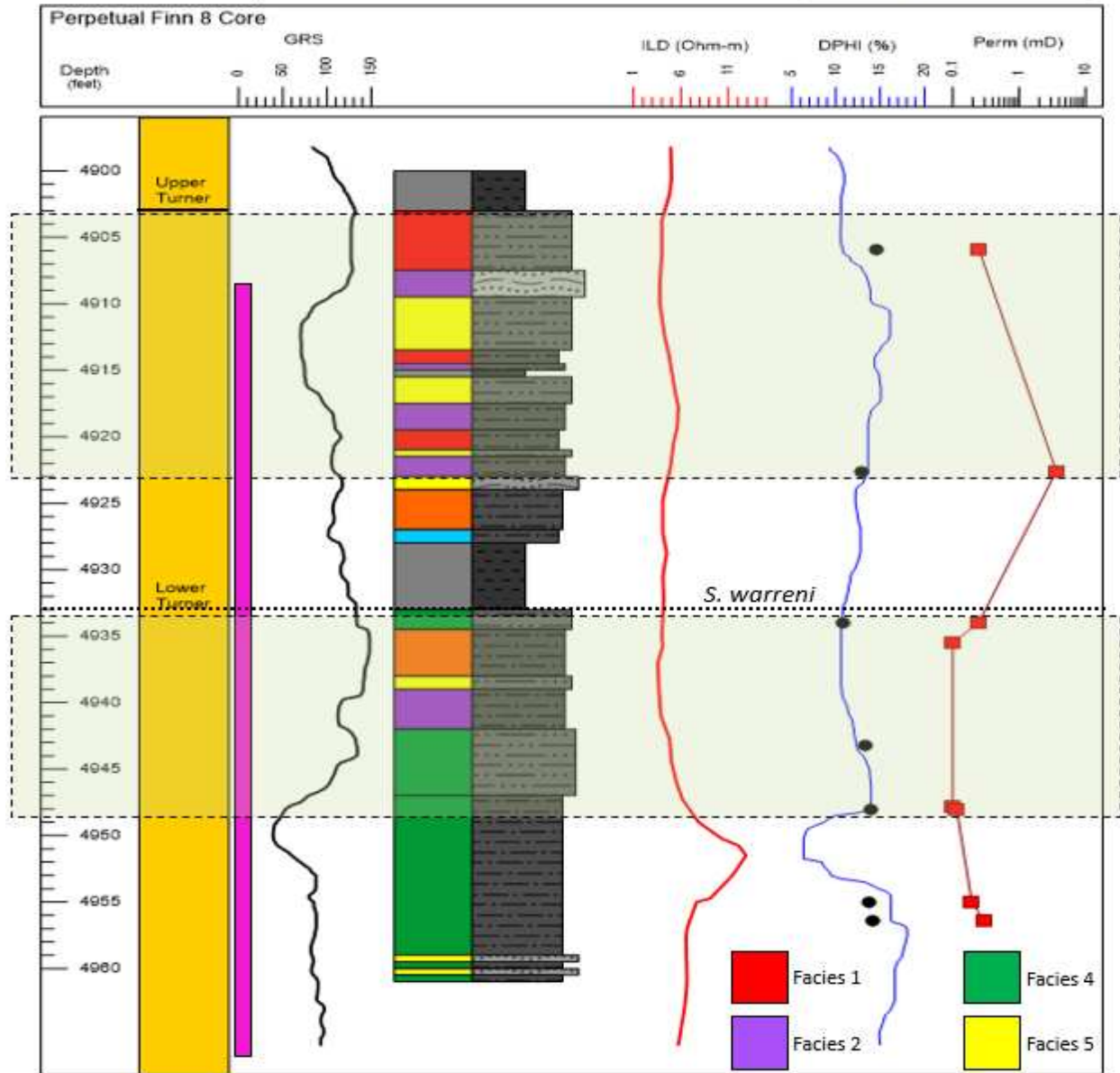


Figure 5.9: Chosen reservoir targets (green shaded intervals) for the Perpetual Finn 8 well based upon facies classification, gamma ray signature, a resistivity cutoff, high porosity values, and high permeability values. Well location is shown on the map in the right corner, and current production information is on the right corner where the perforated interval is shown in pink.

## 5.5 Reservoir Mapping

Reservoir maps were created utilizing 700 wells in the study area at Finn-Shurley Field, located in south central Weston County. Figure 5.10 displays an west to east cross section of the four study area wells that were analyzed in great detail. Due to the vintage of the majority of the wells located in the field, the petrophysical log suite primarily consisted of gamma ray, spontaneous potential (SP), and resistivity curves. Approximately a dozen wells in the study area had density porosity (DPHI) logs through the Turner interval. However, there was not enough coverage to include these logs when creating pay maps. From the data set, isopach and resistivity maps were generated for the lower Turner interval as well as the entire Turner interval. Maps for the individual Turner one and two zones were possible due to the ability to correlate these surfaces in gamma ray and resistivity logs across Finn-Shurley. Isopach maps show the thickness of the Turner reservoir across the study area, where the isopach map with pay shows the thickness of the Turner where there is believed to be hydrocarbons, or a resistivity value greater than 5 ohm-m. This resistivity cutoff was chosen based upon extensive analysis of resistivity logs in the field, and a thorough understanding of the resistivity of the shale baseline of areas not believed to be charged with hydrocarbons. Resistivity of this interval is interpreted to be low based on the high percentage of clay that is present throughout the Turner. Resistivity logs were the primary petrophysical log used in reservoir mapping and are pervasive throughout Finn-Shurley where many other petrophysical logs are not. From logs, resistivity kicks appear throughout the lower Turner interval and begin to diminish moving into the lower Turner two. The upper Turner generally has a single resistivity spike at the very top of the interval (Figure 5.10). From these observations, the entire lower Turner interval appears to be saturated with hydrocarbons.

Figure 5.11a illustrates an isopach of the entire Turner interval, from the top of the Turner to the basal unconformity. The entire Turner interval thickens across Finn-Shurley Field and thins slightly moving outward. This seems to be a result of extra accommodation space available for the Turner, specifically the lower Turner one zone. This accommodation



space could be a result of a paleo-low associated with the Clareton lineament shown by Slack (1981) that trends NE-SW just north of the study area. Pay, or resistivity greater than 5 ohm-m, correlates to the thick in the Finn-Shurley Field. Figure 5.11b shows a resistivity map of the Turner across the Finn-Shurley area. This map was created by summing the thickness of Turner that had resistivity greater than 5 ohm-m and contoured to show where the thickest interval of high resistivity rock is located across the field.

Figure 5.12a illustrates an isopach of the lower Turner interval, from the top of lower Turner to the unconformity. The lower Turner interval thickens across Finn-Shurley and thins moving outward. Pay in the form of resistivity correlates to the thick in Finn-Shurley. Figure 5.12b shows a resistivity map of the lower Turner across the Finn-Shurley area. Again, this map was calculated by summing the thickness of the lower Turner that had resistivity greater than 5 ohm-m. Contours highlight the thickest interval of high resistivity.

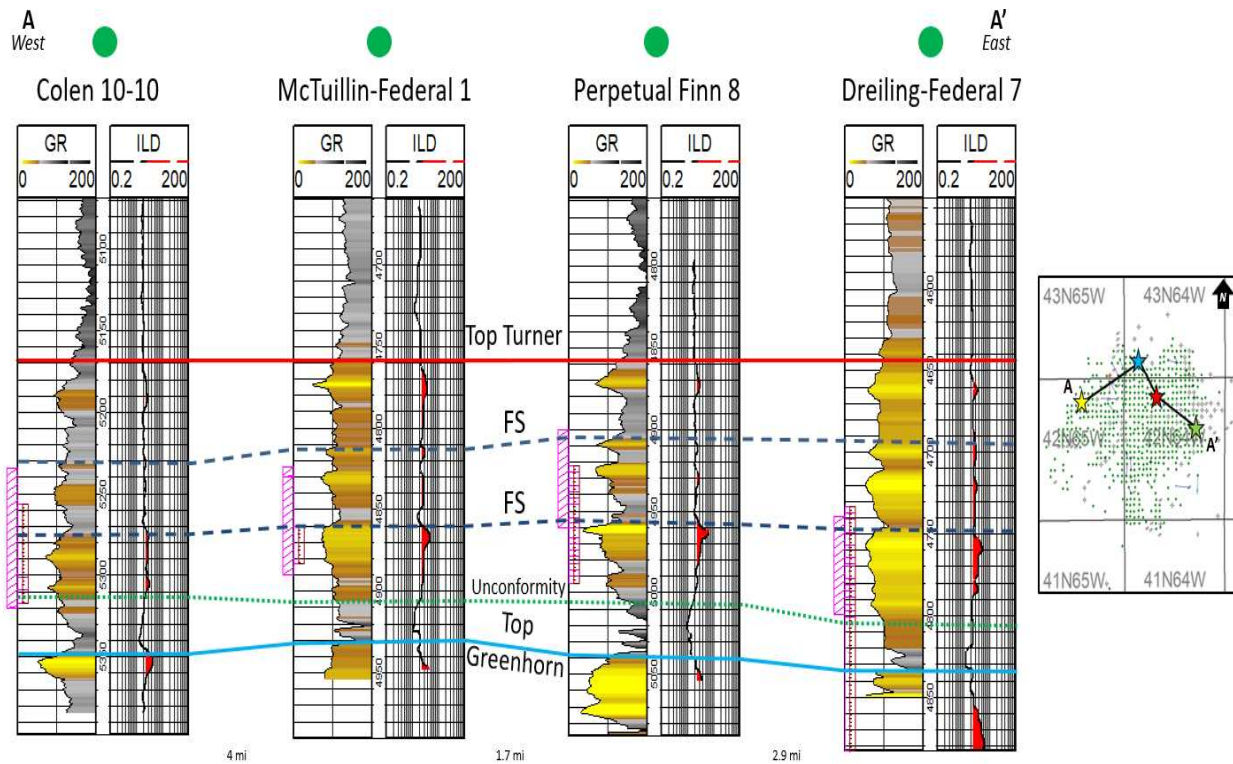


Figure 5.10: Stratigraphic cross section of key cored wells flattened on top of the Turner. Logs including gamma ray and resistivity logs with a cutoff of 5 ohm-m. Pink dotted bars show perforated interval and pink stippled bars show cored interval.

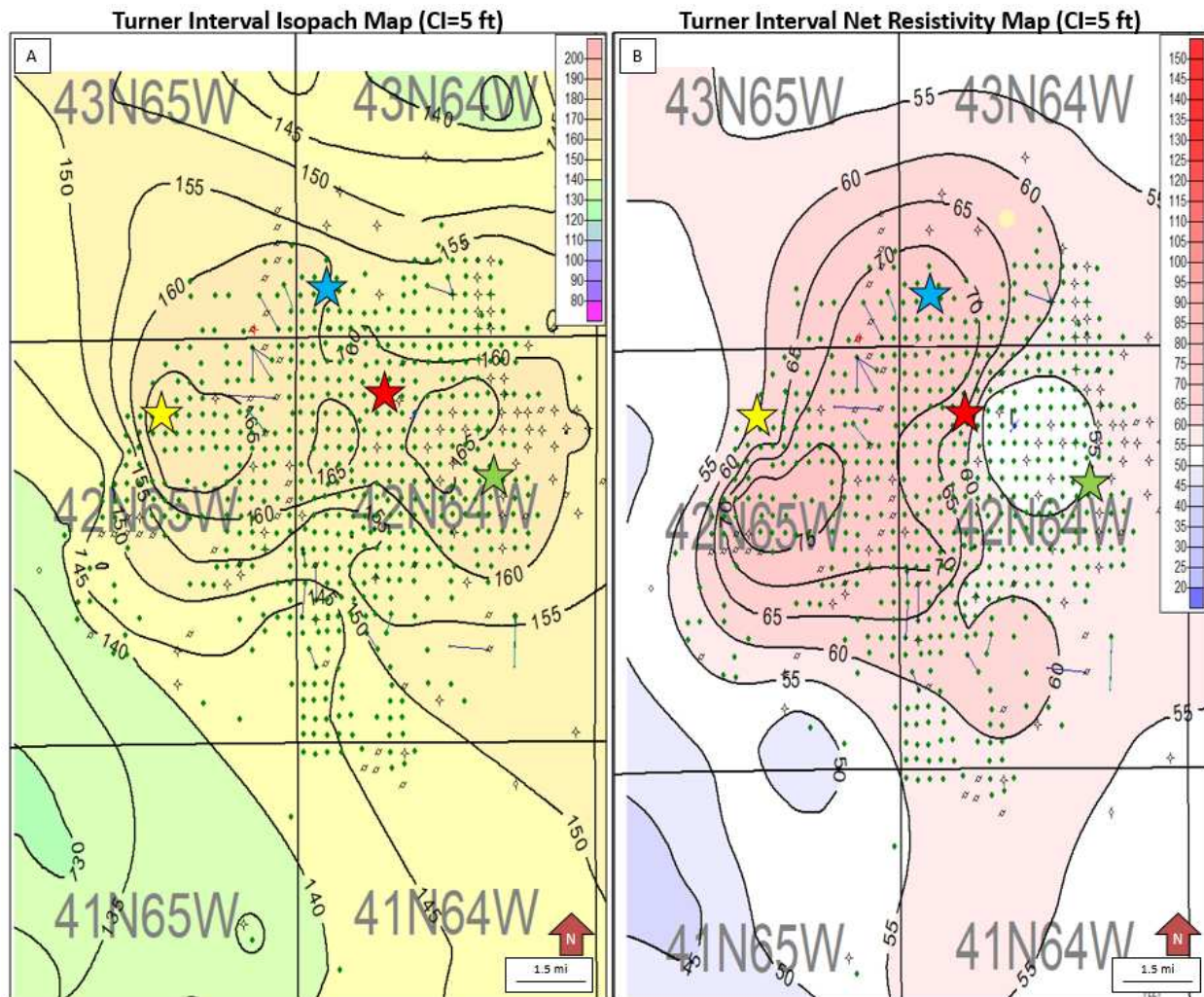


Figure 5.11: Maps generated for the entire Turner interval (Top Turner to Basal Unconformity). A) Isopach of the Turner in Finn-Shurley area. The thickest interval is located in the center of the study area. B) Net resistivity map of the Turner. Resistivity map is created by summing the thickness of the Turner where resistivity is greater than 5 ohm-m. Contoured map shows the thickest interval of resistive rock is located in the center of the study area. Stars represent the locations of the key cored wells for this study.

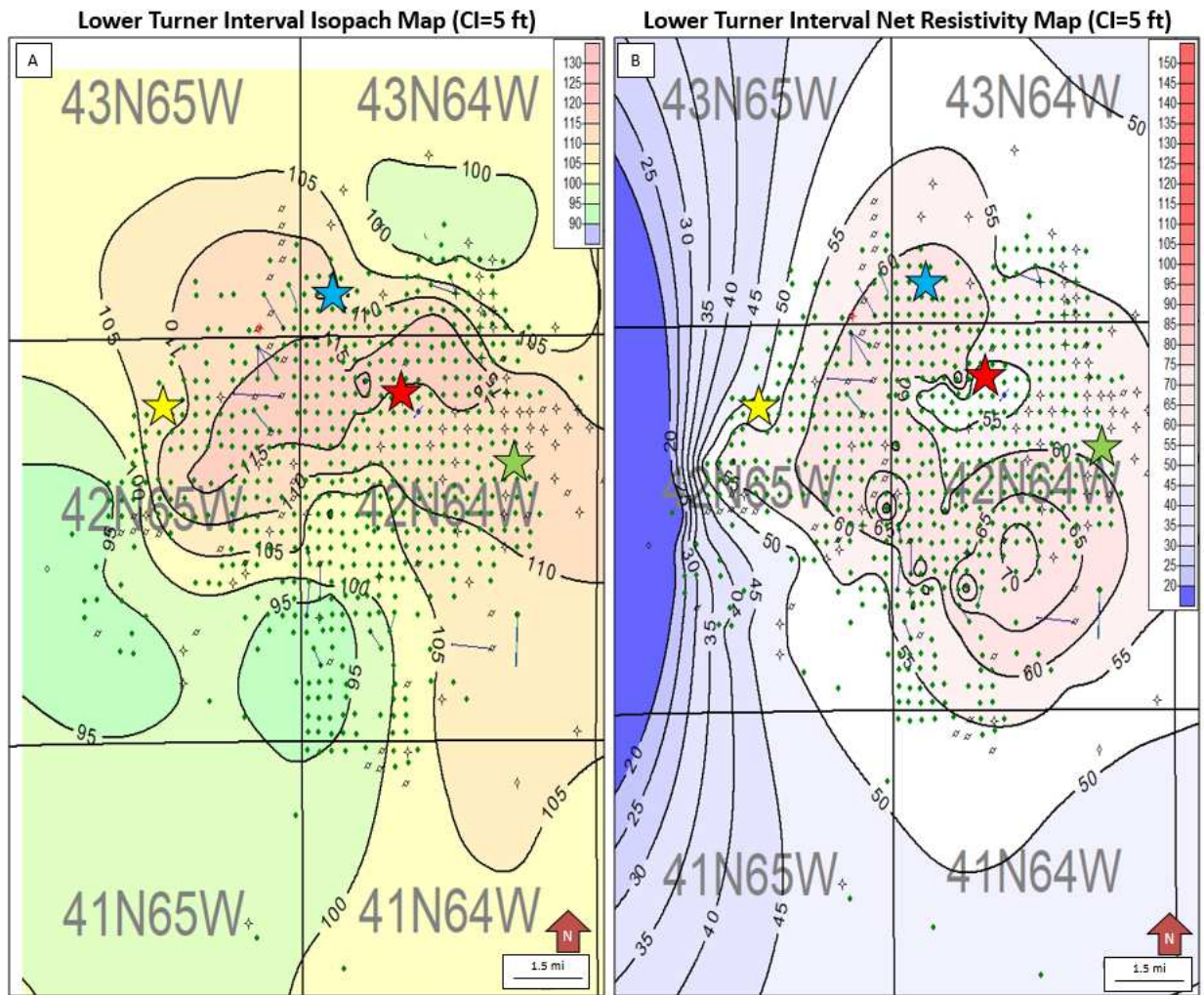


Figure 5.12: Maps generated for the lower Turner interval (Top Lower Turner to Basal Unconformity). A) Isopach of the lower Turner in Finn-Shurley area. The thickest interval is located in the center of the study area. B) Net resistivity map of the lower Turner. Resistivity map is created by summing the thickness of the lower Turner where resistivity is greater than 5 ohm-m. Contoured map shows the thickest interval of resistive rock is located in the center of the study area. Stars represent the locations of the key cored wells for this study.

## 5.6 Production

### 5.6.1 Historical Production

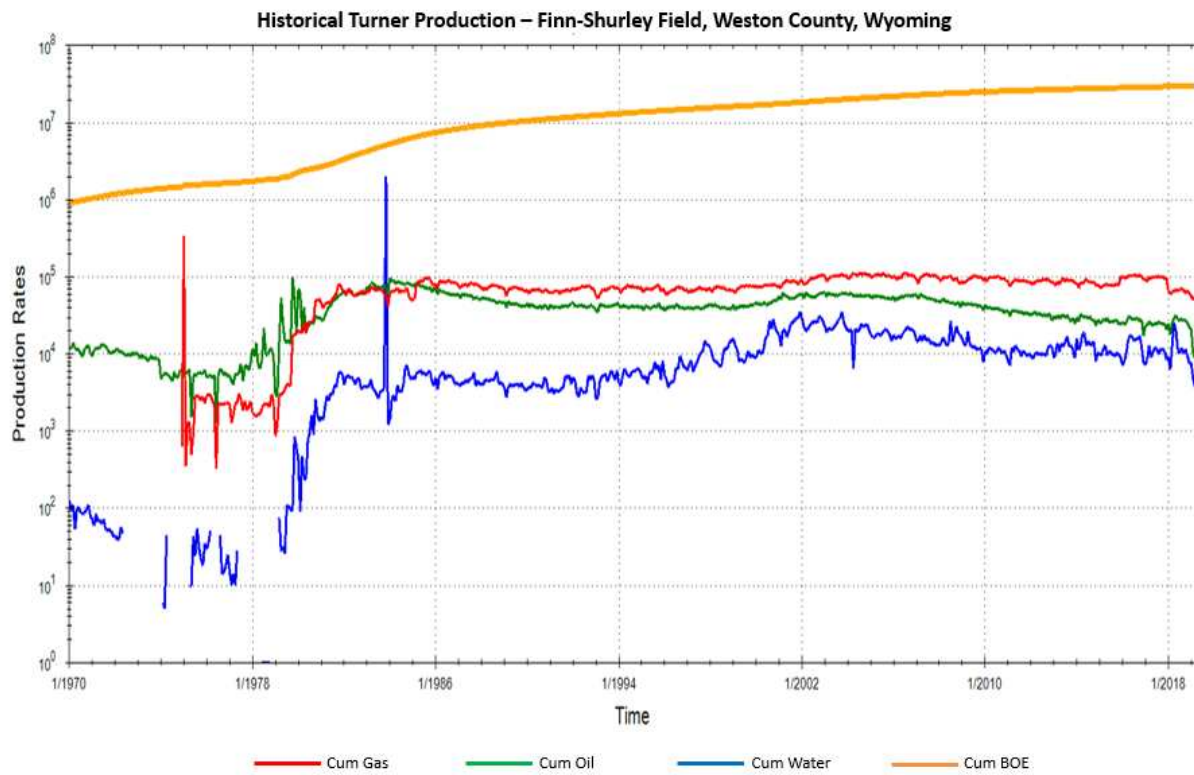
Finn-Shurley Field was first discovered in 1965 and further developed to target the prolific Turner sandy member reservoir. This field has continued to produce from the Turner

since the 1980's (Figure 5.13). Historically, this field has produced conventionally from vertical wells (Figure 5.14), but in recent years there has been an increase in production and horizontal drilling. The production increase in this area is largely due to improved drilling and completion techniques. Horizontal drilling in and around Finn-Shurley began around 2010 and is expected to continue in the coming years to stretch the boundaries of Turner pay outside the study area (Figure 5.14). In addition, historical vertical wells have been subjected to modern re-fracturing methods, or enhanced oil recovery methods, to extend the life of the well. The wells have been re-stimulated by methods such as a "huff and puff", a method which reduces oil viscosity with water injection, and cleans pores by heating the fluid. The addition of both horizontal drilling and re-fracturing of vertical wells, unlocks resources previously unavailable to wells drilled in Finn-Shurley, and expands the potential for economic production in Weston County. To date, Finn-Shurley has produced 23.5 million barrels of oil (MMBO) and 38.6 billion cubic feet of gas (BCFG) from the 748 wells drilled in the field.

### **5.6.2 Production Implications**

The thickness and resistivity trends illustrated in the previous reservoir mapping section was later compared to current production. This can aid to best understand the implications of geologic controls on hydrocarbon production from the Turner in Finn-Shurley Field. Figure 5.15 compares the thickness trends and resistivity trends with historical production in a bubble map. IHS production data was available for 707 wells in Petra for the study area. The available production data did not specify the target zone and could be the cause of any irregular trends. In general, the production is located in areas of thickest Turner interval seen across Finn-Shurley. In addition, most of the production is located in a region of high resistivity. These resistivity trends indicate hydrocarbon presence through thick sections of the lower Turner in Finn-Shurley Field. The introduction of horizontal drilling of the lower Turner sands across Finn-Shurley suggests that with modern completion techniques, untapped resource potential in these sands would be unlocked and produce in high volumes

in and around Finn-Shurley.



**Finn-Shurley Production:**  
**748 Wells**  
**Cum: 23.5 MMBO , 38.6 BCFG**  
**Avg per Well: 31.5 MBO, 51.6 MMCF**

Figure 5.13: Historical production chart of the Turner within the study area of Finn-Shurley field in south central Weston County. Shows cumulative oil (green line), gas (red line), and water (blue line) produced from the field with the total cumulative barrels of oil equivalent (BOE) (orange line).

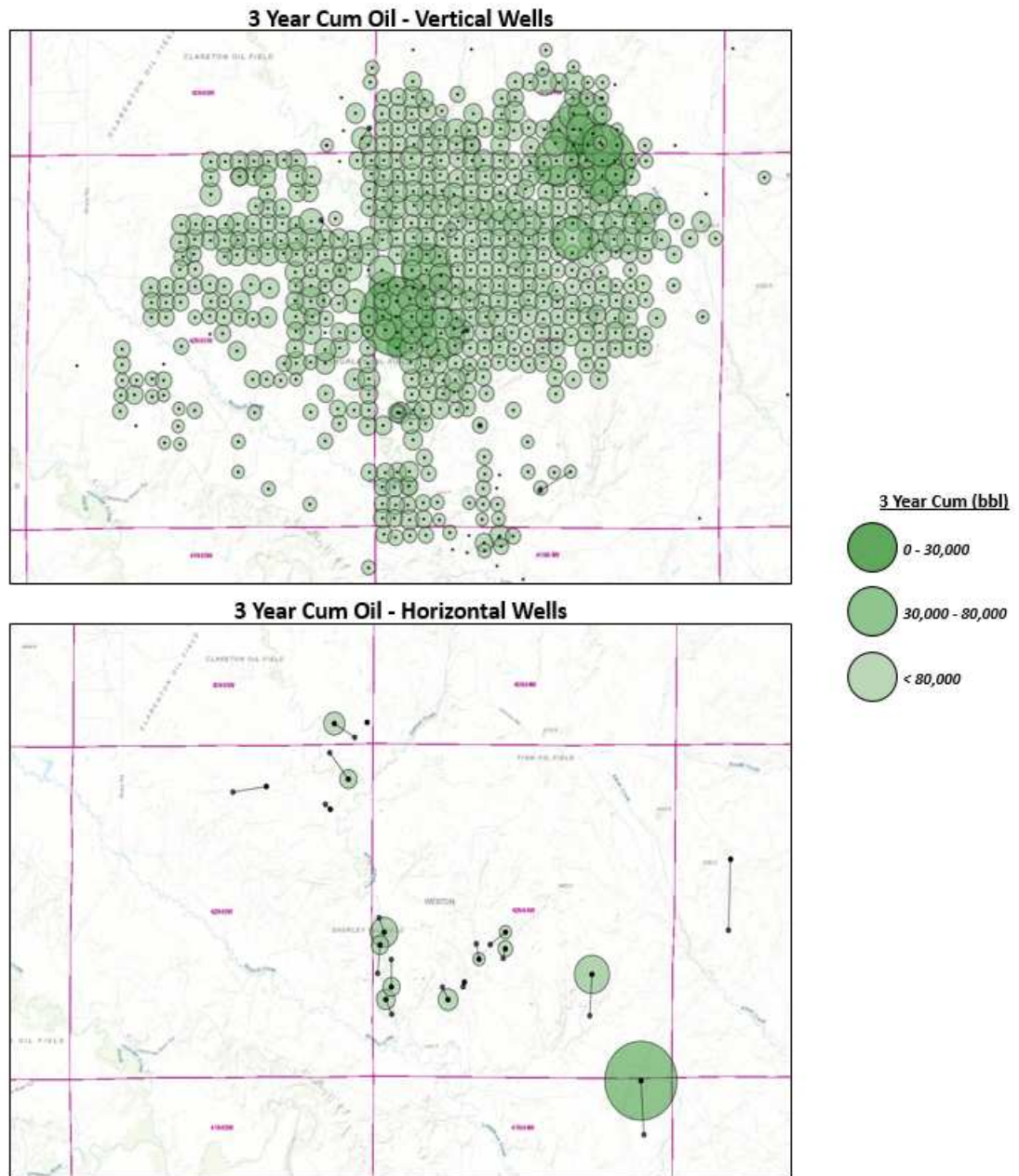


Figure 5.14: Historical production map of the Turner within the study area of Finn-Shurley field in south central Weston County. Illustrates a bubble map of 3 year oil cum's from historical vertical wells (top). In addition, it illustrates a bubble map of 3 year cum's from historical horizontal wells (bottom).

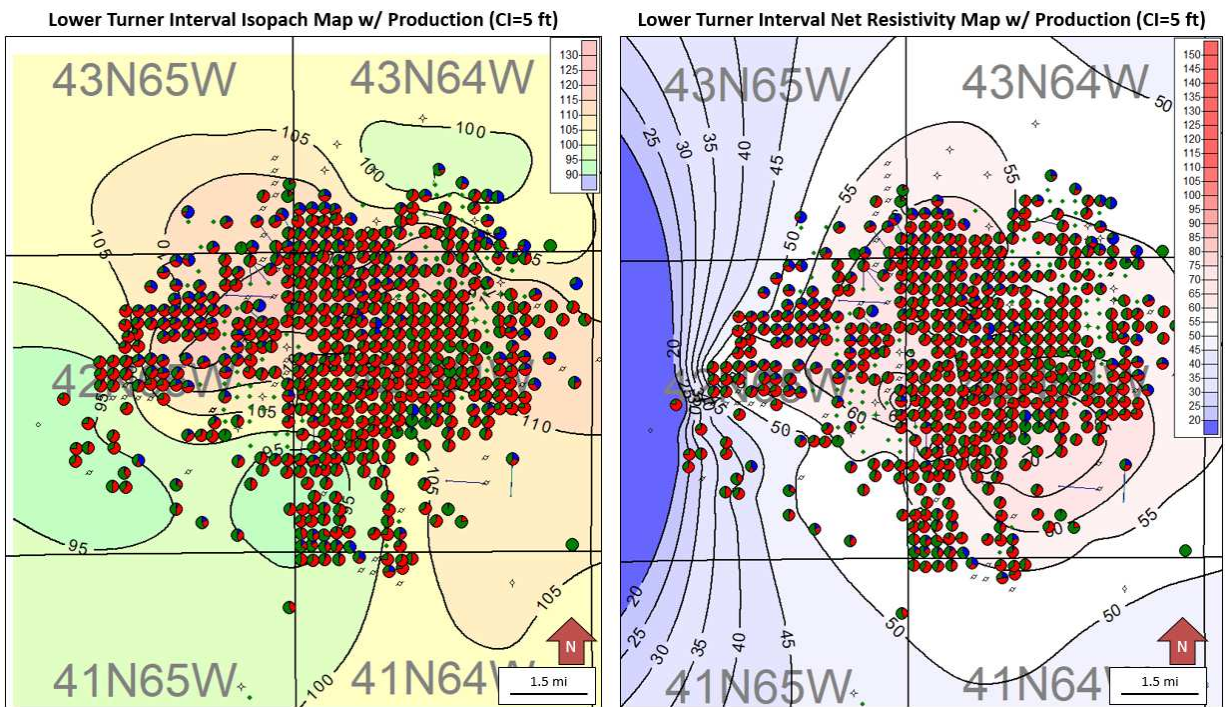


Figure 5.15: Lower Turner (Top Lower Turner to Basal Unconformity) production map for Finn-Shurley field. A) IHS Production is displayed on top of the Lower Turner isopach. B) IHS Production is displayed on top of the net resistivity map for the lower Turner.

## 5.7 Discussion of Total Unconventional Petroleum System

Based upon the multi-scale analysis conducted on the available dataset, each element of the unconventional petroleum system plays a critical role in creating an ideal environment for economic hydrocarbon production at Finn-Shurley Field. Each element of the unconventional system has a direct effect on the environment which allows for a hydrocarbon saturated reservoir interval to exist in an economic quantity be targeted and produced from. A thorough understanding of each petroleum system element at Finn-Shurley is required to comprehend the total hydrocarbon potential of this unconventional system in southern Weston County. The Turner has proven to be a prolific target interval in Weston County due to a specific accumulation of facies that have sustained and preserved excellent porosity and permeability values. The Turner has also acted as a combination unconventional

stratigraphic trap for migrated hydrocarbons in an active petroleum system.

The preservation of initial porosity and permeability is largely a result of both mineralogical and diagenetic controls on reservoir quality. In general, cleaner, fine-grained sandstone facies with early grain coats of chlorite and authigenic microcrystalline quartz were critical in preventing secondary quartz cements, which is proven to decrease porosity and permeability. In addition to preserving porosity and permeability, from mineralogy-based brittleness calculations, these facies tend to have a higher brittleness index due to the overall lack of ductile minerals such as clay. High clay content can be unfavorable for geomechanical properties, but the high percentage of silica and lithics throughout the entire interval suggest the Turner has excellent mechanical stratigraphy and a sought after completion target for hydraulic fracture stimulation. Additional geomechanical research could be done with the addition of petrophysical logs, such as dipole sonic, to the dataset in order to calculate Poisson's ratio and Young's modulus.

The Turner is stratigraphically positioned between two world class source rocks, the Mowry and the Niobrara formations. Both source rocks have been proven to generate and expel mature hydrocarbons into the basin. The Turners location in stratigraphic order, along with the structural complexity that occurs throughout the PRB, suggests multiple migration pathways could occur. Lafargue et al., (1994) shows that in conventional petroleum systems with marginally-rich source rocks, hydrocarbon expulsion efficiencies is higher when in close proximity to carrier beds. These migration pathways allow for the peak maturity oil from these two formations to migrate updip into the Finn-Shurley area, where it can be trapped in a tight sandstone carrier bed. From petrophysical analysis, the entire lower Turner appears to be saturated with hydrocarbons based on resistivity logs and production data. Changes in lithology and the loss of porosity and permeability moving up section appear to act as a local seal top for hydrocarbons.

Understanding the controls on hydrocarbon production from the Turner can aid in choosing targets, drilling wells, and picking proper completion techniques. The targets for the



Turner in Finn-Shurley Field suggest dependency on high porosity and permeability zones which correlate to the lower laminated, cleaner, fine-grained sandstone facies. These primary reservoir facies are a result of prograding sandstones that have been reworked by tides and storms and bioturbated to an extent that was not harmful to rock quality. Post deposition, these reservoir facies experienced excessive grain coating which continued to preserve initial porosity and permeability and were not deterrents to continued diagenetic processes such as quartz overgrowths and calcite cements. Post deposition, thermally mature hydrocarbons from two potential source rocks were able to migrate into the system, and become trapped in economic quantities. With the more mature Mowry Formation sourced hydrocarbons being the more likely, proximal source. Only by integrating microscopic scale, core scale, and log scale data, the lower Turner unconventional petroleum system can be properly understood and developed in Weston County, Wyoming.

CHAPTER 6  
CONCLUSIONS AND FUTURE RECOMMENDATIONS

**6.1 Conclusions**

- 1) Eight facies were identified from 271 feet of core from four key wells, the Colen 10-10, the Perpetual Finn 8, the McTuillin-Federal 1, and the Dreiling-Federal 7. Facies were classified and named based upon lithology, grain size, bioturbation intensity, and sedimentary structures. Due to the heterolithic nature of the Turner microscope scale observations were integrated with core based measurements such as mineralogy, porosity, and permeability to determine four reservoir facies, one primary and three secondary, and four non-reservoir facies.
- 2) Facies 1, 2, 4, and 5 are considered reservoir facies for the Turner. These were determined based upon a criteria of an average porosity measurements greater than 12%, an average permeability measurements greater than 0.1 mD, and a large average  $R_{35}$  value, ideally greater than 0.5. Reservoir quality was further confirmed by petrographic thin section and FE-SEM analysis.
- 3) The Turner is comprised of three major coarsening upward sequences each capped with a flooding surface. The flooding surfaces correlates to a change in the Western Interior biozone. This trend can be observed and correlated in petrophysical logs, core observations, and vertical facies assemblages.
- 4) Facies 1, and 4 are heavily bioturbated, which does not appear to always be detrimental to initial porosity and permeability, suggesting bioturbation may have inhibited other diagenetic mechanisms from diminishing initial porosity and permeability.
- 5) Both type and diversity of ichnofauna combined with intensity of bioturbation influence the ability for a rock to be considered reservoir or non-reservoir quality. Facies with

higher intensity of bioturbation and larger diversity of ichnofauna appear to have inhibited mechanisms that destroy initial porosity and permeability compared to intervals of low diversity and lower intensity.

- 6) The Turner was deposited in a shallow marine environment after a worldwide drop in sea level. This allowed for sediments to prograde out into the basin and be later reworked by tidal and storm processes on the shelf.
- 7) The distribution of facies generally is uniform across the study area. Isopach maps suggest this field was a thicker paleo-depocenter at the time of deposition. Increased accommodation space may have resulted from proximity to paleo-lows associated with basement faults, such as the Clareton lineament, seen throughout the PRB.
- 8) Origin and type of silica is important for reservoir quality. Early grain coating of authigenic microcrystalline quartz resulted in the preservation of initial porosity and permeability by inhibiting the nucleation and growth of secondary quartz cement in the pore space.
- 9) Early coating of authigenic microcrystalline quartz in addition to a secondary grain coating of chlorite blades corresponds to zones of higher porosity and permeability in the Turner.
- 10) Intervals with patchy or missing early grain coats have lower porosity and permeability due to the addition of secondary quartz cements. These intervals tend to be fine-grained with a higher percentage of mud. These quartz cements are likely sourced from pressure solution, feldspar dissolution, and authigenic clays.
- 11) The medium-grained sandstones were highly influenced by diagenesis with the addition of late calcite cements filling available pore space. This does not occur as frequently in the fine-grained muddier intervals.

- 12) There is a thick pay interval across Finn-Shurley in a east-west orientation. This was determined primarily from resistivity logs through the Turner corresponding to known productive wells.
- 13) Integrating multi-scale analyses can optimize targeting for the lower Turner sands in Finn-Shurley Field.

## **6.2 Future Recommendations**

- 1) Obtain more cores within southern Weston county throughout the entire Turner interval. More core could help to better understand the facies trends, both laterally and vertically, across the study area for the reservoir rock.
- 2) Gather MICP data in addition to more core based porosity and permeability measurements to better understand the connectivity of the reservoir and the porosity and permeability relationships with core facies.
- 3) Collect and interpret seismic data to understand and constrain the macro-scale depositional and structural framework for Finn-Shurley field. This would add a structural and paleo-structural component to reservoir development in the PRB.
- 4) Refine the XRF calculated mineral model and calibrate to best match XRD data. More XRD data would be ideal in constraining the calibration and in addition could be used to create more mineralogy-based geomechanical curves.
- 5) Further analyze brittleness of the Turner using XRD and computed XRF to mineral model. Mineralogy based brittleness models were created for the Colen 10-10 well but are preliminary and need better constraint. Again, more XRD data would be useful in calculating brittleness of other cores.
- 6) Collect XRF data on all cores available in Finn-Shurley to further refine the chemofacies analysis and better calibrate the number of chemofacies necessary to visualize all the

elemental trends within the core. These trends can then be integrated with other reservoir properties, such as porosity, mechanical stratigraphy, or diagenetic features.

- 7) Incorporate more samples representative of more facies in a diagenetic study of the Turner. By integrating more samples and more cores, further understanding of the diagenetic effects on reservoir quality can be assessed using EDS, CL, BSE, and SE images.
- 8) Include a more detailed and extensive thin section analysis, using florescent dyes and stains to constrain timing and sources of silica and chlorite.
- 9) Integrate production and pressure data with interpreted reservoir facies and targets to better understand potential sweet spots and refine targeting.
- 10) Expand regional well log sections and subsurface mapping to establish Turner depositional fairways and potential stratigraphic traps.
- 11) Analyze recent horizontal drilling trends, completion techniques, and production trends to refine targeting and sweet spot identification.
- 12) Map production and pressure data, and integrate with Mowry and Niobrara maturity maps to define future sweet spots for development.
- 13) Collect more source rock analysis on the Mowry, Niobrara, and other prospective source rock intervals such as the Greenhorn and Pool Creek, to better establish quality, quantity, and maturity trends. Produced oils at Finn-Shurley can then be compared to source rock extracts to determine most likely source(s).
- 14) Collect more petrophysical log data to see what core scale trends can be scaled to petrophysical logs, such as geomechanical logs, sonic logs, mineralogy logs, and porosity logs.

## REFERENCES CITED

- Anna, L.O., 1986, Geologic framework of the ground water system in Jurassic and Cretaceous rocks on the Northern Great Plains, in parts of Montana, North Dakota, South Dakota, and Wyoming: U.S. Geological Survey Professional Paper 1402-B, 36 p.
- Anna, L.O., 2009, Geologic assessment of undiscovered oil and gas in the Powder River Basin Providence, Wyoming and Montana: USGS Digital Data Series DDS-69-U, USGS, 93 p.
- Asquith, D.O., 1970, Depositional topography and major marine.
- Blakey, R, 2013, North American Key Time-slices Series. Colorado Plateau Geosystems, Inc.
- Cobban W.A., 1952, Cretaceous rocks on the north flank of the Black Hills uplift, in Sonnenberg, F.P., ed., Billings Geological Society, 3rd annual field conference, Black Hills-Williston Basin, Guidebook, p. 86-88.
- Cecil, C.B and Heald, M.T., 1971, Experimental investigation of effects of grain coatings on quartz growth. *Journal of Sedimentary Petrology*, 41(2): 582-
- Craigie, N.W., 2018. Principles of Elemental Chemostratigraphy: A Practical User Guide. Principles of Elemental Chemostratigraphy.
- Deer, W.A., Howie, R.A. and Zussmn, J., 2013a Chlorite Group: Clinochlore  $(Mg)_{10}Al_2[Al_2Si_6O_{20}](OH)_{16}$  - Chamosite  $(Fe^{2+})Al_2[Al_2Si_6O_{20}](OH)_{16}$ . In: W.A Deer, R.A. Howie and J. Zussman (Editors), *An Introduction to the Rock-Forming Minerals*, Mineralogical Society of Great Britain and Ireland.
- Dolton, G.L., and Fox, J.E., 1995, Powder River Basin Province (033): U.S. Geological Survey Web site [http:// energy.cr.usgs.gov/oilgas/noga/1995.html](http://energy.cr.usgs.gov/oilgas/noga/1995.html), Powder River Basin.
- Gustason, E.R., 2015, Playing Battleship in the Powder River Basin—Exploring for isolated, shelf sandstone bodies and associated halo plays of the Wall Creek and upper Turner Sandstone: Rocky Mountain Section-SEPM luncheon talk, September 29, 2015.
- Hancock, J. M. Kauffman, E. G. 1979. The great transgressions of the Late Cretaceous. *journal of the Geological Society of London* 136, 175-186.
- Haun, J. D., 1958, Early Upper Cretaceous stratigraphy, Powder River Basin, Wyoming: Powder River Basin of Wyoming; 13th Annual Field Conference Guidebook.

- Hartmann, D.J., and Beaumont, E.A., 1999, Predicting reservoir system quality and performance: In Exploring for Oil and Gas Traps, AAPG Treatise of Petroleum Geology, Handbook of Petroleum Geology, edited by Edward A. Beaumont and Norman H. Foster, p.9-1 to 9-154
- Haq, B.U., 2014, Cretaceous eustasy revisited: Global and Planetary Change, v. 113, p. 44-58, ISSN 0921-8181, <https://doi.org/10.1016/j.gloplacha.2013.12.007>.
- Heger, A.W., 2016, Stratigraphy and reservoir characterization of the Turner Sandstone, southern Powder River Basin, Wyoming: Golden, Colorado School of Mines, M.S. thesis, 160 p.
- Howard, J.D., and Frey, R.W., 1975, Regional animal-sediment characteristics of Georgia estuaries: *Senckenbergiana Maritima*, v. 7, p. 33-107
- Jarvie, D.M., Hill, R.J., Ruble, T.E., Pollastro, R.M., 2007, Unconventional shale-gas systems: The Mississippian Barnett Shale of north-central Texas as one model for thermogenic shale-gas assessment, v.4, p. 475-499, doi.org/10.1306/12190606068
- Kauffman, E. J., 1985, Cretaceous Evolution of the Western Interior Basin of the United States, in Pratt, L.M., Kauffman, E.G., and Zelt, F.B., eds., *Fine-grained Deposits and Biofacies of the Cretaceous Western Interior Seaway: Evidence of Cyclic Sedimentary Processes: Society of Economic Paleontologists and Mineralogists, Second Annual Field Trip*.
- Kegel, J., Mirenda, T., Lenz, N., Keay, J., and O'Reilly, C., 2019, Powder River Basin Production Review from 2011 through 2018: How Refinements in Completions and Operations Have Led to Increasing Production in the Upper Cretaceous Formations of Campbell and Converse Counties, Wyoming: Unconventional Resources Technology Conference, Denver, Colorado, July 22-24, 2019
- Lafargue, W., Espitalie, J., Broks, T.M., Nyland, B., 1994, Experimental simulation of primary migration, *Organic Geochemistry*, Volume 22, Issues 3-5, p. 575-586, ISSN 0146-6380, [https://doi.org/10.1016/0146-6380\(94\)90216-0](https://doi.org/10.1016/0146-6380(94)90216-0).
- Martinsen, R. S., 2003, Depositional remnants; Part 2, Examples from the Western Interior Cretaceous basin of North America: *American Association of Petroleum Geologists*, v.87, p. 1883-1909.
- MacEachern, J. A., and Bann, K. L., 2008, The role of ichnology in refining shallow marine facies models *in* Recent advances in models of siliciclastic shallow-marine stratigraphy: Hampson, G.J., Steel, R.J., Burgess, P.M., and Dalrymple, R.W., eds., *Society for Sedimentology Special Publication*, 90: p. 73-116

- MacQueen J. B., 1967, Some methods for classification and analysis of multivariate observations. Proceedings of the Fifth Symposium on Math Statistics, and Probability, pp.281-297
- Melick, J.J., 2013, Subsurface description and modeling of geologic heterogeneity in large subsurface: datasets—Using tempo-ral and scalar hierarchies, Powder River Basin, WY and MT, U.S.A.: Bozeman, Montana State University, Ph.D dissertation, 222 p.
- Merewether, E.A., 1980, Stratigraphy of mid-Cretaceous formations at drilling sites in Weston and Johnson counties, north- eastern Wyoming: U.S. Geological Survey Professional Paper 1186-A, 25 p.
- Merewether, E.A., 1996, Stratigraphy and tectonic implication of Upper Cretaceous rocks in the Powder River Basin, northeastern Wyoming and southern Montana: U.S Geological Survey Bulletin 1917-T, 92 p.
- Merewether, E.A., Cobban, W.A., and Cavanaugh, E.T., 1979, Frontier Formation and equivalent rocks in eastern Wyoming: *The Mountain Geologist*, v. 6, no. 3, p. 67–102
- Merewether, E.A., and Cobban, W.A, 1985, Tectonism in the mid-Cretaceous foreland, southeastern Wyoming and adjoining areas, in Nelson, G.E., ed., *The Cretaceous geology of Wyoming: Wyoming Geological Association Annual Field Conference, 36th, 1985, Guidebook*, p. 67-73.
- Merewether, E.A., Cobban, W.A., and Obradovich, J.D., 2007, Regional unconformities in Turonian and Coniacian (Upper Cretaceous) strata in Colorado, Wyoming, and adjoining states-biochronological evidence: *Rocky Mountain Geology*, v. 42, n. 2, p. 95-122.
- Merewether, E.A., Cobban, W.A., and Obradovich, J.D., 2011, Biostratigraphic data from Upper Cretaceous formations—eastern Wyoming, central Colorado, and northeastern New Mexico: U.S. Geological Survey Scientific Investigations Map 3175, 2 sheets, pamphlet, 10 p
- Mermut, A. R., and A. F. Cano, 2001, Baseline studies of the clay minerals society source clays: Chemical analyses of major elements: *Clays and Clay Minerals*, 49, 381–386, doi: 10.1346/CCMN.2001.0490504.
- Modica J. C., and Lapierre S. G., 2012, Estimation of kerogen porosity in source rocks as a function of thermal transformation: Example from the Mowry Shale in the Powder River Basin of Wyoming, *AAPG Bulletin*, v. 96, no. 1. p. 87-104.
- Momper, J.A., and Williams, J.A., 1984, Geochemical exploration in the Powder River Basin, in Demaison, Gerard, and Murriss, R.J., eds., *Petroleum geochemistry and basin evolution: American Association of Petroleum Geologists Memoir 35*, p. 181–191.



- Nance, H. Rowe, H., 2015, Eustatic controls on stratigraphy, chemostratigraphy, and water mass evolution preserved in a Lower Permian mudrock succession, Delaware Basin, west Texas, USA. Interpretation. 3. SH11-SH25. 10.1190/INT-2014-0207.1.
- Parks, S.L., and Gale, M.S., 1996, Exploring overpressured, naturally fractured reservoirs, Powder River Basin, Wyoming: a multi-disciplinary effort: American Association of Petroleum Geologists Rocky Mountain Section Meeting 1996, Expanded Abstracts Volume, p. 69-79.
- Rahman, M., Olson, R.K., Symcox, C.W., and Bingham, Sean, 2016, Geochemistry of Cretaceous oils and source rocks in the Powder River Basin: Unconventional Resources Technology Conference, San Antonio, Texas, August 1–3,2016
- Ramkumar, M., 2015, Toward standardization of terminologies and recognition of chemostratigraphy as a formal stratigraphic method: *in* M. Ramkumar (Ed.), Chemostratigraphy—Concepts, techniques, and applications (Chap. 1, pp. 1–22). Amsterdam: Elsevier.
- Reineck, H. E., 1963, Sedimentgefüge im Bereich der südlichen Nordsee: Adhandlungen der Senckenbergische Naturforschende Gesellschaft, 505p.
- Rice, D.D. and Gaskill, C., 1988, Muddy-Turner field trip: Wyoming Geological Association., Earth Science Bulletin., v.20, p. 67-72
- Rice D.D., and Keighin, C.W., 1989, Configuration of shelf sandstone oil reservoirs, Upper Cretaceous (Turonian) Turner Sandy Member of Carlile Shale, Powder River Basin, Wyoming [abs.]: American Association of Petroleum Geologists Bulletin, v. 73, no. 3, p. 405
- Richter, D.K, Götze, Th., Götze, J., Neuser, R.D., 2003, Progress in application of cathodoluminescence (CL) in sedimentary petrology: *in* Mineralogy and Petrology 79, p. 127–166. <https://doi.org/10.1007/s00710-003-0237-4>
- Rubey, W.W., 1930, Lithologic studies of fine-grained Upper Cretaceous sedimentary rocks of the Black Hills region: U.S. Geological Survey Professional Paper 165-A, 54 p.
- Sageman, B. B. and Lyons, T. W., 2009. Geochemistry of Fine-grained Sediments and Sedimentary Rocks *in* Holland, H.D. and Turekian, K. K. (eds) *Readings from the Treatise on Geochemistry*, Elsevier, pp. 424-456
- Seilacher, A., 1954, Die geologische Bedeutung fossiler Lebensspuren Zeitschrift deutschen Geologische Gesellschaft, no. 105, p. 214-227

- Sippel, R.F., 1968, Sandstone petrology, evidence from luminescence petrography: *J Sediment Petrol* 38, p. 530–554
- Slack, P.B., 1981, Paleotectonics and Hydrocarbon Accumulation, Powder River Basin, Wyoming. *AAPG Bulletin*, p. 65. doi:10.1306/2f9199bd-16ce-11d7-8645000102c1865d
- Slaughter, M., and Earley, J.W., 1965, Mineralogy and geological significance of the Mowery bentonites, Wyoming: *Geological Society of America Special Papers*, v. 83, p. 1-96.
- Sonnenberg, S.A., and Weimer, R.J., 1981, Tectonics, sedimentation, and petroleum potential. Northern Denver Basin, Colorado, Wyoming, and Nebraska: *Quarterly Colorado Sch. Mines*, v. 76, no. 2., p. 7-45.
- Taylor, A. M., Goldring, R., 1993, Description and analysis of bioturbation and ichnofabric. *Journal of the Geological Society*, 150(1), 141-148
- Taylor, A. M., Goldring, R., Gowland, S., 2003. Analysis and application of ichnofabrics, In *Earth-Science Reviews*, v. 60, no. 3-4, p. 227-259
- Tillman, R. W., and Almon, W. R., 1979, Diagenesis of Frontier Formation offshore bar sandstones, Spearhead Ranch Field, Wyoming: *Society of Economic Paleontologists and Mineralogists*, Special Publication no. 26, p. 337-378
- Toner, R.N., 2019, Influences on oil and natural gas production from the Wall Creek and Turner sandstone reservoirs, Powder River Basin, Wyoming: Wyoming State Geological Survey Report of Investigations 77, 84 p., online map at [wsgs.maps.arcgis.com/apps/webappviewer/index.html?id=d00fe805fdf04db3b25eb3b56d81a953](https://wsgs.maps.arcgis.com/apps/webappviewer/index.html?id=d00fe805fdf04db3b25eb3b56d81a953).
- Wagstaff, K., Cardie, C., Rogers, S., and Schrödl, S., 2001, Constrained K-means Clustering with Background Knowledge. In *Proceedings of the Eighteenth International Conference on Machine Learning (ICML '01)*. Morgan Kaufmann Publishers Inc., San Francisco, CA, USA, 577–584.
- Weaver, C. E., 1965, Potassium content of illite: *Science*, 147, 603–605, doi: 10.1126/science.147.3658.603
- Weimer, R.J., and Flexer, A., 1985, Depositional patterns and unconformities, Upper Cretaceous, eastern Powder River Basin, Wyoming: Wyoming Geological Association 36th annual Field conference Guidebook, p. 131-147
- Winn, R.D., 1991, Storm deposition in marine sand sheets—Wall Creek Member, Frontier Formation, Powder River Basin, Wyoming: *Journal of Sedimentary Petrology*, v. 61, no. 1, p. 86–101.

Xu, J. and Sonnenberg, S., 2016, Brittleness and Rock Strength of the Bakken Formation, Williston Basin, North Dakota, *in* Unconventional Resources Technology Conference, San Antonio, Texas, 1-3 August 2016, p. 2237-2254